2010

BIO/ORGANIC COMPOUND DETECTION USING SODIUM SULFATE MINERALS: IMPLICATIONS IN THE SEARCH FOR LIFE ON MARS AND EUROPA

Charles Doc Richardson
The University of Montana

BIO/ORGANIC COMPOUND DETECTION USING SODIUM SULFATE MINERALS: IMPLICATIONS IN THE SEARCH FOR LIFE ON MARS AND EUROPA

By:

CHARLES DOC RICHARDSON

Bachelor of Science Geosciences, University of Colorado, Boulder, CO, 2001
Master of Science Geosciences, University of Otago, Dunedin, New Zealand, 2003

Dissertation

Presented in partial fulfillment of the requirements for the degree of

Doctor of Philosophy in Geosciences

The University of Montana
Missoula, MT

Official Graduation Date- December 2009

Approved by:

Perry Brown, Associate Provost for Graduate Education
Graduate School

Nancy Hinman, Chair
Geosciences

Jill Scott,
Chemical Sciences, Idaho National Laboratory

Julia Baldwin
Geosciences

James Sears
Geosciences

Michael DeGrandpre
Chemistry

Carrine Blank
Geosciences

Richardson, C. Doc, Ph.D., Fall 2009 *Geosciences*

Bio/organic compound detection using sodium sulfate minerals: implications in the search for life on Mars and Europa

Chair: Nancy Hinman

ABSTRACT

With the discovery of Na-sulfate minerals (thenardite, mirabilite) on Mars and Europa, recent studies using these minerals have focused on their ability to assist in the detection of biosignatures. On Earth, biotic and biotic processes can assist in the formation and deposition of these minerals. A primary objective of these studies is the detection of bio/organic compounds that may be associated with the mineral. These biosignatures would imply biological involvement during mineral formation. The following research presents a series of natural and synthetic investigations to determine if biological activity is associated with Na-sulfate mineralization, and if these minerals can assist in detecting bio/organic compounds. Evidence for biological activity associated with the formation of Na-sulfate deposits in the basaltic subsurface of Craters of the Moon National Monument, Idaho was examined by laser desorption Fourier transform mass spectrometry (LD-FTMS), infrared spectroscopy and sulfur isotopic fractionation. These experiments show that bio/organic compounds are likely associated with the secondary Na-sulfate minerals, suggesting biological involvement in the mineralization of these deposits. LD-FTMS results of the synthetic bio/organic-mineral combinations show the potential of Na-sulfate minerals to assist in the detection and identification of bio/organic compounds. These results prove the importance of Na-sulfate minerals for future exploration missions that are likely to use LDMS to search for signs of life in the solar system.

ACKNOWLEDGEMENTS

Doc wants to thank YOU!!

PREFACE

The following dissertation discussion is based on my doctoral research conducted between 2005 and 2009 in the Geosciences Department at the University of Montana-Missoula. This discussion focuses on the effectiveness of thenardite (Na_2SO_4) to assist in the desorption and identification of various types of bio/organic compounds. Bio/organic compounds are defined as chemical compounds produced by living organisms or derived from other biogenic organic compounds. These observations underpin the determination of bio/organic compounds are associated with secondary mineralization at Craters of the Moon National Monument, Idaho (COM). The following chapters are arranged to follow this progression. Chapter 1 is a basic introductory chapter that provides the necessary knowledge about thenardite formation on Earth and the solar system. Additionally, it reviews the methodology and rationale behind the laser desorption-Fourier transform mass spectrometry (LD-FTMS) instrument. The chapter also discusses pertinent background information that may not be covered in the subsequent research chapters. Chapter 2 was published in the journal *Geomicrobiology* in August 2008. Its focus is to determine the effectiveness of thenardite in the detection of aliphatic fatty acids, in addition to discovering the limit of detection of the LD-FTMS instrument. Chapter 3 focuses on the identification, formational mechanisms and gas-phase reactions of aromatic amino acids associated with thenardite, it was accepted by the *International Journal of Astrobiology* in July 2009. The following two chapters focus on the secondary mineralization at COM. Chapter 4 uses X-ray powder diffraction, attenuated total reflectance-Fourier transform infrared spectroscopy, and LD-FTMS to identify and characterize the secondary deposits found in the subsurface of COM. In addition, the

chapter introduces the COM basalts as a viable analog to martian basalts. It is currently under review by the journal of *Chemical Geology*. Subsequently, chapter 5 discusses the role of microbial activity in the formation of thenardite in the secondary deposits at COM. It is currently in review by the journal of *Earth and Planetary Science Letters.* Finally, the last chapter offers a quick summary of the overall results of this dissertation research and discusses its implications into the search for life in the solar system.

With the exception of chapter 1, all the chapters were submitted for publication and are still formatted to reflect their respective journal. Thus each chapter has its own reference list and any redundancy in the introduction and methodology between these chapters is inescapable. Fortunately, the numbering of the tables and figures has been changed to reflect this discussion.

Appendix 1 is an excerpt from a recently published review chapter that discusses the occurrence and fate of organic compound in the solar system. The chapter title is called, “The stellar stew: Distribution of extraterrestrial organics in the universe”. It is in the book “Astrobiology: from simple molecules to primitive life”, published by American Scientific Publishers.

TABLE OF CONTENTS

TABLE OF FIGURES

TABLE OF TABLES

CHAPTER 1: INTRODUCTION

1.1. OVERVIEW

The search for extraterrestrial life is primarily focused on Mars and Europa, a moon of Jupiter, as they are thought to, continuously or sporadically in their existence, contain the necessary ingredients for the emergence of life. These planetary bodies have been visited by spacecraft and rovers and observed through terrestrial instruments in the search for bio/organic compounds, which are defined as organic structures that are made by organisms or derived from a bio/organic compound made by a living organism. Since 1976, with the *Viking* mission, these techniques have been used to search for bio/organic compounds on Mars.

Europa has not been directly investigated for evidence of extinct or extant life. However, Europa may contain the three necessary requirements for emergent life; chemical disequilibria, prebiotic compounds, and liquid water (Kargel et al., 2000). Subsequently, in 2020, a joint ESA/NASA endeavor called the *Europa Jupiter System* mission will further investigate the possibility of extant or extinct life on Europa. Due to the oxidizing and radiolytic atmospheres of Mars and Europa, respectively, any bio/organic compound on the surface will easily degrade unless they are incorporated into a mineral structure. Thus, finding, effective host minerals that can sequester and preserve any associated bio/organic compounds in addition to having the ability to facilitate the detection and characterization of bio/organic compounds is of the utmost importance.

Na-sulfate minerals are excellent targets for sequestering bio/organic compounds, as these minerals are key components in numerous geological and chemical reactions in the solar system. On Mars, Na-sulfate salts are found in bedded layers as a weathering

product of the host basaltic rocks (Mangold et al., 2008; Zhu et al., 2006b). Due to this aqueous basaltic weathering, Na-sulfate may contain chemical information about past environmental and possibly biological processes on Mars. On Europa, the Na-sulfate system is an abundant solute in the subsurface ocean, and subsequently as a component of the surficial salt deposits (Kargel et al., 2000; McCord et al., 1998a; McCord et al., 1999; Zolotov and Shock, 2001). Terrestrial Na-sulfate minerals occur in evaporitic and basaltic settings and are important in many abiotic and biotic chemical pathways (Aubrey et al., 2006; Bowden and Parnell, 2007; Richardson et al., 2008). As terrestrial Na-sulfate minerals are known to harbor bio/organic compounds in several evaporitic and volcanic settings (Dongyan et al., 1998; Richardson et al., 2009b; Richardson et al., 2008), their presence on Mars and Europa signifies their importance in the search for life beyond Earth.

Sodium and sulfate combine to form two stable minerals, mirabilite ($Na_2SO_4 \bullet 10H_2O$) and thenardite (Na_2SO_4). Cell dimensions of the two minerals are only slightly different in the a- and b-axes, while the c-axis is approximately doubled in mirabilite. Another key difference between these two minerals, is the ease in which mirabilite will effloresce, which makes it extremely vulnerable to dehydration, occurring within minutes depending on air temperature and relative humidity (Rodriquez-Navarro et al., 2000). This rapid dehydration occurs at a relative humidity below 71% (at 20 °C) forming thenardite; above this value mirabilite will form at the expense of thenardite. As a result of the efflorescent susceptibility of mirabilite, thenardite likely exists under the dry conditions of the martian atmosphere (Zhu et al., 2006b), while the cold, icy surface of Europa favors the formation and preservation of mirabilite (McCord et al., 2001a).

A critical aspect in the search for biological activity is the ability to detect organic compounds associated with the mineral matrix. This detection is dependent on the formation constraints (biotic vs. abiotic and aqueous precipitation vs. adsorption) and the type of association (sorption, inclusion and substitution). These mineral-bio/organic compound associations can be accurately and effectively investigated using an imaging laser desorption/ionization Fourier transform ion cyclotron resonance-mass spectrometer (FTICR-MS), which is a laboratory-designed instrument, located at Idaho National Laboratory, Idaho Falls, ID. Its ability to detect inorganic and organic chemical signatures associated with mineral matrices, demonstrates its importance in future laser desorption mass spectrometry techniques, such as the Mars Organic Molecular Analyzer (MOMA) slated to be aboard NASA's *ExoMars* rover.

1.2. Occurrence of Terrestrial Na-sulfate Minerals

Na-sulfate minerals are the second most common, naturally occurring water-soluble minerals in the world. Thenardite is one of several sulfate minerals formed in non-marine environments, such as massive salt deposits, as a constituent in evaporitic salt flats (sabkhas, playas), or in fumarolic exhalations (Wiedemann and Smykatz-Kloss, 1981). Additionally, Na-sulfate deposits are found as speleothems in both volcanic lava tubes and, to a lesser extent, in limestone caves if an excess of Na ions are present in the host lithologies (Hill and Forti, 1997).

1.2.1. Evaporitic Settings

The presence of Na-sulfate minerals in evaporitic environments is focused on playa lakes and their resulting mineralogy. Playa lakes are ephemeral lakes that usually lack an outgoing channel; thus, loss of water is strictly through evaporitic processes.

Since these waters contain various ions, other than Na^+ and SO_4^{2-}, a diverse range of mineralogy is expected, with a high degree of mixed-mineral assemblages. Although, the steep solubility curve for Na-sulfate minerals, which is unique relative to other minerals, leads to the preferential formation of mirabilite, even in highly diverse and concentrated brine waters (Eugster and Hardie, 1978). This results in layered deposits of massive, fairly pure mirabilite, that can easily dehydrate to thenardite (Garrett, 2001). Along with abiotic chemical deposition, organic compounds suggesting the influence of microbial activity during the formation of thenardite layers are observed in several evaporitic assemblages throughout the world (Dongyan et al., 1998; Richardson et al., 2008).

1.2.2. Craters of the Moon National Monument

Although most thenardite deposits are found in evaporitic environments, its presence has also been observed in volcanic cave settings. These occurrences have been well documented from lava tubes and caves throughout the world (Hill and Forti, 1997). Unfortunately, studies of thenardite in basaltic settings have been limited to on-site observations offering no in-depth analytical investigations. As a result, no detailed investigations regarding the mineralization have been conducted in relation to thenardite in basaltic cave settings.

Nowhere in the world are the extent and abundance of secondary thenardite as prevalent and mysterious, as in the basaltic caves and lava tubes of Craters of the Moon National Monument, ID (COM). These basaltic flows cover an approximate area of 1,600 km^2 and are the northernmost and largest of the 3 youngest lava fields (the others being Wapi and Kings Bowl) in the Eastern Snake River Plain (ESRP) in southern Idaho (Fig. 1.1). The ESRP is composed of sub-5 km diameter monogenetic tholeiitic and low-

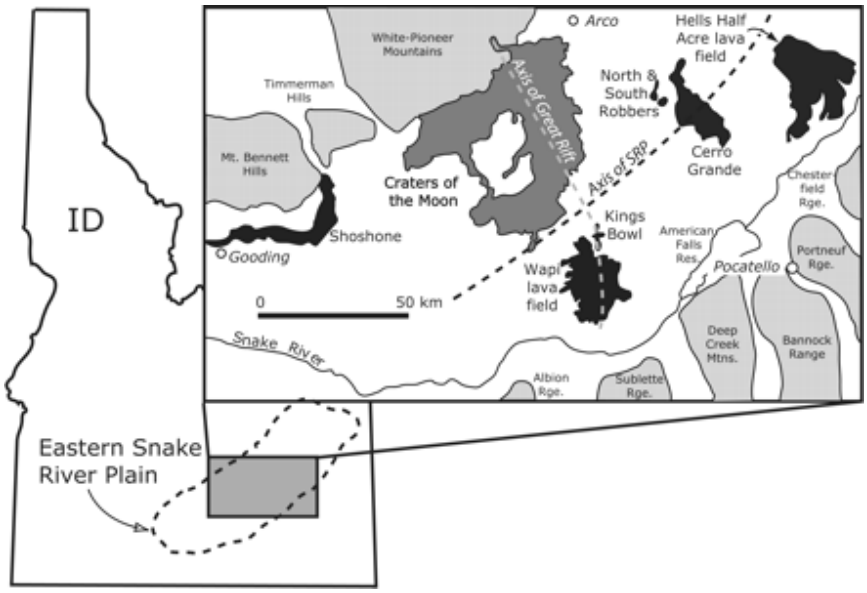

Figure 1.1. Map of Idaho showing location of Craters of the Moon National Monument and other basaltic lava fields in Eastern Snake River Plain. Taken from (Putirka et al., 2009)

angle basalt shield volcanoes intermittent dispersed between Quaternary-aged sedimentary layers (Kuntz et al. 1992). These low-angle coalescent shields, subdued topography and shallow depositional slopes of the basaltic flows are generalized as "plains-style volcanism" proposed by Greeley and King (1977), which was later modified by Greeley (1982). COM is a composite field made up of at least 60 individual lava flows and 25 tephra cones, emplaced due to eight eruptive periods between 15 ka to 2.1 +/- 0.2 ka along the Great Rift (Kuntz et al., 1992; Reid, 1995). The Great Rift is a tensional related series trending parallel to the basin and range fault system (Fig. 1.1), consisting of open cracks, eruptive fissures, shield volcanoes and cinder cones possibly are related to the extension of basement faulting (Leeman et al., 1976).

The approximately 60 basaltic flows in COM are chemically and petrologically atypical of the olivine tholeiites elsewhere in the ESRP (Hughes et al. 1999; Kuntz et al. 1986). Relative to ESRP basalts, the COM flows exhibit elevated Ti, Fe, Na, K, P and

depleted Mg and Ca (Hughes et al. 1999). Since all basaltic flows in the ESRP are considered to originate from a single parent magma, the variance seen in the COM basalts likely reflect large degrees of crustal assimilation or magma fractionation (Kuntz et al., 1986; Kuntz et al., 1992; Leeman et al., 1976).

The majority of the secondary sulfate minerals found in the ESRP are located at COM, although a limited amount of sulfate salts are found lining the walls and ceilings of lava tubes at Hell's Half Acre, Wapi, and Shoshone lava fields (Karlo et al., 1980). These assemblages consist primarily of Ca-sulfate (gypsum, bassanite) and Mg-sulfate (bloedite, epsomite) minerals (Karlo et al., 1980). Contrarily, Na-sulfate minerals dominate the secondary assemblages at COM (Richardson et al., 2009a). The cation differences (Na vs. Ca, Mg) between the lava fields, likely reflect variations in the chemical composition of the respective host basalts, as COM basalts are enriched in alkali elements and depleted in alkali-earth elements relative to basaltic flows elsewhere in the ESRP (Hughes et al., 1999).

Of the 60 cumulative flows that comprise COM, the young Blue Dragon flow (~2.1 ka) contains the majority of the accessible caves and lava tubes found at COM (Richardson et al., 2009a). These subterranean features reflect the younger age of the flow, as they have had less time to undergo gravitational collapse. Within the flow, three separate locations where choose for this purposes of this study. These include Wilderness Caves area, Cave Trail caves and within two hollow magma chambers beneath adjacent spatter cones (Snow Cone Pit, Crystal Pit). These locations were based on personal communication with park officials, preliminary field observations and previous reports (Karlo et al., 1980; Morris et al., 1995; Peck, 1974). These features vary in size from 15

m to nearly 2 km in length and between 2 m and 40 m in diameter. The secondary sulfate deposits occur in caves of all sizes. A more detailed explanation of the subsurface features and the associated secondary minerals can be found in Chapters 5 and 6.

1.3. Occurrence of Na-sulfate Minerals in the Solar System

Excluding Earth, the occurrence of surficial Na-sulfate minerals in the solar system is limited to Mars and the Galilean moons of Europa, Io and Ganymede (Fanale et al., 2001; Johnson, 2000; Kargel et al., 2000; Mangold et al., 2008; McCord et al., 1998b; McCord et al., 2001b; McCord et al., 1999; Wiens et al., 1997; Zhu et al., 2006b; Zolotov and Shock, 2001).

1.3.1. Io

Evidence of solid $NaSO_4$ species on the surface of Io is observed by sputtering of molecular ion clouds from localized surface locations (Wiens et al., 1997). These molecular clouds contain significant quantities of sodium-bearing molecular ions (Na_xO_y, Na_xS_y), evident by their interaction with Jupiter's magnetosphere (Wilson and Schneider, 1994). Regardless of whether the endogenic Na neutrals originate from the atmosphere or from the surface, the Na must have once been associated with Na-bearing minerals on the surface (Wiens et al., 1997). Spectroscopic observations of Io's surface support the occurrence of Na-bearing sulfates with surficial concentration reaching up to 40% (Howell et al., 1989). These surficial deposits are likely formed due to interaction of solid Na-silicates with oxidized SO_2 atmospheric gases (Burnett, 1995; Johnson and Burnett, 1993).

1.3.2. Ganymede

Ganymede is the largest of the Galilean moons, and the third most distant from Jupiter. The near infrared mapping specrometer (NIMS) aboard the *Galileo* spacecraft observed evidence of H_2O-bearing salt minerals, inferred to be Mg-sulfates with minor concentrations of hydrated Na-sulfate minerals (McCord et al., 2001b). Ganymede, like Europa, is considered to have a subsurface liquid water ocean, containing a brine-type liquid ocean consisting of dissolved Mg, Na, and sulfate (Grundy et al., 2007; Kivelson et al., 2002; McCord et al., 2001b).

1.3.3. Formation and Emplacement of Na-sulfate Minerals on Europa

Europa is the second closest moon to Jupiter with a diameter nearly equal to Earth's moon. Unlike the Moon, Europa has a differentiated internal structure, comprised of a Fe-metallic-silicate core, water-rich rocky mantle and an icy lithosphere encompassing a subsurface liquid ocean (Kargel et al., 2000; McCord et al., 2001b; Zolotov and Shock, 2001). The subsurface ocean was detected by its induced magnetic field by the magnetometer aboard the *Galileo* spacecraft, which indicated the existence of a salt-rich, liquid water ocean beneath approximately 100-150 km of solid ice (Khurana et al., 1998; Kivelson et al., 1997). Determining the composition of this outer layer has been limited to geochemical and thermodynamic modeling (Zolotov and Shock, 2001), sputtering of surficial components produced by charged-particle irradiation associated with Jupiter's magnetosphere (Brown and Hill, 1996), and by near-infrared reflectance spectroscopy (Carlson et al., 1996). These observations suggest that the surface of Europa is heterogeneously composed of water ice with intermittently dispersed regions of hydrated salts. These non-icy regions consist primarily of polyhydrated Mg- and Na-

sulfate minerals ($MgSO_4 \cdot 7H_2O$; $MgSO_4 \cdot Na_2SO_4 \cdot 4H_2O$; $Na_2SO_4 \cdot 10H_2O$) and possibly sodium carbonate ($Na_2CO_3 \cdot 10H_2O$) (McCord et al., 1998a; McCord et al., 1999). These surficial sulfate minerals may comprise up to 90% of the non-icy regions with nearly 40% attributed to polyhydrated Na-sulfate (Kargel et al., 2000; Orlando et al., 2005).

The occurrence of surficial hydrated Na-sulfate minerals provides direct insight into the chemical constituents and speciation of the subsurface ocean. These salts are strongly associated with well-defined, tectonically disrupted areas (lineaments, mottled and chaotic terrains), suggesting an endogenic emplacement followed by sublimation and sputtering of ice (McCord et al., 1998a; McCord et al., 1998b). The presence of solutes in the subsurface ocean is undeniable assuming terrestrial investigations of water-rock interactions and ocean chemistries. Thus, similar water-rock interactions during the onset of ocean formation on Europa would have led to multiple solute constituents. These solutes were likely the result of leaching and degassing of elements from Europa's silicate mantle (Fanale et al., 2001). Unfortunately, the only insight into the chemical constituents and concentrations in the subsurface oceans is based on theoretical geochemical modeling. Such modeling has implied that the europan ocean contains 0.087 mol/kg of SO_4^{2-} and 0.049 mol/kg of Na^+, corresponding to 0.014 mol/kg of dissolved Na_2SO_4 (Zolotov and Shock, 2001). The uppermost layer of this ocean is likely in chemical equilibrium with the overlying ice, with the remaining ocean saturated with sulfate and chlorine salts (Fanale et al., 2001). Freezing of the ocean water on the water-ice interface leads to the preferential deposition of Mg and Na-sulfate minerals, further causing the remaining oceanic composition to be concentrated in chlorine and chloride salts (Orlando et al., 2005). Due to this preferential deposition and their subsequent

emplacement, surficial Mg- and Na-sulfate minerals offer direct insight into the chemical composition of the subsurface ocean.

1.3.4. Formation of Secondary Na-sulfate Minerals on Mars

The production of secondary mineral assemblages depends on a number of interrelated factors, including primary igneous lithologic composition, alteration environment (i.e., gas, aqueous, subsurface, etc), pH, temperature and duration. These characteristics ultimately dictate which assemblages will mineralize from the host lithology. On Mars, investigations of secondary mineralogy and the formational pathways of these deposits have largely focused on phyllosilicates, Fe-sulfates and Fe-bearing oxides and hydroxides (Chevrier and Mathe, 2006). These minerals assemblages comprise the majority of secondary minerals found on Mars, although localized concentrations of sulfate minerals have been observed. These sulfate minerals were first detected on the martian regolith by the *Viking* rover (Clark et al., 1976) and later confirmed in 2004 by the Mars Exploration Rovers *Spirit* and *Opportunity* (Christensen et al., 2004; Clark et al., 2005; Squyres and Knoll, 2005). These rovers found that secondary sulfate minerals comprise approximately 40% of the mineralogy in certain evaporitic-like terrains (McLennan et al., 2005).

With the ubiquitous occurrence of Na-sulfate minerals on Earth, similar deposits are likely to be present within the martian regolith. Until recently, Na-sulfates were undetected from the surficial mineral assemblages seen on Mars. This apparent absence is likely due to Na-sulfate minerals having similar characteristic bands as Mg-, Fe-, and Ca-sulfates minerals, rather than the complete absence of Na-sulfate minerals (Mangold et al., 2008). Additionally, Na-sulfate minerals are often intermixed with other secondary

minerals and Fe-oxides, which further conceals their signatures (Gendrin et al., 2005). Despite these similarities, characteristic spectra suggestive of Na-sulfate minerals were observed in the low-albedo region of Syrtis Major (Zhu et al., 2006b). In addition, Na-sulfate minerals are a constituent in the West Candor Chasma, which is one of the largest sulfate deposits known on Mars (Mangold et al., 2008).

Indirect evidence of Na-sulfate deposits on Mars comes from thermal spectra and from geochemical modeling. Thermal spectrometry data obtained from the boundaries of the seasonal polar caps provide evidence of rapid seasonal hydration-dehydration cycles (Kuzmin et al., 2004). To explain these observations, Kuzmin et al. (2004) concluded that mirabilite likely dehydrates to thenardite in the summer months. This is followed by the hydration of thenardite forming mirabilite in winter seasons. Chemical and mineralogical evidence of Na-sulfate species also suggests the presence of Na-sulfates using a series of evaporation calculations based on known martian basaltic chemistries (Tosca and McLennan, 2006).

The atmospheric conditions on Mars, except near the seasonal polar caps, favor the presence of thenardite at the expense of mirabilite. The occurrence of thenardite is likely intermixed with other anhydrous and polyhydrated sulfate minerals, suggesting these species have similar formational pathways. Two scenarios have been proposed to explain the occurrence of sulfate minerals on Mars (Fig. 1.2).

1) The first scenario involves chemical weathering of sulfide-rich mineral assemblages in the presence of oxic, acidic aqueous solutions (Fig. 1.2A). This process begins with oxidation of the basaltic host rock well below the surface. As the percolating groundwater rises it brings soluble cations (Mg^{2+},

Fe^{2+}, Ca^{2+}, Na^{+}), along with carbonates and sulfate oxyanions to the surface. Once on the surface, layered precipitation occurs due to evaporation of the lacustrine water and the solubility of the precipitates (Burns, 1987; Burns and Fisher, 1990a; Burns and Fisher, 1990b; Zolotov and Shock, 2005).

2) High concentrations of SO_2 gas in the atmosphere could also be a factor in the formation of sulfate deposits (Fig. 1.2B). The high SO_2 is due to degassing volcanoes and by meteoric impact causing the release of volatiles (Chevrier and Mathe, 2006; Tosca et al., 2004; Wanke et al., 2001). The SO_2 is then converted to H_2SO_4 in presence of water, forming acid fog. Subsequent percolation of the acid rain downward through the basalts interacts with the sulfide-rich basaltic deposits forming sulfate minerals (Banin et al., 1997; Tosca and McLennan, 2006). As the formation and abundance of sulfate is dependent on volcanic activity and meteoric impacts this pathway is largely controlled by these episodic cycles during martian history (Tosca et al., 2004).

In each proposed formational pathway, one of the main factors is the presence and subsequent interaction of aqueous solutions. The abundance of water, either in the atmosphere or in the subsurface, is a limiting factor in the chemical weathering potential of martian basalts (Borg and Drake, 2005). Therefore weathering rates and subsequent sulfate mineral formation are limited by the amount of atmospheric, surficial and/or subsurface water (Madden et al., 2004).

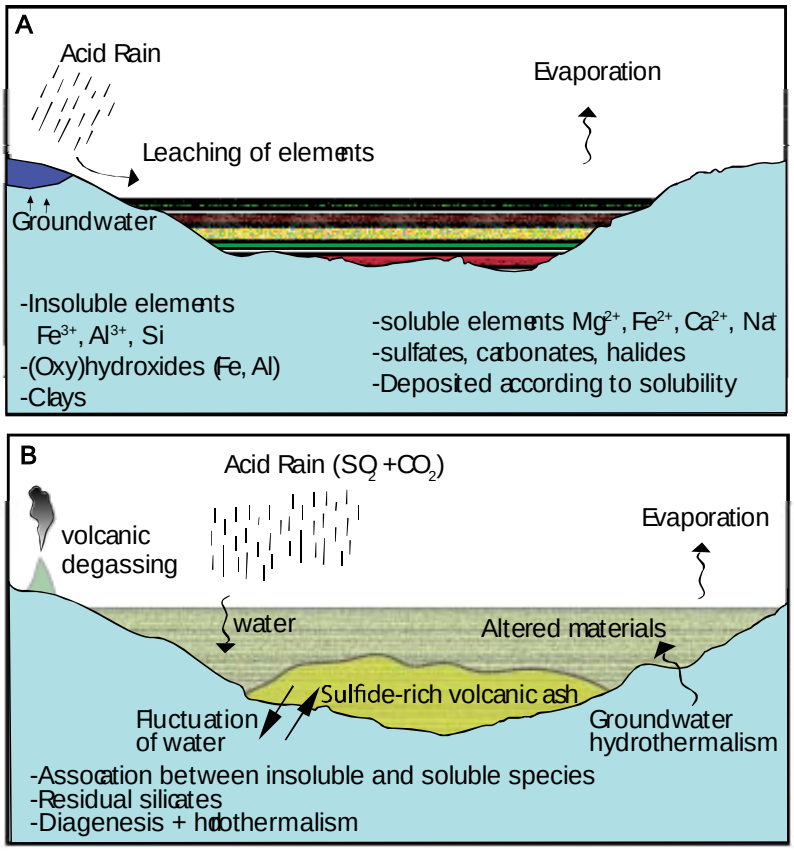

Figure 1.2. Two possible processes for the formation of sulfate deposits on Mars. (A) Hypothesis of alteration, leaching, transport and deposition in a lake or sea. (B) In situ alteration and transformation of minerals by input of acid rain and evaporation of water. Modified from Chevrier and Mathe (2006).

The abundance of sulfate minerals on Mars reflects the enrichment of sulfur in the martian lithosphere (Chevrier and Mathe, 2006). Sulfur concentrations in martian soils are nearly two-orders of magnitude higher than sulfur concentrations in terrestrial soils (Yen et al., 2005). This abundance of sulfur is a direct result of the lack of differentiation on Mars due to the absence of tectonic activity and mantle dynamics (Burns and Fisher, 1990a; Clark and Baird, 1979). This homogeneity is observed by the lack of petrologic and mineralogical variations observed throughout the martian basaltic landscape (McSween, 2004).

1.4. ORGANIC COMPOUNDS AND FORMATIONAL PATHWAYS OF BIO/ORGANIC COMPOUNDS

Sulfate minerals are the predominant salts detected on the two main targets for extraterrestrial life, Mars and Europa. On Earth, life requires liquid water, organic building blocks (prebiotic amino acids), and chemical disequilibria. It is still unclear exactly how life arose on Earth, so it is difficult to determine how and if similar biotic pathways would develop in other planetary bodies. Mars in particular was, and is still, considered the most earth-like of all planets, as it shows polar caps, an atmosphere with meteorological activity over a rocky surface, a comparable rotation period, seasonal variations, and moderate temperatures not too different from certain environments on Earth. In addition to these similarities, early Mars may have contained the necessary ingredients for life. In contrast, Europa's surface environment and conditions are much different than Earth; nonetheless conditions on Europa may have continuously or sporadically fulfilled the requirements of emergent life in its subsurface ocean.

1.4.1. Chemical Pathways of Bio/organic Compounds on Europa

The presence of liquid water, prebiotic organic compounds, and an adequate energy source suggest the possibility of emergent life on Europa. Exogenous delivery by comets early in europan history delivered an estimated 1-10 Gt of carbon and other biogenic elements (H, O, P, N, and S) based on modeling experiments, cometary impact velocities, and escape thresholds of the europan atmosphere (Pierazzo and Chyba, 2002). Estimates of organic compounds within the low-temperature, primordial ocean is nearly 100 ppm, corresponding to about 4.8×10^{18} kg (Kargel et al., 2000). These values imply that carbon could be in excess in the ocean, with concentrations much higher than present-day terrestrial oceans (Zolotov and Shock, 2001). As a result, the europan ocean

would have contained the necessary constituents for organic compound synthesis (Chyba, 2000; Gaidos et al., 1999; Kotler et al., 2009).

Hydrothermal activity is also putatively agreed to produce numerous vents on the europan ocean floor (Fig. 1.3). This energy gradient is likely due to upwelling water from metamorphic dehydration in the deep mantle (Prieto-Ballesteros and Kargel, 2005). Upwelling water would have carried soluble minerals in addition to forming non-uniform hydrothermal vents on the ocean floor. This outgassing and leaching would have further modified the chemical composition of the subsurface ocean (Kargel et al., 2000). The driving force for the hydrothermal circulation is a consequence of a Jupiter-induced tidal dissipation and radiogenic heat from rocky sub-ocean lithosphere (Lowell and Dubose, 2005). Combined, these processes may induce a total heat flux that is comparable to the present-day radiogenic heat flux on Earth. However, due to Europa's low acceleration of gravity, individual hydrothermal output on Europa is ten times less than vents on Earth (Lowell and Dubose, 2005; Vance et al., 2007). Regardless, the energy output from the hydrothermal vents on the europan seafloor would satisfy the necessary energy gradient needed for emergent life (Chyba, 2000). Biological activity by chemoautotrophic organisms could occur near the hydrothermal vents on Europa (Chyba, 2000; Gaidos et al., 1999). Physiochemical conditions likely associated with the hydrothermal vents are within the acceptable range of hospitable conditions for numerous terrestrial microorganisms (Kargel et al., 2000). If present, remnant biogenic compounds would be present in the subsurface ocean and intermix with inorganic solutes. These interactions would subsequently trap the bio/organic compounds in the sulfate mineral lattice. The sulfate minerals would become preferentially frozen at the ice-water interface and

emplaced on the surface by sublimation, cryovolcanism upwelling in fractures and/or impact events (McCord et al., 1998b; McCord et al., 1999; Orlando et al., 2005). Thus, bio/organic compounds could be incorporated in Mg- and Na-sulfate deposits and preserved on the surface of Europa (Fig. 1.3) (Chela-Flores, 2006).

Preservation of bio/organic compounds is dependent on the stability of sulfate minerals on the europan surface. The persistence and concentration of mirabilite in the ice-free lag deposits is dependent on their emplacement rate as well as its radiolytic and thermodynamic stability. On the surface, incoming radiation has the most influential degradation effect on the stability of Na-sulfate minerals (Zolotov and Shock, 2001). This radiolytic bombardment is due to Jupiter's immense magnetosphere (Johnson, 2000). Fortunately, the sulfate anion and the associated hydrogen bonds are effective in stabilizing the mineral from such degradation effects (Cooper et al., 2001). However, minerals containing monovalent cations are not as stable, and much of the surface-layer sodium and hydrogen ions will desorb from the crystal lattice into the atmosphere (Johnson, 2000). The sputtering rate and extent of neutral sodium loss is also dependent on depth within the lag deposits and the ice, because effective radiation can only penetrate the upper most ~ 0.1- 1 cm of the surface (Cooper et al., 2001; Johnson, 2000). Thus, below 1cm depth mirabilite should be relatively stable. A similar depth profile is observed in the thermal dehydration of mirabilite. At depth, mirabilite is thermodynamically stable for millions of years because of Europa's surface temperatures and pressures, along with the dehydration kinetics and thermodynamic stability of the salts (McCord et al., 2001a; Zolotov and Shock, 2001). Once the dehydration threshold

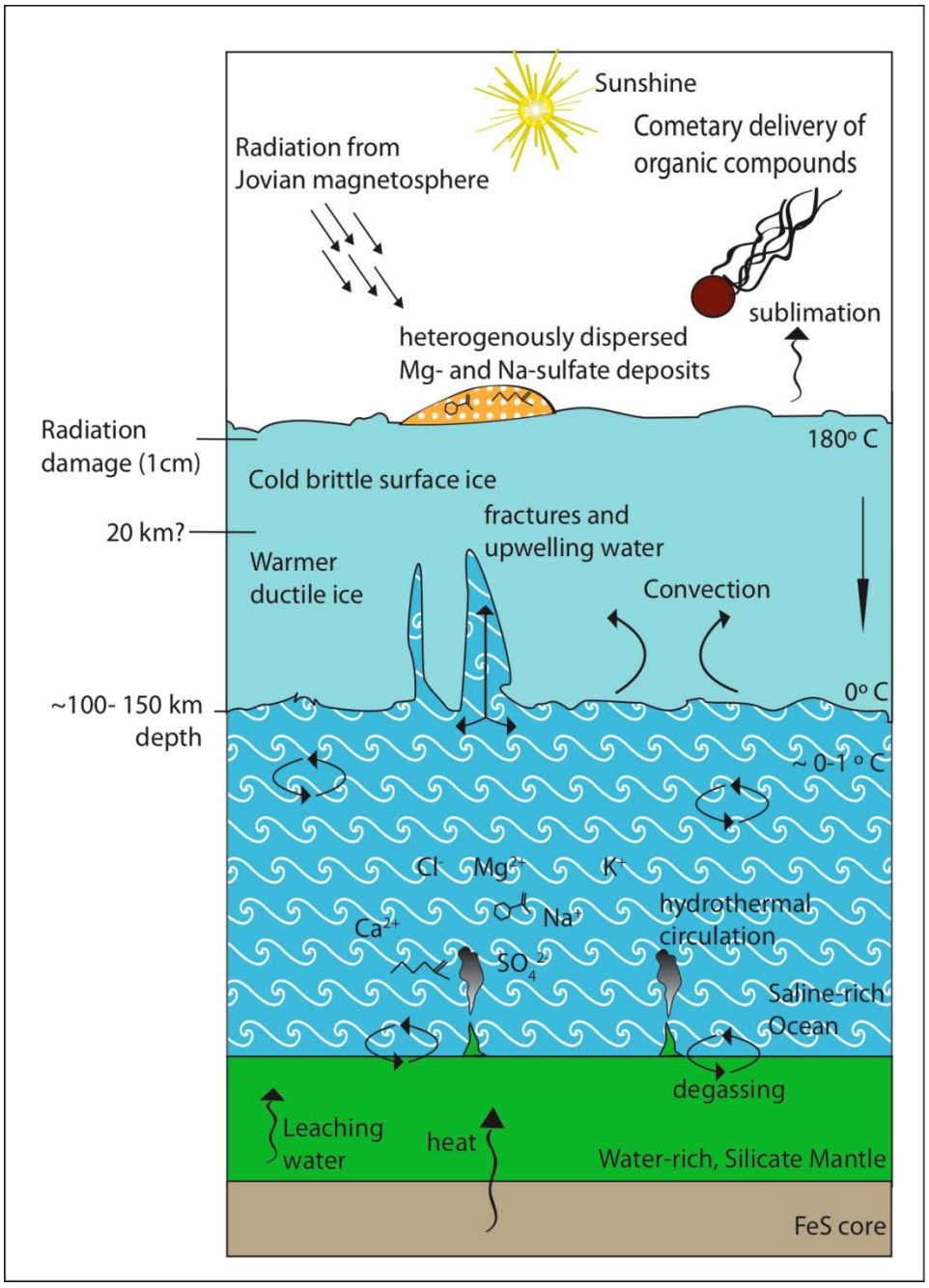

Figure 1.3. Schematic of Europa illustrating the dynamic processes that lead to the formation, emplacement and degradation of surfical Na-sulfate minerals and possibly association of bio/organic compounds. Not to scale.

is breached, mirabilite will quickly dehydrate into thenardite, causing dehydration stratification in the upper layers of the surface. This desiccation further increases the amount of sputtered sodium into the atmosphere due to the loss of bonded water molecules from the mineral lattice (Johnson, 2000).

Regardless of the fate of Na-sulfate species on the surface or within the icy outer crust, Na-sulfates are a significant constituent of the non-icy lag deposits on the europan surface. Their presence on the surface gives valuable insights into the past and present physiochemical processes that lead to their formation and emplacement, along with possibly hosting evidence of past biological activity on Europa (Fig. 1.3).

1.4.2. Chemical Pathways and Preservation of Bio/organic Compounds on Mars

Without a protective atmosphere, the martian regolith is continually exposed to solar ultraviolet radiation, which likely results in photochemical production of oxidants and subsequent oxidation of any organic molecules that might be present (Encrenaz et al., 2004; Oyama et al., 1977). As a result, *in situ* investigations by martian rovers and landers have failed to detect the occurrence of organic compounds. The *Phoenix* lander identified perchlorate (ClO_4^-) at concentrations between 0.3-0.6 wt% in the soil, its presence is problematic as it can easily oxidize organic compounds, erasing any evidence of their past existence (Aubrey et al., 2009).

Fortunately, the detection of organic compounds is not restricted to *in situ* experiments, as the Planetary Fourier Spectrometer aboard the Mars *Express* Orbiter detected methane gas in the martian atmosphere (Formisano et al., 2004). Its occurrence was later confirmed by Earth-based Fourier Transform Spectrometry (Krasnopolsky et al., 2004). Atmospheric methane concentrations are between 0 and 30 ppbv (parts per

billion by volume), with a global mixing ratio of 10 ppbv (Formisano et al., 2004). High concentrations were observed in spatially heterogeneous locations, signifying the methane is released from localized sources on the surface. Continuous observations show that the methane has a short residence time, implying it is being replenished at rates faster than meteorite impact or magmatic activity can control (Oze and Sharma, 2005). As these are no longer a valid source, other explanations of the atmospheric methane include a by-product of methanogenic metabolism, emission through degassing by thermal activity, and cometary delivery (Formisano et al., 2004; Krasnopolsky et al., 2004; Kress and McKay, 2004).

The bulk of the knowledge regarding martian organic matter comes from detailed investigations of the SNC (shergotite-nakhlite-chassignite) martian meteorites. SNC meteorites contain many low and high mass complex organic molecules, such as aromatic, alkyl-substituted aromatic, oxygen-containing, and nitrogen-bearing aromatic hydrocarbons (Kotler et al., 2009; Sephton, 2002). Organic compounds have also been identified when incremental combustion experiments released CO_2 between 200–400°C, which is the typical range of carbon-bearing compounds (Jull et al., 1998; Wright et al., 1989).

Due to the link between liquid water and biological activity on Earth, evidence of past surficial water have been taken as hopeful signs that Mars might once have supported life. The presence of fluvial features provides direct evidence that liquid water was once present on the martian surface (Jolliff et al., 2006; Knoll and Grotzinger, 2006). Present-day conditions on Mars are too cold; with an atmosphere that is too thin, to support liquid water on its surface. Thus, Mars must have had a thicker atmosphere in

order to sustain liquid water even sporadically in its past. Presently, the martian surface does not appear to have the necessary conditions to support life. By analogy with Earth, life may have originated on Mars early in its history, possibly during the end of the late heavy bombardment (3.8- 4.0 Ga) when the surface of Mars was wetter and warmer (Bibring et al., 2006; Knoll and Grotzinger, 2006; McKay, 1997).

The abundance of sulfate minerals on the martian evaporitic terrains and their association with water during their formation makes them ideal targets for biosignature investigation (Parnell et al., 2004). Small quantities of bio/organic compounds can be preserved in the sulfate mineral lattice as intracrystalline inclusions or substitutions (Aubrey et al., 2006; Bowden and Parnell, 2007). Such associations are often observed in terrestrial sulfate minerals, indicating the direct or indirect influence of biological activity in their formation (Aubrey et al., 2006; Bowden et al., 2005; Kotler et al., 2008; Richardson et al., 2008). Sulfate deposits are easily susceptible to dissolution and erosion on Earth. Fortunately, surficial water has been much less prevalent on Mars, implying sulfate minerals have not been exposed to much, if any, water (Aubrey et al., 2006; Martinez-Frias et al., 2006). Thus, preservation of sulfate minerals is feasible over long geological time scales due to the martian atmospheric and dry, cold surface conditions. As a result, bio/organic compounds may also be preserved over billions of years when shielded within a sulfate mineral matrix (Aubrey et al., 2006; Kminek and Bada, 2006).

Evidence of microbial activity may also be found in the martian subsurface (Boston et al., 2001; Leveille and Datta, 2009). Orbiter imagery and thermal anomalies have confirmed the presence of lava tubes and related structure in the large-scale basaltic edifices of Mars (Cushing et al., 2007; Riedel and Sakimoto, 2002; Wyrick et al., 2004).

On Earth, caves and lava tubes are unique environments that provide stable physiochemical conditions for both secondary mineralization and microbial growth. Such environments offer valuable insight into the diversity and resilience of past microbial and aqueous activity. Likewise, martian caves and lava tubes may contain subsurface groundwater and provide habitable environments, both past and present (Grin et al., 1998; Schulze-Makuch et al., 2005). These subsurface features may contain secondary minerals and water ice that harbor paleoenvironmental indicators and bio/organic compounds. Such environments would also offer pristine conditions for secondary mineral and bio/organic compound preservation, providing shelter from surficial ultraviolet radiation, temperature fluctuations, and desiccation (Boston et al., 2001). Due to the low gravity, dry arid conditions, and extremely slow weathering rates, it is possible that subsurface features seen today could have existed during warmer and wetter periods of martian history (Leveille and Datta, 2009). By offering shelter from harsh surface conditions, caves and lava tubes may preserve minerals and associated bio/organic compounds for longer than typical surface deposits. As a result, caves and lava tubes may provide the most likely environment for preserving and finding bio/organic compounds on Mars (Leveille and Datta, 2007, 2009).

1. 5. Organic Compounds and their Relationship to Biotic and Abiotic Processes

Terrestrial organic matter is so ubiquitous that is difficult to determine bio/organic compounds and organic matter of nonbiological origin. Past studies of terrestrial samples largely suggest that the most accurate methodology is the use of carbon chemistry. Other methods (morphological, mineralogical, isotopic) may always be part of planetary

explorations, but no one single methodology provides as much pertinent information as organic analysis.

Because of the harsh atmospheric conditions on Mars and Europa, bio/organic compounds are not stable unless they can be associated with a protective mineral matrix. Size restraints between the mineral lattice and complex bio/organic compounds (nucleic acids, proteins, phospholipids, carbohydrates, steroids) make these organic compounds unlikely to be associated with minerals. However, their precursor bio/organic compounds (amino acids, fatty acids, hydrocarbons) and other smaller bio/organic compounds may be adequately sized to be associated with the mineral matrix. Unfortunately, many of these smaller bio/organic compounds also have a nonbiological origin. Therefore, in the search for molecular evidence of past or present biological activity in the solar system, it is imperative to be able to distinguish between organic compounds formed by abiotic processes and those synthesized by biological processes (Parnell et al., 2007a). Abiogenic processes can make a wide range of organic compounds, such as amino acids, hydrocarbons and sugars. Fortunately, bio/organic compounds have specific chemical characteristics (chirality, preferential number of carbons, isotopic distribution, structural isomers) that can distinguish them as having a biotic or abiotic origin (Table 1.1) (Kotler et al., 2009; Simoneit, 2004; Simoneit et al., 1998).

An important aspect of terrestrial life, and thus identifying biological activity, is the fact that all organisms utilize a distinct set of small compounds as building blocks to construct more complex bio/organic compounds. Some of the more understood subunits include the 20 essential amino acids of proteins, the four nucleotides of DNA, and acetate

($C_2H_3O_2$) of fatty acids and lipids. For example, the preferential accumulation of acetate subunits is seen in the formation of fatty acids (in the bacterial and eukaryotic domains of life) by the addition of acetate subunits. Acetate accumulation will always result in an even number of carbons in the fatty acid, thus growth of the fatty acid is accomplished by binding of additional acetate units producing an even number of carbons (e.g., C_{16}, C_{18}, C_{20}) (Mathews et al., 2000). The ability of acetate and other molecular subunits to construct more complex compounds reflects the propensity of these smaller compounds to be arranged in distinct chemical and structural configurations. These configurations are called isomers, which are molecules having identical formulas but exhibit different spatial arrangements of their atoms. These different configurations can lead to a number of important biological properties. Biogenic amino acids are synthesized exclusively as using one of these isomeric structures (Peters et al., 2004). These structures, called enantiomers, are compounds with different chirality but identical chemical formulas. In contrast to biogenic amino acid formation, abiotic synthesis of amino acids has no preferential production regarding chirality, resulting in 1:1 racemic ratio of the enantiomers. This preference of one enantiomer over another also pertains to sugars. Enantiomeric excess in either amino acids or sugars would strongly indicate a biological origin (Peters et al., 2004). This biologic preference, to utilize one specific isomer, is in direct contrast to the thermodynamically-controlled pathways of abiotic organic synthesis (Lambert, 2008).

Table 1.1. Select biocompounds, their biological function, and distinguishing characteristics in their identification.

Biocompound	Biological Function	Characteristics
Nucleic Acids	Genetic information	Complex structure
Proteins	Building blocks of enzymes	Complex structure
Nucleotides	Building blocks of nucleic acids	Complex structure
Hydrocarbons	Building blocks of membranes	Distinct number of carbons
Isoprenoids*	Membranes, quinones	Repeating 5-carbon subunits
Peptides	Breakdown products of proteins	Short chain of L-amino acids
Amino Acids	Building blocks of proteins	Chirality
Sugars	Energy source, biosynthetic precursor	Chirality
Nucleobases	Building blocks of nucleotides	Fragile, contain N

* Stable for longer periods of geological time

The discovery of any complex family of organic compounds associated with life on Earth would have dramatic implications if found on Mars and Europa. However, discovery of these large complex bio/organic compounds is unlikely due to the harsh surficial conditions of these planetary bodies. As a result, the search for unambiguous signs of biological activity is largely focused on smaller bio/organic compounds, which could be protected and preserved within surficial minerals. The discovery of repeating preference or patterns of carbon number, chirality, or structural isomers in these organic compounds would be extremely significant in interpreting and elucidating the emergence of life in the solar system.

1.6. Background of Geomatrix-Assisted Laser Desorption/Ionization Fourier Transform Ion Cyclotron Resonance Mass Spectrometry

Laser desorption mass spectrometry (LDMS) has been proposed to be a viable method in the search for extraterrestrial bio/organic compounds. Biosignature detection is dependent on the concentrations of the bio/organic compound, ionization efficiency between the matrix and the analyte, and the instrument capabilities. Therefore, maximizing the ionization efficiency of the matrix and improving the mass accuracy, resolution, detection limits and other instrument parameters are particularly important.

Geomatrix-assisted laser desorption/ionization (GALDI) combined with a FTICR-MS has shown repeatedly to detect biosignatures in a wide host of mineral matrices (Kotler et al., 2008; Richardson et al., 2008; Richardson et al., 2009c; Yan et al., 2007a; Yan et al., 2007c). This technique is capable of much greater resolution and mass accuracy than traditional LDMS techniques. For example, the FTICR-MS has high resolution (< 10, 000), high mass accuracy (mass error of ± 0.003 amu), high sensitivity (≤ 400 ions for peaks with signal-to-noise ratio ~3), high spatial resolution, automated mapping capabilities, low detection limits (~ 3 parts per trillion), and automated data acquisition and interpretation capabilities (Richardson et al., 2008; Yan et al., 2007a), all of which can be acquired using a single laser shot, which is unusual compared to conventional LDMS instruments.

Most bio/organic compounds require assistance in desorption and ionization processes to produce ions that can be observed, exceptions being polycyclic aromatic hydrocarbons and some aromatic compounds (Macha et al., 2000; Richardson et al., 2009c; Yan et al., 2007c). Thus, the focus of GALDI-FTICR-MS studies is the ability of a mineral matrix to facilitate the desorption and ionization of bio/organic compounds. Previous studies using GALDI-FTICR-MS have shown that the type of mineral moiety directly influences the bio/organic peaks observed in the spectrum (Kotler et al., 2008; Richardson et al., 2008; Richardson et al., 2009c; Yan et al., 2007a; Yan et al., 2007c). For example, certain Fe-bearing oxides are incapable of assisting in analyte detection as they produce either no signal or highly fragmented peaks (Yan et al., 2007a). The concentration of the bio/organic compound is also particularly important, because as the ratio of the bio/organic compound to mineral decreases, the signal attributable to a

bio/organic compound tends to increase (Richardson et al., 2008). This is likely due to the bio/organic compound being completely surrounded and incorporated into the mineral matrix. Thus, biosignatures can be easily and accurately detected even at extremely low concentrations. Not only does this matrix surrounding the analyte lower the limit of detection, but results in the improved ability to detect minute quantities of remnant bio/organic compounds that may have been heterogeneously dispersed within a mineral.

The type of bio/organic compound-mineral association (e.g., sorption, inclusion, substitution) is another critical aspect in bio/organic signature detection in the solar system. Exogenous ultraviolet radiation, on solar bodies that lack a substantial protective atmosphere, will easily degrade bio/organic compounds if not properly shielded by a mineral. On the surface, the bio/organic compound can survive if adequately entrained within the mineral matrix, where it would have a much greater chance of being shielded. Thus, understanding the differences between these associations (inclusion, adsorption, or substitution) is essential in GALDI-FTICR-MS studies.

The ability and parameters of GALDI in conjunction with the FTICR-MS, makes this a unique and crucial instrument in the search for biosignatures in the solar system. Although the instrument is too large for space exploration, it accurately detects and characterizes organic, biological, and mineralogical constituents in a range of terrestrial samples. Furthermore, its ability to assist in characterizing a wide range of bio/organic compounds associated with relevant extraterrestrial minerals can further assist in future space-based LDMS missions searching for life in the solar system as well as analysis of samples returned to Earth.

1.7. REFERENCES

Aubrey, A., Cleaves, H.J., Chalmers, J.H., Skelley, A.M., Mathies, R.A., Grunthaner, F.J., Ehrenfreund, P. and Bada, J.L., 2006. Sulfate minerals and organic compounds on Mars. Geology 34(5), 357-360.

Aubrey, A., Parker, E., Grunthaner, F. and Bada, J., 2009. Implications of the presence of surface perchlorate for in situ detection of organic compounds during future missions, The New Martian Chemistry Workshop, Medford, Ma, pp. 1.

Banin, A., Han, F. and Cicelsky, A., 1997. Aciditic volatiles and the Mars soil. J. Geophys. Res 102(E6), 13341-13356.

Bibring, J.P., Langevin, Y., Mustard, J.F., Poulet, F., Arvidson, R., Gendrin, A., Gondet, B., Mangold, N., Pinet, P. and Forget, F., 2006. Global mineralogical and aqueous mars history derived from OMEGA/Mars express data. Science 312(5772), 400-404.

Borg, L. and Drake, M., 2005. A review of meteorite evidence for the timing of magmatism and of surface or near-surface liquid water on Mars. J. Geophys. Res 91(B13), E207-E214.

Boston, P., Spilde, M., Northup, D., Melim, L., Soroka, D., Kleina, L., Lavoie, K., Hose, L., Mallory, L., Dahm, C., Crossey, L. and Schelble, R., 2001. Cave biosignatures suites: microbes, minerals, and Mars. Astrobiology 1, 25-55.

Bowden, S., Cooper, J. and Parnell, J., 2005. The extraction of organic compound from sulfate minerals for astrobiological exploration. Lunar and Planetary Science XXXVI(Abstract 1325).

Bowden, S. and Parnell, J., 2007. Intracrystalline lipids within sulfates from the Haughton Impact Structure-implications of survival of lipids on Mars. Icarus 187, 422-429.

Brown, M. and Hill, R., 1996. Discovery of an extended sodium atmosphere around Europa. Nature 380, 229-231.

Burnett, D., 1995. Competition between Na2SO4 and Na sulfide in teh upper crust of Io. Journal of Geophysical Research 100, 21265-21270.

Burns, R.G., 1987. Ferric Sulfates on Mars. Journal of Geophysical Research 92(B4), E570-E574.

Burns, R.G. and Fisher, D.S., 1990a. Evolution of Sulfide Mineralization on Mars. Journal of Geophysical Research-Solid Earth and Planets 95(B9), 14169-14173.

Burns, R.G. and Fisher, D.S., 1990b. Iron-sulfur mineralogy of Mars: Magmatic evolution and chemical weathering products. J. Geophys. Res. 95, 14,415 – 14,421.

Carlson, R., Smythe, W., Baines, K., Barbinis, E., Becker, K., Burns, R., Calcutt, S., Calvin, W., Clark, R., Danielson, G., Davies, A., Drossart, P., Encrenaz, T., Fanale, F., Granahan, J., Hanse, G., Herrera, P., Hibbitts, C., Hui, J., Irwin, P., Johnson, T., Kamp, L., Kieffer, H., Leader, F., Lellouch, E., Lopes-Gautier, R., matson, D., McCord, T., Mehlman, R., Ocampo, A., Orton, G., Roos-Serote, M., Segura, M., Shirley, J., Soderblom, L., Stevenson, A., Taylor, F., Torson, J., Weir, A. and Weissman, P., 1996. Near-infrared spectroscopy and spectral mappping of Jupiter and teh Galilean satellite: results from Galileo's initial orbit. Science 274, 385-388.

Chela-Flores, J., 2006. The sulphur dilemma: are there biosignatures on Europa's icy and patchy surface? International Journal of Astrobiology 5, 17-22.

Chevrier, V. and Mathe, P.E., 2006. Mineralogy and evolution of the surface of Mars: A review. Planetary and Space Science 55(3), 289-314.

Christensen, P.R., Wyatt, M.B., Glotch, T.D., Rogers, A.D., Anwar, S., Arvidson, R.E., Bandfield, J.L., Blaney, D.L., Budney, C., Calvin, W.M., Faracaro, A., Fergason, R.L., Gorelick, N., Graff, T.G., Hamilton, V.E., Hayes, A.G., Johnson, J.R., Knudson, A.T., McSween, H.Y., Mehall, G.L., Mehall, L.K., Moersch, J.E., Morris, R.V., Smith, M.D., Squyres, S.W., Ruff, S.W. and Wolff, M.J., 2004. Mineralogy at Meridiani Planum from the Mini-TES experiment on the Opportunity Rover. Science 306(5702), 1733-1739.

Chyba, C., 2000. Energy for microbial life on Europa. Nature 406(6794), 391-395.

Clark, B. and Baird, A., 1979. Is the martian lithosphere sulfur rich? Journal of Geophysical Research 84(B14), 8395-8403.

Clark, B., Baird, A., Rose, H., Toulmin, P., Keil, K., Castro, A.J., Kelliher, W.C., Rowe, C.D. and Evans, P.H., 1976. Inorganic analyses of martian surface samples at the Viking landing sites. Science 194, 1283-1288.

Clark, B.C., Morris, R.V., McLennan, S.M., Gellert, R., Jolliff, B., Knoll, A.H., Squyres, S.W., Lowenstein, T.K., Ming, D.W., Tosca, N.J., A., Y., Christensen, P.R., Gorevan, S., Bruckner, J., Calvin, W., Dreibus, G., Farrand, W., Klingelhoefer, G., Waenke, H., Zipfel, J., Bell III, J.F., Grotzinger, J., McSceen, H.Y. and Rieder, R., 2005. Chemistry and mineralogy of outcrops at Meridiani Planum. Earth and Planetary Science Letters 240, 74-94.

Cooper, J., Johnson, R., Mauk, B., Garrett, H. and Gehrels, N., 2001. Energetic ion and electron irradiation of the icy galilean satellites. Icarus 149, 133-159.

Cushing, G.E., Titus, T.N., Wynne, P.R. and Christensen, P.R., 2007. Themis observes possible cave skylights on Mars. Geophysical Research Letters 34(L17201), Doi:10.1029/2007/2007GL030709.

Dongyan, W., Zhenmin, L., Xiaolin, D. and Shaokang, X., 1998. Biomineralization of mirabilite deposits of Barkol Lake, China. Carbonates & Evaporites 13, 86-89.

Encrenaz, T., Bezard, B., Greathouse, T., Richter, L., Lacy, J., Atreya, S., Wong, A., Lebonnis, S., Lefevre, F. and Forget, F., 2004. Hydrogen peroxide on Mars:evidence for spatial and seasonal variations. Icarus 170(2), 424-429.

Eugster, H. and Hardie, L., 1978. Saline Lakes. Lakes: chemistry, geology, physics. Springer-Verlag, 237-293 pp.

Fanale, F.P., Li, Y.-H., De Carlo, E., Farley, C., Sharma, S.K., Horton, K. and Granahan, J.C., 2001. An experimental estimate of Europa's "ocean" composition independent of Galileo orbital remote sensing. Journal of Geophysical Research 106(E7), 14595-14600.

Formisano, V., Atreya, V., T., E., Ignatiev, N. and Giuranna, M., 2004. Detection of methane in the atmosphere of Mars. Science 306, 1758-1761.

Gaidos, E., Nealson, K. and Kirschvink, J., 1999. LIfe in Ice-Covered Oceans. Science 284, 1631-1633.

Garrett, D., 2001. Sodium sulfate: handbook of deposits, processing, properites, and use. Academic Press, London, UK.

Gendrin, A., Mangold, N., Bibring, J., Langevin, Y., Gondet, B., Poulet, F., Bonello, G., Quantin, C., Mustard, J., Arvidson, R. and LeMouelic, S., 2005. Sulfates in Martian Layered Terrains: The OMEGA/Mars Express View. Science 307(5715), 1587-1591.

Grin, E., Cabrol, N. and McKay, C., 1998. Caves in the martian regolith and their significance for exobiology exploration, 29th Lunar and Planetary Science Conference, Houston, TX, pp. Abstract #1012.

Grundy, W., Buratti, B., Cheng, A., Emery, J., Lunsford, A., McKinnon, W., Moore, J., Newman, S., Olkin, C., Reuter, D., Schenk, P., Spencer, J., Stern, S., Throop, H. and Weaver, H., 2007. New Horizons mapping of Europa and Ganymede. Science 318, 234-237.

Hill, C. and Forti, P., 1997. Cave minerals of the world, 2nd National Speleological Society, Huntsville, AL.

Howell, R., Nash, D., Geballe, T. and Cruikshank, D., 1989. High-resolution infrared spectroscopy of Io and possible surface materials. Icarus 78, 27-37.

Hughes, S.S., Smith, R., Hackett, W. and Anderson, S., 1999. Mafic volcanism and environmental geology of the eastern Snake River Plain. In: S.S. Hughes and G. Thackray (Editors), Guidebook to the geology of eastern Idaho. Idaho Museum of Natural History, Pocatello, Idaho, pp. 143-168.

Johnson, M. and Burnett, D., 1993. SO2-rock interaction on Io: reaction under highly oxidizing conditions. Journal of Geophysical Research 98, 1233-1230.

Johnson, R.E., 2000. Sodium at Europa. Icarus 143, 429-433.

Jolliff, B., McLennan, S. and Team, a.t.A.S., 2006. Evidence for water at Meridiani Elements 2, 163-167.

Jull, A., Courtney, C., Jeffrey, D. and Beck, J., 1998. Isotopic evidence for a terrestrial source of organic compounds found in martian meteorites Allan Hills 84001 and Elephant Moraine 79001. Science 279(5349), 366-369.

Kargel, J.S., Kaye, J.Z., Head, J.W.I., Marion, G.M., Sassen, R., Crowly, J.K., Ballesteros, O.P., Grant, S.A. and Hogenboom, D.L., 2000. Europa's crust and ocean: origin, composition, and the prospects for life. Icarus 148, 226-265.

Karlo, J.H., Jorgenson, D.B. and Shineldecker, C.L., 1980. Sulfate minerals in Snake River Plain volcanoes. Northwest Science 54(3), 178-182.

Khurana, K., Kivelson, M., Stevenson, D., Schubert, G., Russell, C., Walker, R. and Polansky, C., 1998. Induced magnetic fields as evidence for subsurface oceans in Europa and Callisto. Nature 395, 777-780.

Kivelson, M., Khurana, K., Joy, S., Russell, C., Southwood, D., Walker, R. and Polansky, C., 1997. Europa's magnetic signature: report from Galileo's pass on 19 December 1996. Science 276, 1239-1241.

Kivelson, M., Khurana, K. and Volwerk, M., 2002. The permanent and inductive magnetic moments of Ganymede. Icarus 157, 507-522.

Kminek, G. and Bada, J., 2006. The effect of ionizing radiation on the preservation of amino acids next term on Mars. Earth and Planetary Science Letters 245(1-2), 1-5.

Knoll, A. and Grotzinger, J., 2006. Water on Mars and the prospect of martian life. Elements 2, 169-173.

Kotler, J.M., Hinman, N.W., Yan, B., Stoner, D.L. and Scott, J.R., 2008. Glycine identification in natural jarosites using laser-desorption Fourier transform mass spectrometry: Implications for the search for life on Mars. Astrobiology 8, 253-266.

Kotler, J.M., Richardson, C.D., W., H.N. and Scott, J.R., 2009. The stellar stew: distribution of extraterrestrial organics in the universe. In: V.A. Basiuk (Editor), From simple molecules to primitive life. American Scientific Publishers, Valencia, CA, pp. in press.

Krasnopolsky, V., Maillard, J. and Owen, T.C., 2004. Detection of methane in the martian atmosphere: evidence for life? Icarus 172, 537-547.

Kress, M. and McKay, C.P., 2004. Formation of methane in comet impacts: Implications for Earth, Mars, and Titan. Icarus 168(2), 475-483.

Kuntz, M., Champion, D., Spiker, E. and Lefebvre, R., 1986. Contrasting magma types and steady-state, volume-predictable volcanism along the great rift, Idaho. GSA bulletin 97, 579-594.

Kuntz, M., Covington, H. and Schorr, L., 1992. An overview of basalitc volcanism of the eastern Snake River Plain, Idaho. In: P. Link, M. Kuntz and L. Platt (Editors), Regional geology of eastern Idaho and western Wyoming. Geological Society of America memoir, pp. 227-267.

Kuzmin, R.O., Christensen, P.R. and Zolotov, M.Y., 2004. Results of global mapping of bound water distribution in the martian surface material base on TES data. Geophysical Research Abstracts 6(07008).

Lambert, J., 2008. Adsorption and polymerization of amino acids on mineal surfaces: A review. Origins of Life and Evolution of the Biosphere 38, 211-242.

Leeman, W., Vitaliano, C. and Prinz, M., 1976. Evolved lavas from the Snake River Plain: Craters of the Moon National Monument, Idaho. Contributions to Mineralogy and Petrology 56, 35-60.

Leveille, R. and Datta, S., 2007. Basaltic caves and lava tubes: astrobiological targets on Earth and Mars, Lunar and Planetary Science XXXVIII, Houston, TX.

Leveille, R. and Datta, S., 2009. Lava tubes and basaltic caves as astrobiological targets on Earth and Mars: A review. Planet. Space Sci, 10.1016/j.pss.2009.06.004.

Lowell, R. and Dubose, M., 2005. Hydrothermal systems on Europa. Geophysical Research Letters 32, L05202.1-L05202.4.

Macha, S.F., Limbach, P.A. and Savickas, P.J., 2000. Application of nonpolar matrices for the analysis of low molecular weight nonpolar synthetic polymers by matrix-assisted laser desorption/ionization time-of-flight mass spectrometry. Journal Of The American Society For Mass Spectrometry 11(8), 731-737.

Madden, M.E.E., Bodnar, R.J. and Rimstidt, J.D., 2004. Jarosite as an indicator of water-limited chemical weathering on Mars. Nature 431(7010), 821-823.

Mangold, N., Gendrin, A., Gondet, B., LeMouelic, S., Quantin, C., Ansan, V., Bibring, J., Langevin, Y., Masson, P. and Neukum, G., 2008. Spectral and geological study of the sulfate-rich region of West Candor Chasma, Mars. Icarus 194, 519-543.

Martinez-Frias, J., Amaral, G. and Vazquez, L., 2006. Astrobiological significance of minerals on Mars surface environment. Reviews in Environmental Science and Biotechnology 5, 219-231.

Mathews, C., van Holde, K. and Ahern, K., 2000. Biochemistry. Addison Wesley Longman, San Francisco.

McCord, T., Orlando, T., Teeter, G., Hanse, G., Sieger, M., Petrik, N. and van Keulen, L., 2001a. Thermal and radiation stability of the hydrated salt minerals epsomite, mirabilite, and natron under Europa environmental conditions. Journal Geophysical Research 106, 3311-3319.

McCord, T.B., Hansen, G., Clark, R.N., Martin, P., Hibbitts, C.A., Fanale, F., Granahan, J., Segura, M., Matson, D.L., Johnson, T., Carlson, R., Smythe, W., Danielson, G. and Team, T.N., 1998a. Non-water-ice constituents in the surface material of the icy Galilean satellites from the Galileo near-infrared mapping spectrometer investigation. J. Geophys. Res 103(E4), 8603-8626.

McCord, T.B., Hansen, G., Fanale, F., Carlson, R., Matson, D.L., Johnson, T., Smythe, W., Crowley, J., Martin, P., Ocampo, A., Hibbitts, C.A., Granahan, J. and Team, N., 1998b. Salts on Europa's surface detected by Galileo's near infrared mapping spectrometer. Science 280, 1242-1245.

McCord, T.B., Hansen, G.B. and Hibbitts, C.A., 2001b. Hydrates salt minerals on Ganymede's surface: Evidence of an ocean below. Science 292, 1523-1525.

McCord, T.B., Hansen, G.B., Matson, D.L., Johnson, T.V., Crowley, J.K., Fanale, F.P., Carlson, R.W., Smythe, W.D., Martin, P.D., Hibbitts, C.A., Granahan, J.C. and Ocampo, A., 1999. Hydrated salt minerals on Europa's surface from the Galileo near-infrared mapping spectrometer (NIMS) investigation. Journal of Geophysical Research 104, 11827-11851.

McKay, C.P., 1997. The search for life on Mars. Origins of Life and Evolution of the Biosphere 27(1-3), 263-289.

McLennan, S.M., Bell, J.F., Calvin, W.M., Christensen, P.R., Clark, B.C., de Souza, P.A., Farmer, J., Farrand, W.H., Fike, D.A., Gellert, R., Ghosh, A., Glotch, T.D., Grotzinger, J.P., Hahn, B., Herkenhoff, K.E., Hurowitz, J.A., Johnson, J.R., Johnson, S.S., Jolliff, B., Klingelhofer, G., Knoll, A.H., Learner, Z., Malin, M.C., McSween, H.Y., Pocock, J., Ruff, S.W., Soderblom, L.A., Squyres, S.W., Tosca, N.J., Watters, W.A., Wyatt, M.B. and Yen, A., 2005. Provenance and diagenesis of the evaporite-bearing Burns formation, Meridiani Planum, Mars. Earth and Planetary Science Letters 240(1), 95-121.

McSween, H.Y., 2004. Basaltic rocks analyzed by the Spirit Rover in Gusev Crater. Science 305, 842-845.

Morris, R.C., Anderson, R.C., Earl, S., McCurry, M. and Pearson, L., 1995. A Mineral and Biotic Survey of Two Caves at Craters of the Moon National Monument. Environmental Science and Research Foundation.

Orlando, T.M., McCord, T.B. and Grieves, G.A., 2005. The chemical nature of Europa surface material and the relation to a subsurface ocean. Icarus 177, 528-533.

Oyama, V., Berdahl, B. and Carle, G., 1977. Preliminary findings of the Viking gas exchange experiment and a model for martian surface chemistry. Nature 265, 100-114.

Oze, C. and Sharma, M., 2005. Have olivine, will gas: serpentinization and the abiogenic production of methane on Mars. Geophysical Research Letters 32, L10203.

Parnell, J., Cullen, D., Sims, M., Bowden, S., Cockell, C., Court, R., Ehrenfreund, P., Gaubert, F., Grant, W., Parro, V., Rohmer, M., Sephton, M., Stan-Lotter, H., Steele, A., Toporski, J. and Vago, J., 2007. Searching for Life on Mars: Selection of Molecular Targets for ESA's Aurora ExoMars Mission. Astrobiology 7, 578-604.

Parnell, J., Lee, P., Cockell, C. and Osinski, G., 2004. Microbial colonization in impact-generated hydrothermal sulphate deposits, Haughton impact structure, and implications for sulphates on Mars. International Journal of Astrobiology 3, 247-256.

Peck, S.B., 1974. Unusual mineralogy of the Crystal Pit Spatter Cone, Craters of the Moon National Mounument, Idaho. NSS Bulletin 36(1), 19-24.

Peters, K., Moldowan, J. and Walters, C., 2004. The Biomarker Guide. Cambridge University Press, Cambridge, MA.

Pierazzo, E. and Chyba, C., 2002. Cometary delivery of biogenic elements to Europa. Icarus 157, 120-127.

Prieto-Ballesteros, O. and Kargel, J., 2005. Thermal state and complex geology of a heterogeneous salty crust of Jupiter's satellite, Europa. Icarus 173, 212-221.

Putirka, K., Kuntz, M., Unruh, D. and Vaid, N., 2009. Magma evolution and ascent at the Craters of the Moon and neighboring volcanic fields, southern Idaho, USA: Implications for the evolution of polygenetic and monogenetic volcanic fields. Journal of Petrology 50, 1639-1665.

Reid, M., 1995. Processes of mantle enrichment and magmatic differentiation in the eastern Snake River Plain: Th isotope evidence. Earth and Planetary Science Letters 131, 239-254.

Richardson, C., Hinman, N., McHenry, L., Kotler, J. and Scott, J., 2009a. Secondary sulfate mineralization and basaltic chemistry of Craters of the Moon National Monument, Idaho: A view into the martian subsurface. Chemical Geology, submitted.

Richardson, C., Hinman, N., McHenry, L. and Scott, J., 2009b. Biological activity in the mineralization of secondary deposits within the basaltic subsurface of Craters of the Moon National Monument: Implications for the search for life on Mars. Earth and Planetary Science Letter, in prep.

Richardson, C., Hinman, N., McJunkin, T., Kotler, J. and Scott, J., 2008. Exploring biosignatures associated with thenardite by geomatrix-assisted laser desorption/ionization Fourier transform ion cyclotron resonance mass spectrometry (GALDI-FTICR-MS). Geomicrobiology Journal 25(7), 432-440.

Richardson, C., Hinman, N. and Scott, J., 2009c. Effect of thenardite on the direct dectection of aromatic amino acids: Implications for the search for life in the solar system. International Journal of Astrobiology 8(4), 291-300.

Riedel, S. and Sakimoto, S., 2002. MOLA topgraphic constraints on lava tube effusion rates for Alba Patera, Mars, 33rd Lunar and Planetary Science Conference, pp. Abstract #1410.

Rodriquez-Navarro, C., Doehne, E. and Sebastian, E., 2000. How does sodium sulfate crystalllize? Implications for the decay and testing of building materials. Cement and Concrete Research 30, 1527-1534.

Schulze-Makuch, D., Irwin, L., Lipps, J., LeMone, D., Dohm, J. and Fairen, A., 2005. Scenarios for the evolution of life on Mars. Journal of Geophysical Research E: Planets 110, 1-12.

Sephton, M.A., 2002. Organic compounds in carbonaceous meteorites. Natural Product Reports 19(3), 292-311.

Simoneit, B., 2004. Biomarker (molecular fossils) as geochemical indicators of life. Advances in Space Research 33, 1255-1261.

Simoneit, B., Summons, R. and Jahnke, L., 1998. Biomarkers as tracers for life on early Earth and Mars. Origins of Life and Evolution of the Biosphere 28, 475-483.

Squyres, S.W. and Knoll, A.H., 2005. Sedimentary Geology at Meridiani Planum, Mars. Earth and Planetary Science Letters 240(1), 1-10.

Tosca, N.J. and McLennan, S.M., 2006. Chemical divides and evaporite assemblages on Mars. Earth and Planetary Science Letters 241, 21-31.

Tosca, N.J., McLennan, S.M., Lindsley, D.H. and Schoonen, M.A.A., 2004. Acid-sulfate weathering of synthetic Martian basalt: The acid fog model revisited

.Journal of Geophysical Research 109.

Vance, S., Harnmeijer, J., Kimura, J., Hussmann, H., deMartin, B. and Brown, J., 2007. Hydrothermal systems in small ocean planets. Astrobiology 7, 987-1005.

Wanke, H., Bruckner, J., Dreibus, G., Rieder, R. and Ryabchikov, I., 2001. Chemical composition of rocks and soils at the Pathfinder site. Space Sci. Rev 96, 317-330.

Wiedemann, H. and Smykatz-Kloss, W., 1981. Thermal studies of thenardite. Thermochimica Acta 50, 17-29.

Wiens, R.C., Burnett, D.S., Calaway, W.F., Hansen, C.S., Lykke, K.R. and Pellin, M.J., 1997. Sputtering products of sodium sulfate: Implications for Io's surface adn for sodium-bearing molecules in the Io torus. Icarus 128(2), 386-397.

Wilson, J. and Schneider, N., 1994. Io's fast sodium: implications for molecular and atomic atmospheric escape. Icarus 111, 31-44.

Wright, I., Grady, M. and Pillinger, C., 1989. Organic materials in a martian meteorite. Nature 340, 220-222.

Wyrick, D., Ferrill, D., Morris, A., Colton, S. and Sims, D., 2004. Distribution, morphology, and origins of martian pit crater chains. Journal of Geophysical Research 109, E06005.

Yan, B., Stoner, D.L., Kotler, J.M., Hinman, N.W. and Scott, J.R., 2007a. Detection of biosignatures by geomatrix-assisted laser desorption/ionization (GALDI) mass spectrometry. Geomicrobiology Journal 24, 379-385.

Yan, B., Stoner, D.L. and Scott, J.R., 2007b. Direct LD-FTMS detection of mineral-associated PAHs and their influence on the detection of other organics. Talanta 72, 634-641.

Yen, A., Gellert, R., Schroder, C., Morris, R.V., Bell III, J.F., Knudson, A.T., Clark, B.C., Ming, D.W., Crisp, J.A., Arvidson, R., Blaney, D., Bruckner, J., Christensen, P.R., Des Marais, D.J., de Souza, P.A., Economou, T., Ghosh, A., Hahn, B.C., Herkenhoff, K.E., Haskin, L., Hurowitz, J.A., Jolliff, B., Johnson, J., Klingelhoefer, G., Madsen, M.B., McLennan, S.M., McSween, H.Y., Richter, L., Rieder, R., Rodionov, D., Soderblom, L., Squyres, S.W., Tosca, N.J., Wang, A., Wyatt, M. and Zipfel, J., 2005. An integrated view of the chemistry and mineralogy of martian soils. Nature 436, 49-57.

Zhu, M., Xie, H., Guan, H. and Smith, R., 2006. Mineral and lithologic mapping of martian low albedo regions using OMEGA data, Lunar and Planetary Science XXXVII pp. 2173.pdf.

Zolotov, M.Y. and Shock, E.L., 2001. Composition and stability of salts on the surface of Europa and their oceanic origin. Journal of Geophysical Research 106(E12), 32815-32827.

Zolotov, M.Y. and Shock, E.L., 2005. Formation of jarosite-bearing deposits through aqueous oxidation of pyrite at Meridiani Planum, Mars. Geophysical Research Letters 32(21).

CHAPTER 2: EXPLORING BIOSIGNATURES ASSOCIATED WITH THENARDITE BY GEOMATRIX-ASSISTED LASER DESORPTION/IONIZATION FOURIER TRANSFORM ION CYCLOTRON RESONANCE MASS SPECTROMETRY (GALDI-FTICR-MS)

C. Doc Richardson[1], Nancy W. Hinman[1], Timothy R. McJunkin[2a], J. Michelle Kotler[1], and Jill R. Scott[2b]

[1]Geosciences Department, University of Montana, Missoula, MT 59812
[2a]Industrial Technology and [2b]Chemical Sciences, Idaho National Laboratory, Idaho Falls, ID 83415

Short title: BIOSIGNATURES IN THENARDITE BY GALDI-FTICR-MS

2.1 ABSTRACT

Geomatrix-assisted laser desorption/ionization (GALDI) in conjunction with a Fourier transform ion cyclotron resonance mass spectrometer (FTICR-MS) has been employed to determine how effectively bio/organic molecules associated with the mineral thenardite (Na_2SO_4) can be detected. GALDI is based on the ability of the mineral host to assist desorption and ionization of bio/organic molecules without additional sample preparation. When glycine was mixed with thenardite, glycine was deprotonated to produce $C_2H_4NO_2^-$ at m/z 74.025. The combination of stearic acid with thenardite produced a complex cluster ion at m/z 390.258 in the negative mode, which was assigned a composition of $C_{18}H_{39}O_7Na^-$. A natural sample of thenardite from Searles Lake in California also produced a peak at m/z 390.260. The bio/organic signatures in both the laboratory-based and natural samples were heterogeneously dispersed as revealed by chemical imaging. The detection limits for the stearic acid and thenardite combination were estimated to be 3 parts per trillion or ~7 zeptomoles (10^{-21}) per laser spot. Attempts to improve the signal-to-noise ratio by co-adding FTICR-MS data predetermined to

contain the biosignatures of interest revealed problems due to a lack of phase coherence between data sets.

Key words: glycine, stearic acid, geomatrix, evaporite, GALDI, laser desorption, mass spectrometry, FTICR-MS.

2.2. INTRODUCTION

Laser desorption mass spectrometry (LDMS) has been suggested as a method for searching for signs of life for both terrestrial and extraterrestrial geological samples because it should not require sample preparation as do many other methods under consideration for detecting bio/organic compounds (Botta and Bada, 2002; Kujawinski et al., 2002; Navarro-Gonzalez et al., 2006; Rodier et al., 2001). In addition, it is also possible to simultaneously obtain both mineral and bio/organic signatures from the same analysis (Yan et al., 2007b). Most of the initial research using LDMS to detect organic compounds associated with geological matrices has been on samples, such as meteorites (Elsila et al., 2004; Kovalenko et al., 1992), that contain polycyclic aromatic hydrocarbons (PAHs) (Bezabeh et al., 1997; Dale et al., 1994; Hankin and John, 1999; Rodgers et al., 2000; Zimmermann et al., 2000). However, PAHs appear to ionize well with LDMS when associated with any mineral because they can self-ionize and even assist the ionization of other bio/organic compounds (Macha et al., 2000; Vermillion-Salsbury and Hercules, 2002; Yan et al., 2007b). Most other bio/organic compounds require some assistance for desorption and ionization processes to produce ions that can be observed by the mass spectrometer (Karas and Hillenkamp, 1988; Stump et al., 2002; Tanaka et al., 1988). Our research focuses on the ability of minerals to perform this

desorption/ionization assistance, a method referred to as geomatrix-assisted laser desorption/ionization (GALDI) (Yan et al., 2007b).

Previously, GALDI in conjunction with a laser desorption Fourier transform ion cyclotron resonance mass spectrometer (FTICR-MS) was investigated using halite (NaCl) and hematite (Fe_2O_3) with the amino acids histidine, threonine, and cysteine as well as the small cyclical protein gramicidin S (Yan et al., 2007b). In general, halite samples produced the expected cation-attached bio/organic ions (i.e., $[M+Na]^+$, where M is the molecular formula). The laboratory-based samples were prepared by two different methods: 1) application of a solution of the bio/organic compound to the geomatrix surface and 2) physically mixing the dry bio/organic compound with the geomatrix. The surface applied sample preparation used by Yan et al. (2007a) is similar to surface-assisted laser desorption/ionization (SALDI) (Chen et al., 2008; Kim and Kang, 2000; Speir and Amster, 1992; Wu et al., 2007), while the physically mixed sample preparation is analogous to matrix-assisted laser desorption/ionization (MALDI) (Karas and Hillenkamp, 1988b; Stump et al., 2002; Tanaka et al., 1988). Yan et al. (2007a) reported that the physically mixed samples tended to yield mass spectra with less fragmentation and better signal-to-noise ratios than those samples that were applied to the surface. This observation was attributed to bio/organic molecules being surrounded by an excess number of geomatrix particles in the physically mixed samples. Thus, the excess geomatrix particles absorbed most of the laser power and protect the bio/organic molecules from fragmentation. In MALDI and SALDI, the matrix or surface substrate are typically chosen because they absorb efficiently at the laser wavelength (Allwood et al., 1997). For GALDI, Yan et al. (2007a) used a laser wavelength of 355 nm for all of

the mineral samples, including the sodium salt NaCl (halite) that only absorbs strongly in the deep ultraviolet (~245 nm) (Müller, 1927). Thus, the sodium salt/laser interaction most likely involved multiphoton interactions. While the mechanism(s) for laser-induced desorption of alkali salts has been investigated (Fernandez-Lima et al., 2008), the process is not thoroughly understood. Yan et al. (2007a) speculated that the ionization efficiency for the physically mixed samples was increased relative to the surface-applied samples because more geomatrix particles were desorbed per laser shot providing a greater chance for the cationization of the analytes. In the case of hematite, no bio/organic signatures were observed with either sample preparation. There are few reports of cationization of organic compounds by iron using LDMS and results are generally poor compared to cationization by alkali metals (Budimir et al., 2007; Speir et al., 1993; Yalcin et al., 2002). Iron cationization has only been observed successfully using GALDI for the siderophore desferrioxamine B (Scott et al., 2007).

Jarosite as a geomatrix for GALDI has also been studied because the jarosite group minerals have been discovered on the martian surface by the Mars Exploration Rover Opportunity (Kotler et al., 2008a). Natural samples from 7 locations around the world were analyzed by GALDI-FTICR-MS. Organic matter was detected in several of the jarosite samples. One of the biosignature ions ($C_{11}H_{19}O_2N_2S_2^+$) from the natural jarosites was attributed to a complex cluster ion formed from interaction of jarosite with glycine. While the mass-to-charge ratio (m/z) for the biosignature peak was 275.087, which is significantly larger than the monoisotopic molecular weight of glycine (75.032 u), a systematic study revealed that the same peak was observed in spectra from combinations of glycine with synthetic ammonium and potassium jarosites as well as

Na_2SO_4 and K_2SO_4 in the positive mode. Therefore, the complex cluster ion formation was attributed to the presence of sulfur as sulfate. According to Kotler et al. (2008), the mechanism for the formation of the complex cluster ion is not currently known, but could occur either in the initial laser desorption/ablation plume or latter in the gas phase.

In this article, we extend the use of GALDI-FTICR-MS for analysis of bio/organic compounds associated with the mineral thenardite (Na_2SO_4). Thenardite is one of several sulfate minerals formed in non-marine environments, such as evaporitic salt flats (sabkhas, playas), fumarolic exhalations, and in the dehydration of mirabilite ($Na_2SO_4 \cdot 10H_2O$) (Wiedemann and Smykatz-Kloss, 1981). Thenardite has also been suggested to be a constituent of the martian regolith based on chemical/mineralogical modeling (Tosca and McLennan, 2006)and recent spectroscopy data from the Mars *Express* Orbiter (Zhu et al., 2006b). The existence of thenardite and other sulfate minerals on Mars indicates the past existence of water on the planet. Results of interactions of thenardite with glycine and stearic acid are used to illustrate two types of GALDI ionization mechanisms: proton abstraction and complex cluster ion formation. Preliminary results from a natural sample from Searles Lake in California are also presented and compared to the laboratory-based samples. In addition, the stearic acid and thenardite combination is used to demonstrate issues related to sample heterogeneity and detection limits, including attempts to increase the signal-to-noise ratio (S/N) by signal averaging.

2.3. EXPERIMENTAL

2.3.1. Materials

Anhydrous Na_2SO_4 (thenardite) was purchased from Fischer Scientific (Pittsburgh, PA), which contained≤0.02% chloride. Glycine, palmitic acid, and arachidic acid were

purchased from Sigma-Aldrich (St. Louis, MO), while stearic acid was obtained from Fischer Scientific (Pittsburgh, PA). All chemicals were used as received.

2.3.2. Laboratory-based Sample Preparation

Physical mixtures of thenardite with either glycine or stearic acid were prepared based on procedure (Yan et al., 2007b). Approximately 1×10^{-4} mole (0.0075 g) of glycine was added to 10 g of thenardite (Na_2SO_4) in a glass vial. The sample was then mixed for 5 min at 70 Hz using a vortex mixer (Model 231, Fisher Scientific, Pittsburgh, PA) with two 4.5 mm zinc-plated steel ball bearings (Premium Grade BBs, Daisy Outdoor Products, Rogers, AR) to produce a relatively homogeneous 1 μM (~0.8 ppm) sample. The palmitic acid, stearic acid, and arachidic acid samples were produced in a manner similar to glycine. For example, 0.028 g of stearic acid was added to 10 g of thenardite. The sample was then mixed in a glass vial for 5 min at 70 Hz using a vortex mixer with two ball bearings to produce a 1 μM sample corresponding to a bulk concentration of ~3 ppm. Lower concentrations of stearic acid with thenardite were made by dry serial dilutions with incremental steps of 10^{-3} molar, resulting in bulk sample concentrations of stearic acid down to 1 pM or 3 ppt. Higher concentrations of stearic acid were made in a similar manner starting with larger amounts of stearic acid. Vortex mixing occurred between all dilution steps to facilitate homogenization of the samples. Because Yan et al. (2007a) reported that the organic analyte, gramicidin S, appeared to cling to surface of the vial after vortex mixing, the vials were visually inspected after transferring the sample. No obvious organic material appeared on the surfaces of the vials or ball bearings. To prevent cross contamination, new ball bearings and vials were used for each sample. Samples were then pressed into pellets using a 0.5-

inch Beckman dye with a Carver Laboratory Press (Menomonee Falls, WI) at an approximate pressure of 3.5 x 10^{-7} Pa prior to mounting on copper discs using epoxy (Devcon 5 minute epoxy, Danvers, MA). Epoxy was allowed to dry for almost 5 min before the pressed pellet was applied to prevent the sample from absorbing any epoxy. The pellet press dye was cleaned with distilled water and ethanol between samples.

2.3.3. Natural Sample

Natural thenardite was obtained from Searles Lake by Valley Mineral Co. (Trona, CA). The natural sample was ground into a powder using a corundum mortar and pestle to help homogenize the sample.

2.3.4. FTICR-MS Instrumentation and Parameters

Mass spectra were obtained using a laboratory-built laser desorption Fourier-transform mass spectrometer (Scott and Tremblay, 2002) equipped with a 7 T Oxford (Oxford, England) superconducting magnet, a 2-inch cubic cell and an Odyssey control and data acquisition computer system (Finnigan, FT/MS, Bremen, Germany). A Nd:YAG laser (Continuum, Santa Clara, Ca) operating at 355 nm with a 6 ns pulse width was used for desorption/ionization, with a laser irradiance of 1 x 10^{8} W/cm^{2} for a ~10 μm diameter. While the term desorption is use, it should be noted that the laser parameters may be more consistent with the ablation regime (Aubriet et al., 2005; Haglund, 1996). Using these settings, the imaging LD-FTICR-MS has high mass accuracy (mass error of ± 0.003 Da), resolution (approximately >10,000), high sensitivity (≤400 ions for peaks with signal-to-noise ratio ~3 (Limbach et al., 1993; Marshall et al., 1998)), and high spatial resolution (~6 μm) (Yan et al., 2007b). Samples were located ~0.5 cm from the front electrostatic plate in the ionization cell. During ionization, voltage potential

between the front and back plates was maintained at 0 V. After ionization, a trapping potential of either –2 V was applied to both trap plates. The applied trap potentials were then maintained throughout the experiment until the quench event. A delay of 0.5 s was allowed prior to chirp excitation over the range of 50 Hz to 4 MHz (corresponding m/z 10^5 and 26.9, respectively) with a sweep rate of 3600 Hz/μs. Each spectrum was collected from a single laser shot having a diameter of 10 μm and an approximate depth of 0.2 μm. Ions were detected in direct mode using 64 K data points. After acquisition, data were baseline corrected, Hamming apodized, zero filled, and Fourier transformed. All spectra are negative mode spectra unless specified otherwise. Pressure during analysis was $\leq 5 \times 10^{-9}$ Torr.

2.3.5. Chemical Imaging

The chemical map was made taking advantage of the automated laser scanning mechanism associated with the laboratory-based FTICR-MS system (McJunkin et al., 2002a; Scott and Tremblay, 2002; Scott et al., 2006). The mapping area covered a 2 mm × 2 mm area. The center-to-center distance between laser desorption spots was set to 100 μm for a closest packed pattern. The Fuzzy Logic Inference Engine (FLIE) was used to automate the analysis (McJunkin and Scott, 2006; Scott et al., 2003; Yan et al., 2005; Yan et al., 2006). FLIE was modified to allow the program to classify peaks based on the signal-to-noise ratio.

2.4. RESULT AND DISCUSSION

Two different bio/organic compounds were chosen to mix with thenardite for GALDI-FTICR-MS investigation. The first bio/organic compound chosen was the amino acid glycine ($C_2H_5NO_2$). Degradation of amino acids on Mars is expected to be less than

on Earth (Aubrey et al., 2006). The second biomolecule chosen was the lipid stearic acid ($C_{18}H_{36}O_2$), which is a straight chain fatty acid that forms portions of cell membranes of eukaryotes and prokaryotes (Bowden and Parnell, 2007). Although straight chain fatty acids can also be synthesized abiotically via Fischer-Tropsch Process, the probability that a large C_{18} chain produced in this manner is extremely low (Parnell et al., 2007b). Both glycine and stearic acid are considered very stable relative to other bio/organic compounds in the martian environment and are ubiquitous in terrestrial life.

2.4.1. Glycine and Thenardite

Previous research has focused predominantly on positive bio/organic ions generated by GALDI from various minerals. In these studies, ionization of glycine occurred either as simple cation attachment to form species such as $C_2H_5NO_2Na^+$ with halite (Yan et al., 2007b) or complex cluster ion formation to form species such as $C_{11}H_{19}O_2N_2S_2^+$ with jarosite (Kotler et al., 2008). The focus of the current study is on negative ions produced from thenardite with and without glycine present (Figure 2.1).

Figure 2.1A has a host of high mass peaks that might suggest that thenardite interacts with glycine to produce a complex cluster ion similar to that observed with glycine and jarosite (Kotler et al., 2008). However, Figure 2.1B shows a typical negative ion spectrum from thenardite alone that is almost identical to that in Figure 2.1A. As is also true for positive ion spectra of simple sulfate salts (Kotler et al., 2008a), there are a number of inorganic peaks produced that include several high mass peaks, such as those at m/z 184.97, 350.91, 516.82, and 682.71, that are present in negative mode spectra of thenardite with and without glycine present (Figure 2.1). The high m/z peaks observed are different from those observed by (Van Vaeck et al., 1998a) for Na_2SO_4 using a laser

wavelength of 266 nm. In addition to the difference in laser wavelength, there differences in the FTICR-MS parameters used to obtain the spectra that may be important because Van Vaeck et al. (1998) did demonstrate that the production of higher m/z cluster ions is dependent on gas-phase reactions. There may also be differences in sample preparation that could influence ions observed.

Besides the fact that the thenardite sample used to create Figure 2.1B is from a purely inorganic sample, these high m/z peaks can also be easily identified as inorganic in nature based on their mass defects (i.e., the number after the decimal point). Most common inorganic elements have mass defects between 0.90 to 0.99 u (NIST; 1984) with exceptions being low atomic weight elements such as Li and Be and high atomic weight elements $>^{211}$Rn. Common non-hydrogen elements associated with bio/organic compounds have mass defects closer to 0.000 u (e.g., ^{12}C at 12.000 u, ^{16}O at 15.995 u, ^{14}N at 14.003 u). Hydrogen has an elemental mass of 1.008 u and tends to dominate the mass defect in bio/organic molecules because there are usually twice as many hydrogen atoms as other elements. However, one caveat is that inorganic cluster ions that are highly hydrated (Gianotto et al., 2004) can have sufficient H atoms such that the mass defects are similar to organic compounds. Hence, it is necessary to have sufficient mass accuracy and resolution to distinguish between peaks related to inorganic and organic cluster ions.

While the negative mode spectrum of thenardite with glycine (Figure 2.1A) appeared very similar to that of thenardite alone (Figure 2.1B), closer inspection revealed that there was indeed a peak distinct for deprotonated glycine ($C_2H_4NO_2^-$) at m/z 74.025 (Figure 2.2A) that was not present in spectra from thenardite alone (Figure 2.2B). The

other peaks between m/z 67 and 77 were related to isotopes of Cl_2^- at m/z 69.938 ($^{35}Cl_2^-$), m/z 71.935 ($^{35}Cl^{37}Cl^-$), m/z 73.932 ($^{37}Cl_2^-$). Even if the concentration of chloride in a sample is small (≤0.02% chloride in the thenardite), chloride-related peaks may be

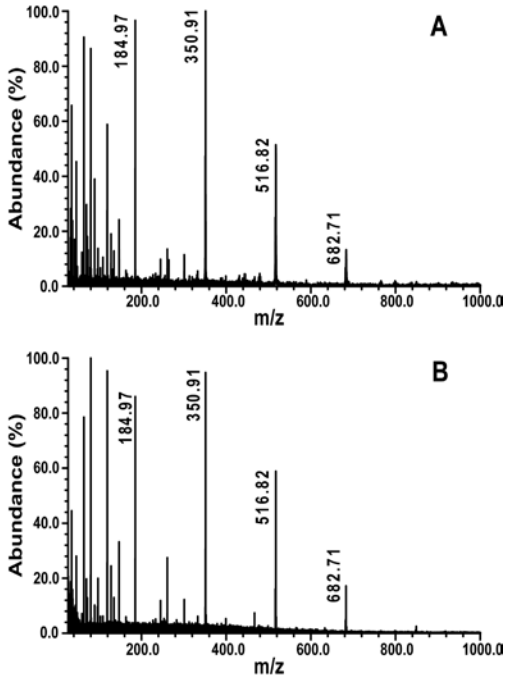

Figure 2.1. Negative ion GALDI-FTICR-MS spectra of thenardite (A) with and (B) without glycine

abundant in a mass spectrum because halogens are easily ionized. Thus, the abundance of ions in a LDMS spectrum is not only dependent on the amount of the substance in the sample, but also by how efficiently it is desorbed and ionized (Yan et al., 2006). In addition, less abundant HCl_2^- isotope peaks at m/z 70.946 and m/z 72.943 are also observed in the combined glycine and thenardite sample (Figure 2.2A).

Analysis of a pellet of glycine alone did not produce any peaks in positive or negative mode, which is consistent with the reports by Yan et al. (2007a) and Kotler et al. (2008) for the same experimental conditions. Therefore, it is possible that one or more inorganic cluster ions or neutrals may have a gas-phase basicity (i.e., proton affinity)

(Raczyńska et al., 2007) sufficient to abstract a proton from glycine either in the desorption plume or in the gas phase. However, the exact mechanism for the formation

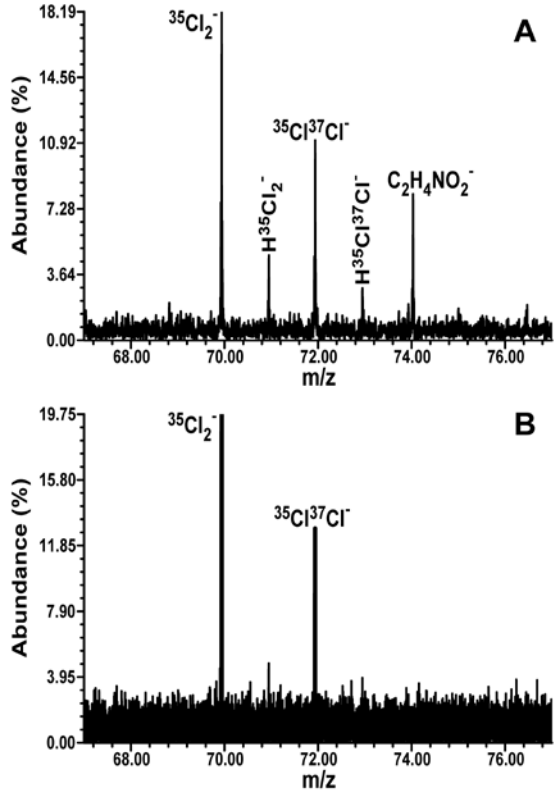

Figure 2.2. Expanded m/z 67–77 region for negative ion GALDI-FTICR-MS spectra of (A) glycine mixed with thenardite and (B) thenardite alone.

of deprotonated glycine in thenardite is not yet known. Previous combination of glycine with other, similar minerals did not produce a deprotonated glycine peak as summarized in Table 2.1.

The variation in ionization for the different samples may be due to subtle differences in the geomatrices and how they interact with the laser light. It is likely that there multiple reactions **p**ossible in the laser desorption plume that compete with each other, especially because the experimental condition might actually be in the laser ablation regime where rearrangements are expected (Aubriet et al. 2005). The closest two

Table 2.1. List of observed m/z peaks for various combinations of bio/organic compounds and minerals.

Sample	Na^+ attached peak (m/z)	Deprotonated peak (m/z)	Complex cluster ion peak (m/z)	Ref.
Glycine + NaCl	98.02			Yan et al. 2007
Glycine +Jarosite			259.11, 275.09	Kotler et al. 2008
Glycine + Na_2SO_4			259.11, 275.09	Kotler et al. 2008
Glycine + Thenardite		74.02		This study
Palmitic acid + Thenardite	279.23	255.23		This study
Stearic Acid + Thenardite			390.26	This study
Arachidic Acid + Thenardite			393.32, 421.32	This study

experments were the glycine with high purity Na_2SO_4 by Kotler et al. (2008) and the glycine with thenardite in this study. In the Kotler et al. (2008), glycine with Na_2SO_4 producd as complex cluster ion peak at m/z 275 that was consistent with the glycine and jarosite sample. The primary difference between these two experiments was the presence of chloride in the thenardite. Chloride was obviously present in the glycine and NaCl (halite) samples analyzed by Yan et al. (2007a and b); however, these samples only produce Na^+-attached ions at m/z 74.02 in the positive mode and not deprotonated ions in the negative mode. Interestingly, in negative ion mode the primary chloride species observed by Yan et al. (2007a) were elemental only (i.e., $^{35}Cl^-$ and $^{37}Cl^-$), whereas the current thenardite produced Cl_2^- isotope peaks. Therefore, ion formation is dependent on the exact constitution of the geomatrix because there are multiple competitive reactions that can affect which bio/organic signature is observed for a particular compound in a given geomatrix. Natural thenardite is an evaporate mineral that is likely to also contain chloride because it may be mixed with other evaporate minerals (e.g., halite).

2.4.2. Natural Thenardite—Searles Lake

A negative mode spectrum from a natural thenardite sample acquired from Searles Lake in California is shown in Figure 2.3. Searles Lake is an evaporitic basin related to a succession of Pleistocene lakes located in southeastern California. Lacustrine assemblages consist of halite, bedded thenardite and mud layers, capped by a massive halite layer deposited during the last lake event (Li et al., 1996). Because of the halite (NaCl) present, it is not surprising that a set of peaks for Cl_2^- isotopes was observed in spectra from Searles Lake (Figure 2.3), similar to that observed in Figure 2.1. However, to date, no definitive deprotonated glycine peaks have been observed in any of the spectra acquired from this natural sample. However, some spectra do have small peaks with S/N 2 to 3 at the expected m/z 74.025. Approximately 30% of the negative ion spectra acquired from a Searles Lake sample did have a peak at m/z 390.260, which has a mass defect suggestive of a bio/organic compound.

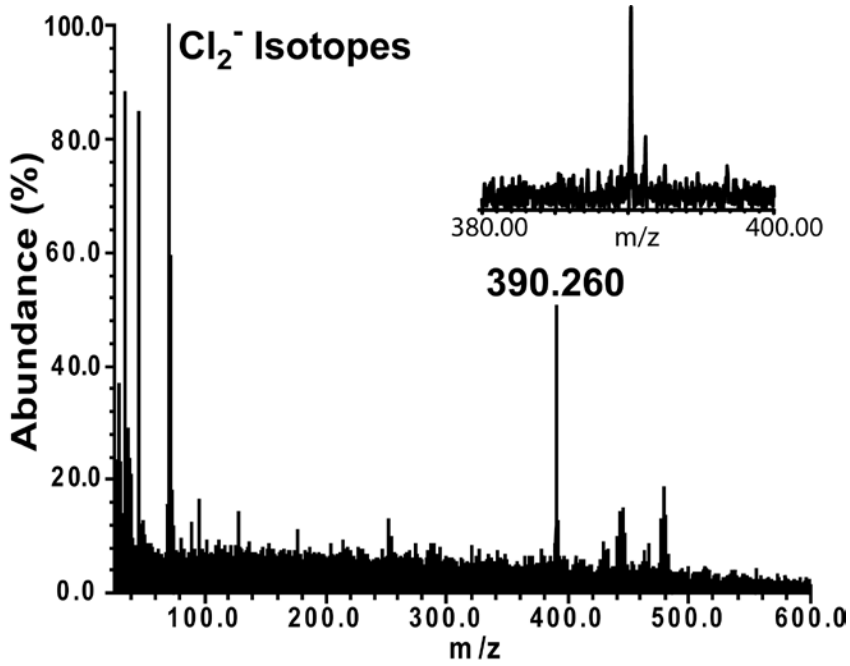

Figure 2.3. GALDI-FTICR-MS spectrum of natural thenardite sample from Searles Lake in California. Inset shows expanded view of m/z 380–400.

2.4.3. Stearic Acid and Thenardite

Because lipids are key components of cell membranes, we investigated the types of biosignatures that common lipids can be produced using different geomatrices. The preliminary results are summarized in Table 2.1. Similar to the case of glycine, the different bio/organic-mineral combinations produced a variety of results, which are probably caused by competition between various gas-phase reactions. We chose to focus on stearic acid because it produced a similar peak to that observed in the Searles Lake sample and only appeared to produce one type of ion.

Under the given experimental conditions, the pellet of stearic acid alone did not produce any peaks in the negative mode. Cation spectra of stearic acid did show peaks for low mass fragment ions (<130 u). This is in contrast the to previous results reported using 337 nm laser desorption/ionization with a time-of-flight mass analyzer that showed deprotonated stearic acid and fragments ions in the negative mode (Soltzberg and Patel, 2004). Besides the difference in laser wavelength and irradiance, Soltzberg and Patel (2004) also used a very thin, transparent film of sample over the stainless steel target. Thus, their sample preparation may have lead to a SALDI-type of ionization mechanism.

When stearic acid was mixed with thenardite, a distinct peak at m/z 390.258 was produced in the negative mode that was not present in spectra of the thenardite by itself (Figure 2.4). A range of bulk stearic acid concentrations were analyzed to determine if any significant loss of the stearic acid had occurred during the sample preparation and to investigate the limit of detection. The spectra actually improved as the concentration of

stearic acid decreased compared to thenardite, which suggests that there was no significant loss of stearic acid during the sample preparation.

Interestingly, similar peaks at m/z 390 were observed in spectra from the natural sample from Searles Lake in California (Figure 2.3). This biosignature peak is not from simple proton abstraction as was observed for glycine. The peak at m/z 390 appears to be an example of complex cluster ion formation similar to that reported for glycine with jarosite (Kotler et al., 2008a). Using the procedure outlined in Kotler et al (2008), the most likely composition for the peak is $C_{18}H_{39}O_7Na^-$ (m/z 390.260). This appears to be a complex cluster ion formed with one stearic acid molecule and adducts from the mineral matrix. Complex reactions often occur in the laser desorption (or ablation) plume or in the gas phase, resulting in ions larger than the expected molecular ion due to formation of adducts (Karas and Kruger, 2003) from addition of matrix (Knochenmuss et al., 1996a) and/or analyte species (Budimir et al., 2007; Ham et al., 2003b). Additionally, it is not uncommon for an alkali metal atom to be observed in both positive and negative singly-charged ions (Budimir et al., 2007; Tomlinson et al., 1999; Yan et al., 2007b), presumably because one alkali metal atom displaces a H atom, especially in carboxylic acid groups. Although the cluster ion has 18 carbon atoms the same as intact stearic acid, it would be presumptuous to assume that this cluster ion is formed by a single stearic acid molecule and mineral adducts. It is possible that that this ion is formed by a combination of stearic acid fragments along with some mineral moieties. The mechanism for the formation of the complex ions is still unknown because experiments to elucidate the mechanism have been hindered by the heterogeneous nature of the samples.

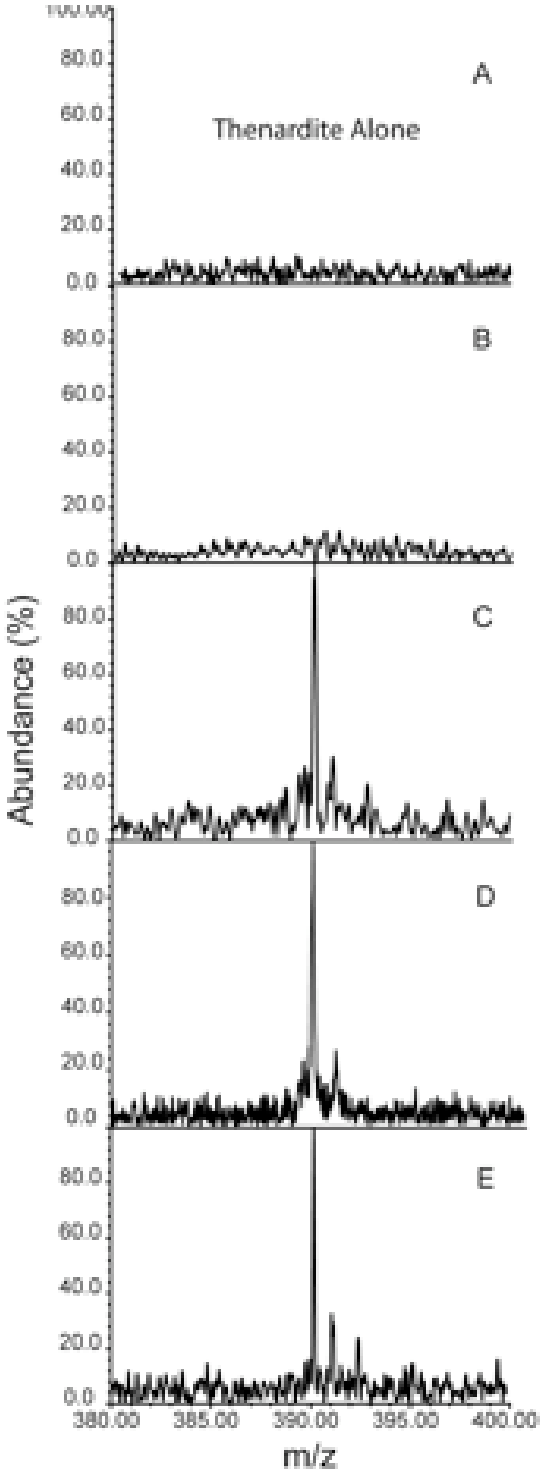

Figure 2.4. Expanded m/z 380–400 region of GALDI-FTICR-MS spectra for (A) thenardite alone and stearic acid mixed with thenardite for bulk stearic acid concentrations of (B) 3‰, (C) 3 ppm, (D) 3 ppb, and (E) 3 ppt.

2.4.4. Heterogeneity and Detection Limits

The laboratory-based stearic acid and thenardite combination was used to investigate issues of heterogeneity and limits of detection. A series of dry serial dilutions were used to produce a final sample equivalent to 2.8×10^{-12} g stearic acid to 1 kg of mineral for a 3 parts per trillion bulk sample that would translate into 6.8 zeptomoles (6.8×10^{-21} moles or 4095 molecules) per laser spot, based on the volume of the laser desorption spot, assuming a homogeneous sample. Even though the dry samples were mixed using a vortex with ball bearing method similar to a dry MALDI preparation (Hanton and Parees, 2005; Trimpin et al., 2001), the samples were not homogeneous as shown in the map in Figure 2.5. While ~40% of spectra contained a peak at m/z 390 with S/N ≥3, only ~6% of all spectra had a peak at m/z 390 with S/N >10.

Initially, it may appear obvious to conclude that the amount of analyte per laser spot is greater than that estimated based on the bulk values and would be closer to ~20 zeptomoles taking into account the percent of spots that produced a positive signal. However, we have observed that as the relative concentration of the organic compound decreases as shown in Figure 2.4 for stearic acid in thenardite, the S/N in the mass spectra increases. In addition, the number of spectra per sample with peaks indicative of the bio/organic compounds also increases. The number of positive spectra for the series shown in Figure 2.4B-E ranged from 0%, ~10%, ~15%, ~35%, and ~40% for bulk stearic acid concentrations of 3 ‰, 3 ppm, 3 ppb, and 3 ppt, respectively. While it is not intuitive that this should be the case, it is consistent with observations for MALDI where the signal improves as the molar ratio of matrix-to-analyte increases. Yao et al. (Yao et al., 1998b) showed that samples that produce no analyte signal with low amounts of matrix

can produce decent signals as the concentration of matrix is drastically increased. Thus, the spectra with higher S/N may actually have fewer bio/organic molecules (i.e., analyte) than those with low or no signal. The signal intensity increases presumably because of more efficient ionization as the bio/organic molecules are more completely surrounded by the mineral matrix.

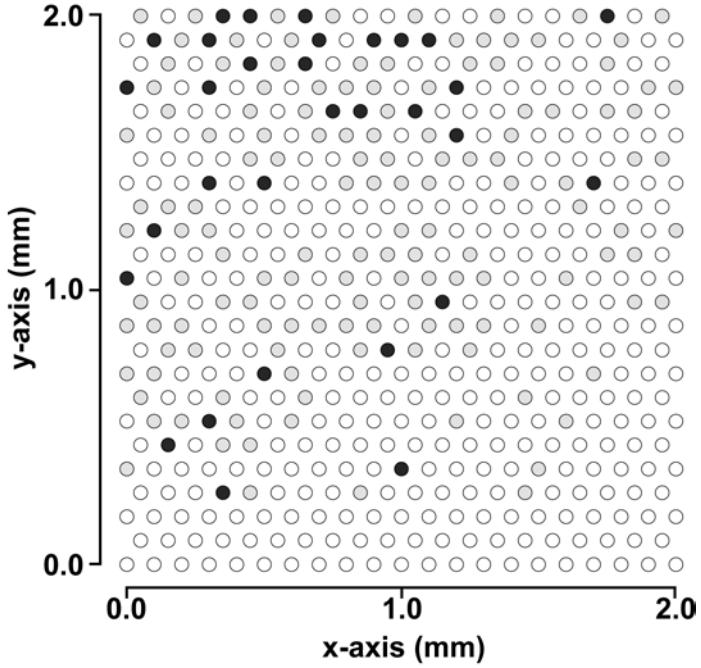

Figure 2.5. Two-dimensional map showing heterogeneity of distribution of stearic acid biosignature in thenardite. Gray spots have m/z 390 peaks with S/N of 3 to 10 and black spots have S/N 10 or greater. The representation of the spot size is not to scale.

2.4.5. Signal-to-Noise Ratio and Co-addition of Spectra

Attempts to increase the signal-to-noise ratio were made in order to improve observation of minor peaks, such as the potential $C_2H_4NO_2^-$ at m/z 74 in the Searles Lake samples. In addition, observation of minor isotopes is necessary to make unequivocal composition assignments for the biosignatures (Kotler et al., 2008a). A common practice in mass spectrometry to increase the S/N is to signal average or co-add spectra. For FTICR-MS, the raw data that is based on measuring the ion cyclotron frequencies is

actually co-added (Kujawinski et al., 2002; Pastor and Wilkins, 1997; Scott et al., 1997). As many as 18,000 spectra from homogeneous samples have been co-added to reveal peaks of interest (Kujawinski et al., 2002). The commercial software associated with the FTICR-MS does allow for co-addition of raw data; therefore, it would appear appropriate to co-add spectra identified to have peaks of interest to increase to ability to observe peaks from lower abundant ion types, such as minor isotopes, that can be lost in the noise. Signal averaging spectra that do not have the peak(s) of interest is actually deleterious and will actually average the desired signal(s) into the noise (Lyons, 2004). Therefore, for heterogeneous samples, predetermining which data from the single laser desorption spots have signal(s) of interest is a necessary prelude to co-addition or signal averaging.

However, the commercial FTICR-MS software does not take into account the phase of the FTICR-MS frequency data. If the frequencies of spectra that are added together are coherent (i.e., perfectly in phase), then the resulting spectrum should have peaks with abundances that are the sum of the co-added spectra. However, if the signals of the FTICR-MS data added together are not in phase, then the resulting amplitude will be less than the sum of the amplitudes as illustrated in Figure 2.6. Figure 2.6 was created by co-adding two of the spectra from the map in Figure 2.5 that had a peak at m/z 390. The resultant spectrum (Figure 2.6C) from the co-addition has a significantly poorer S/N ratio than the single shot spectrum in Figure 2.6B. The general peak quality (e.g., shape and resolution) in the spectrum (Figure 2.6C) resulting from co-addition is degraded compared to either individual spectra (Figures 2.6A and 2.6B). While other co-added combinations did not produce results as poor as Figure 2.6C, none of them produced

results with significant improvements in S/N compared to individual spectra from single laser shots. Hence, a scheme to determine and account for the phase difference to allow for coherent co-addition of FTICR-MS data is currently being developed.

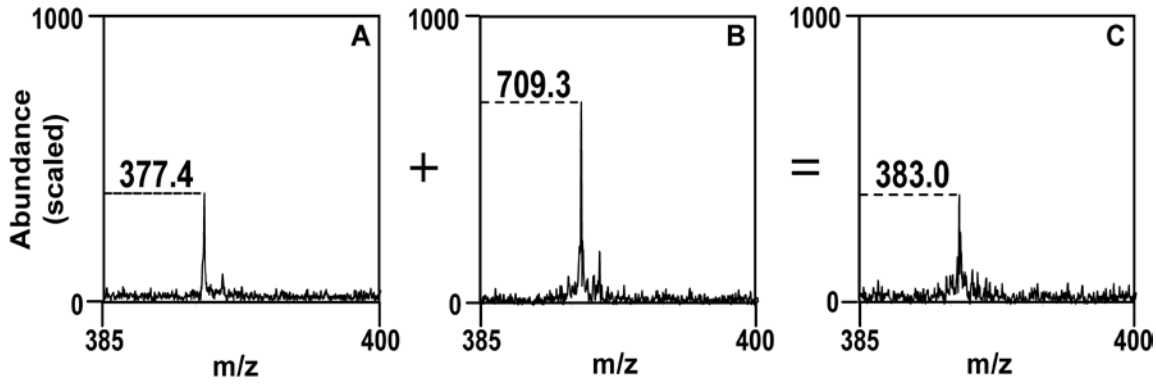

Figure 2.6. Illustration of potential negative effect of co-adding GALDI-FTICR-MS spectra. Raw data from single shot spectra (A and B) were co-added to produce (C) resultant spectrum.

2.5. CONCLUSIONS

As a geomatrix for GALDI, thenardite is capable of ionizing bio/organic compounds either by deprotonation or complex cluster ion formation in the negative mode. In the case of deprotonation of glycine, gas-phase neutral or ionic inorganic species from the thenardite geomatrix are suspected to have basicities appropriate for abstracting a proton from glycine. The complex cluster ion formed with stearic acid is likely due to adducts from the thenardite matrix and is similar to peaks observed in spectra from natural thenardite samples from Searles Lake. Experiments to elucidate the reaction mechanisms responsible for these ionization schemes have been hindered by the heterogeneity of the sample preparation.

Detection limit for GALDI of stearic acid in thenardite was estimated to be at least 3 parts per trillion based on bulk concentration, which would translate into ~7 zeptomoles

per laser spot assuming a homogeneous sample. However, the heterogeneity of the sample leaves the actual detection limit in question, which is further complicated because the S/N tends to increase as the concentration of the biomolecules decreases relative to the mineral. Hence, less bio/organic molecules per sample tends to translate into more abundant biosignature peaks in the mass spectrum, which should be the case until the abundance begins to fall off as one approaches the limit of the number of ions the mass analyzer can detect (~400 for the current FTICR-MS instrument) or ultimately 1.66 yoctomoles (i.e., 1.66×10^{-24} moles or one molecule).

Because bio/organic molecules are heterogeneously dispersed in geological samples, signal averaging data to improve S/N is only a viable option if it is known that the biosignature of interest is present in all of the co-added spectra. However, co-adding the frequency-based FTICR-MS data is more complicated than generally acknowledged because commercial software does not take into account the phase of the frequency data. Therefore, co-adding data where the frequencies are not in phase can actually degrade spectral quality (i.e., S/N, peak shape, etc.).

In general, for simple ionization mechanisms (e.g., cationization and deprotonation), the mass accuracy obtainable with GALDI-FTICR-MS can allow the exact bio/organic molecule to be identified. When complex cluster ions are formed, the mass accuracy affordable by GALDI-FTICR-MS can be used to determine that the ion contains organic constituents. However, because the mechanisms and/or conditions that lead to the formation of complex cluster ions are not thoroughly understood at this time, the identification of the specific bio/organic compound involved in the complex cluster ion

requires laboratory experiments to determine expected fingerprints for different bio/organic-mineral combinations.

2.6. ACKNOWLEDGMENTS

The authors acknowledge support by the National Aeronautics and Space Agency (NASA) Exobiology Program (EXB03-0000-0054). CDR would also like to thank Inland Northwest Research Alliance (INRA) and Montana Space Grant Consortium for support. Research was performed at the Idaho National Laboratory under DOE/NE Idaho Operations Office Contract DE-AC07-05ID14517.

2.7. REFERENCES

Allwood, D.A., Dreyfus, R.W., Perera, I.K. and Dyer, P.E., 1997. Optical absorption of matrix compounds for laser-induced desorption and ionization (MALDI). Applied Surface Science, 110: 154-157.

Aubrey, A. et al., 2006. Sulfate minerals and organic compounds on Mars. Geology, 34(5): 357-360.

Aubriet, F., Carre, V. and Muller, J.F., 2005. Laser desorption and laser ablation Fourier transform mass spectrometry for the analysis of pollutants in complex matrices. Spectroscopy Europe, 17: 14-22.

Bezabeh, D.Z., Allen, T.M., McCauley, E.M., Kelly, P.B. and Jones, A.D., 1997. Negative ion laser desorption ionization time-of-flight mass spectrometry of nitrated polycyclic aromatic hydrocarbons. Journal of the American Society for Mass Spectrometry, 8(6): 630-636.

Botta, O. and Bada, J.L., 2002. Extraterrestrial organic compounds in meteorites. Surveys in Geophysics, 23(5): 411-467.

Bowden, S. and Parnell, J., 2007. Intracrystalline lipids within sulfates from the Haughton impact structure-Implications of survival of lipids on Mars. Icarus, 187: 422-429.

Budimir, N., Blais, J.C., Fournier, F. and Tabet, J.C., 2007. Desorption/ionization on porous silicon mass spectrometry (DIOS) of model cationized fatty acids. Journal of Mass Spectrometry, 42(1): 42-48.

Chen, Y., Chen, H., Aleksandrov, A. and Orlando, T., 2008. Roles of water, acidity, and surface morhology in surface-assisted laser desorption ionization of amino acids. Journal of Mass Spectrometry, C 112: 6953-6960.

Dale, M.J., Jones, A.C., Pollard, S.J.T. and Langridgesmith, P.R.R., 1994. Direct determination of polycyclic aromatic-hydrocarbons in environmental matrices using laser-desorption laser photoionization time-of-flight mass-spectrometry. Analyst, 119(4): 571-578.

Elsila, J.E., de Leon, N.P. and Zare, R.N., 2004. Factors affecting quantitative analysis in laser desorption/laser ionization mass spectrometry. Analytical Chemistry, 76(9): 2430-2437.

Fernandez-Lima, F.A., Ponciano, C.R. and da Silveira, E.F., 2008. UV laser-induced desorption mechanism analyzed through two-layer alkali halide samples. Journal of Mass Spectrometry, 43(5): 587-593.

Gianotto, A.K. et al., 2004. Hydration of alumina cluster anions in the gas phase. Journal of the American Chemical Society, 126(26): 8275-8283.

Haglund, R.F., 1996. Microscopic and mesoscopic aspects of laser-induced desorption and ablation. Applied Surface Science, 96-8: 1-13.

Ham, J.E., Durham, B. and Scott, J.R., 2003. Comparison of laser desorption and matrix-assisted laser desorption/ionization for ruthenium and osmium trisbipyridine complexes using Fourier transform mass spectrometry. Journal of the American Society for Mass Spectrometry, 14(4): 393-400.

Hankin, S.M. and John, P., 1999. Laser time-of flight mass analysis of PAHs on single diesel particulates. Analytical Chemistry, 71(6): 1100-1104.

Hanton, S.D. and Parees, D.M., 2005. Extending the solvent-free MALDI sample preparation method. Journal of the American Society for Mass Spectrometry, 16(1): 90-93.

Karas, M. and Hillenkamp, F., 1988. Laser desorption ionization of proteins with molecular masses exceeding 10000 Daltons. Analytical Chemistry, 60(20): 2299-2301.

Karas, M. and Kruger, R., 2003. Ion formation in MALDI: The cluster ionization mechanism. Chemical Reviews, 103(2): 427-439.

Kim, J. and Kang, W., 2000. Use of graphite plate for homogeneous sample preparation in matrix/surface-assisted laser desorption and ionization of polypropyleneglycol and polystyrene. Bulletin of the Korean Chemical Society, 21(4): 401-404.

Knochenmuss, R., Dubois, F., Dale, M.J. and Zenobi, R., 1996. The matrix suppression effect and ionization mechanisms in matrix-assisted laser desorption/ionization. Rapid Communications in Mass Spectrometry, 10(8): 871-877.

Kotler, J.M., Hinman, N.W., Yan, B., Stoner, D.L. and Scott, J.R., 2008. Glycine identification in natural jarosites using laser-desorption Fourier transform mass spectrometry: Implications for the search for life on Mars. Astrobiology: (in press).

Kovalenko, L.J. et al., 1992. Microscopic organic-analysis using 2-step laser mass-spectrometry - Application to meteoritic acid residues. Analytical Chemistry, 64(6): 682-690.

Kujawinski, E.B., Hatcher, P.G. and Freitas, M.A., 2002. High-resolution Fourier transform ion cyclotron resonance mass spectrometry of humic and fulvic acids: Improvements and comparisons. Analytical Chemistry, 74: 413-419.

Li, J., Lowenstein, T.K., Brown, C.B., Ku, T. and Luo, S., 1996. A 100 ka record of water tables and paleoclimates from salt cores, Death Valley, California. Palaeogeography, Palaeoclimatology, Palaeoecology, 123: 179-203.

Limbach, P.A., Grosshans, P.B. and Marshall, A.G., 1993. Experimental-determination of the number of trapped ions, detection limit, and dynamic-range in Fourier-transform ion-cyclotron resonance mass-spectrometry. Analytical Chemistry, 65(2): 135-140.

Lyons, R., 2004. Understanding Digital Signal Processing. Prentice Hall, Upper Saddle River, NJ.

Macha, S.F., Limbach, P.A. and Savickas, P.J., 2000. Application of nonpolar matrices for the analysis of low molecular weight nonpolar synthetic polymers by matrix-assisted laser desorption/ionization time-of-flight mass spectrometry. Journal of the American Society for Mass Spectrometry, 11(8): 731-737.

Marshall, A.G., Hendrickson, C.L. and Jackson, G.S., 1998. Fourier transform ion cyclotron resonance mass spectrometry: A primer. Mass Spectrometry Reviews, 17: 1-35.

McJunkin, T.R. and Scott, J.R., 2006. Fuzzy logic classification of imaging laser desorption Fourier transform mass spectrometry data. arXiv:cs.AI/0611085.

McJunkin, T.R., Tremblay, P.L. and Scott, J.R., 2002. Automation and control of an imaging internal laser desorption Fourier transform mass spectrometer (I^2LD-FTMS). Journal of the Association for Laboratory Automation, 7: 76-83.

Müller, L.A., 1927. Absorption spectra of the alkali halides in aqueous solutions and in vapors. Ann. Phys., 82: 39-66.

Navarro-Gonzalez, R. et al., 2006. The limitations on organic detection in Mars-like soils by thermal volatilization-gas chromatography-MS and their implications for the Viking results. Proceedings of the National Academy of Sciences of the United States of America, 103(44): 16089-16094.

Parnell, J. et al., 2007. Searching for life on Mars: Selection of molecular targets for ESA's Aurora ExoMars Mission. Astrobiology, 7(4): 578-604.

Pastor, S.J. and Wilkins, C.L., 1997. Analysis of hydrocarbon polymers by matrix-assisted laser desorption/ionization Fourier transform mass spectrometry. Journal of the American Society for Mass Spectrometry, 8(3): 225-233.

Raczyńska, E.D., Gal, J.F., Maria, P.C., Zientara, K. and Szelag, M., 2007. Application of FT-ICR-MS for the study of proton-transfer reactions involving biomolecules. Analytical and Bioanalytical Chemistry, 389(5): 1365-1380.

Rodgers, R.P., Lazar, A.C., Reilly, P.T.A., Whitten, W.B. and Ramsey, J.M., 2000. Direct determination of soil surface bound polycyclic aromatic hydrocarbons in petroleum-contaminated soils by real time aerosol mass spectrometry. Analytical Chemistry, 72(20): 5040-5046.

Rodier, C., Sternberg, R., Raulin, F. and Vidal-Madjar, C., 2001. Chemical derivatization of amino acids for in situ analysis of Martian samples by gas chromatography. Journal of Chromatography A, 915(1-2): 199-207.

Scott, J.R. et al., 2007. Searching for biosignatures as signs of life using GALDI-FTMS. Journal of the Idaho Academy of Science: (in press).

Scott, J.R., McJunkin, T.R. and Tremblay, P.L., 2003. Automated analysis of mass spectral data using fuzzy logic classification. Journal of the Association for Laboratory Automation (JALA), 8(2): 61-63.

Scott, J.R., Schürch, S., Moore, S. and Wilkins, C.L., 1997. Evaluation of MALDI-FTMS for analysis of peptide mixtures generated by ladder sequencing. International Journal of Mass Spectrometry and Ion Processes, 160(1-3): 291-302.

Scott, J.R. and Tremblay, P.L., 2002. Highly reproducible laser beam scanning device for an internal source laser desorption microprobe Fourier transform mass spectrometer. Review of Scientific Instruments, 73(3): 1108-1116.

Scott, J.R., Yan, B. and Stoner, D.L., 2006 Spatially correlated spectroscopic analysis of microbe-mineral interactions. Journal of Microbiological Methods 67: 381-384.

Soltzberg, L.J. and Patel, P., 2004. Small molecule matrix-assisted laser desorption/ionization time-of-flight mass spectrometry using a polymer matrix. Rapid Communications in Mass Spectrometry, 18(13): 1455-1458.

Speir, J.P. and Amster, I.J., 1992. Substrate-assisted laser desorption of neutral peptide molecules. Analytical Chemistry, 64(9): 1041-1045.

Speir, J.P., Gorman, G.S. and Amster, I.J., 1993. Fe^{+} chemical ionization of peptides. Journal Of The American Society For Mass Spectrometry, 4(2): 106-110.

Stump, M.J. et al., 2002. Matrix-assisted laser desorption mass spectrometry. Applied Spectroscopy Reviews, 37(3): 275-303.

Tanaka, K. et al., 1988. Protein and polymer analyses up to m/z 100,000 by laser ionization time-of-flight mass spectrometry. Rapid Communications in Mass Spectrometry, 2(8): 151-153.

Tomlinson, M.J., Scott, J.R., Wilkins, C.L., Wright, J.B. and White, W.E., 1999. Fragmentation of an alkali metal-attached peptide probed by collision-induced dissociation Fourier transform mass spectrometry and computational methodology. Journal of Mass Spectrometry, 34(9): 958-968.

Tosca, N.J. and McLennan, S.M., 2006. Chemical divides and evaporite assemblages on Mars. Earth and Planetary Science Letters, 241: 21-31.

Trimpin, S., Rouhanipour, A., Az, R., Rader, H.J. and Mullen, K., 2001. New aspects in matrix-assisted laser desorption/ionization time-of-flight mass spectrometry: A universal solvent-free sample preparation. Rapid Communications in Mass Spectrometry, 15(15): 1364-1373.

Van Vaeck, L., Adriaens, A. and Adams, F., 1998. Microscopical speciation analysis with laser microprobe mass spectrometry and static secondary ion mass spectrometry. Spectrochimica Acta Part B-Atomic Spectroscopy, 53(2): 367-378.

Vermillion-Salsbury, R.L. and Hercules, D.M., 2002. 9-aminoacridine as a matrix for negative mode matrix-assisted laser desorption/ionization. Rapid Communications in Mass Spectrometry, 16(16): 1575-1581.

Weast, R.C. (Editor), 1984. Handbook of Chemistry and Physics. CRC, Boca Raton.

Wiedemann, H. and Smykatz-Kloss, W., 1981. Thermal studies of thenardite. Thermochimica Acta, 50: 17-29.

Wu, H.P., Su, C.L., Chang, H.C. and Tseng, W.L., 2007. Sample-first preparation: A method for surface-assisted laser desorption/ionization time-of-flight mass spectrometry analysis of cyclic oligosaccharides. Analytical Chemistry, 79(16): 6215-6221.

Yalcin, T., Wallace, W.E., Guttman, C.M. and Li, L., 2002. Metal powder substrate-assisted laser desorption/ionization mass spectrometry for polyethylene analysis. Analytical Chemistry, 74(18): 4750-4756.

Yan, B., McJunkin, T.R., Stoner, D.L. and Scott, J.R., 2005. Mineral identification in basalts using automated mass spectral data analysis. Geochimica et Cosmochimica Acta, 69(10): A797-A797.

Yan, B., McJunkin, T.R., Stoner, D.L. and Scott, J.R., 2006. Validation of fuzzy logic method for automated mass spectral classification for mineral imaging. Applied Surface Science, 253(4): 2011-2017.

Yan, B., Stoner, D.L., Kotler, J.M., Hinman, N.W. and Scott, J.R., 2007a. Detection of biosignatures by geomatrix-assisted laser desorption/ionization (GALDI) mass spectrometry. Geomicrobiology Journal, 24(3-4): 379-385.

Yan, B., Stoner, D.L. and Scott, J.R., 2007b. Direct LDI-FTMS detection of mineral-associated PAHs and their influence on the detection of other organics. Talanta, 72(2): 634-641.

Yao, J., Scott, J.R., Young, M.K. and Wilkins, C.L., 1998. Importance of matrix:analyte ratio for buffer tolerance using 2,5-dihydroxybenzoic acid as a matrix in matrix-assisted laser desorption/ionization Fourier transform mass spectrometry and matrix-assisted laser desorption/ionization time of flight. Journal of the American Society for Mass Spectrometry, 9(8): 805-813.

Zhu, M., Xie, H., Guan, H. and Smith, R., 2006. Mineral and lithologic mapping of martian low albedo regions using OMEGA data, Lunar and Planetary Science XXXVII.

Zimmermann, R., Van Vaeck, L., Davidovic, M., Beckmann, M. and Adams, F., 2000. Analysis of polycyclic aromatic hydrocarbons (PAH) adsorbed on soot particles by Fourier transform laser microprobe mass spectrometry (FT LMMS): Variation of the PAH patterns at different positions in the combustion chamber of an incineration plant. Environmental Science & Technology, 34(22): 4780-4788.

CHAPTER 3: EFFECT OF THENARDITE ON THE DIRECT DETECTION OF AROMATIC AMINO ACIDS: IMPLICATIONS FOR THE SEARCH FOR LIFE IN THE SOLAR SYSTEM.

C. Doc Richardson[1], Nancy W. Hinman[1], and Jill R. Scott [2*]

[1]Geosciences Department, University of Montana, Missoula, 32 Campus Drive #1296, Missoula, MT 59812, United States. Email: Nancy.Hinman@umontana.edu

[2]Chemical Sciences, Idaho National Laboratory, 1765 North Yellowstone Hwy, Idaho Falls, ID 83415, United States. Email: Jill.Scott@inl.gov

Short Title: DIRECT DETECTION OF AROMATIC AMINO ACIDS WITH THENARDITE

3.1. ABSTRACT

With the discovery of Na-sulfate minerals on Mars and Europa, recent studies using these minerals have focused on their ability to assist in the detection of bio/organic signatures. This study further investigates the ability of thenardite (Na_2SO_4) to effectively facilitate the ionization and identification of aromatic amino acids (phenylalanine, tyrosine, and tryptophan) using a technique called geomatrix-assisted laser desorption/ionization in conjunction with a Fourier transform ion cyclotron resonance mass spectrometry. This technique is based on the ability of a mineral host to facilitate desorption and ionization of bio/organic molecules for detection. Spectra obtained from each aromatic amino acid alone and in combination with thenardite show differences in ionization mechanism and fragmentation patterns. These differences are

due to chemical and structural differences between the aromatic side chains of their respective amino acid. Tyrosine and tryptophan when combined with thenardite were observed to undergo cation-attachment ($[M+Na]^+$), due to the high alkali ion affinity of their aromatic side chains. In addition, substitution of the carboxyl group hydrogen by sodium led to formation of $[M- H+Na]Na^+$ peaks. In contrast, phenylalanine mixed with thenardite showed no evidence of Na^+ attachment. Understanding how codeposition of amino acids with thenardite can affect the observed mass spectra is important for future exploration missions that are likely to use laser desorption mass spectrometry to search for bio/organic compounds in extraterrestrial environments.

Key words: biosignature, geomatrix, thenardite, GALDI, aromatic amino acids, FTICR-MS, Mars, Europa

3.2. INTRODUCTION

Both hydrated and unhydrated Na-sulfate minerals exist in numerous bodies throughout the solar system. On Earth, Na-sulfates form in non-marine environments (playas, sabkhas), in basaltic weathering (Hill and Forti, 1997; Karlo et al., 1980), as fumarolic exhalations (Hill and Forti, 1997), in atmospheric aerosols (Rankin et al., 2002), and in subsurface Antarctic ice (Ohno et al., 2006). Beyond Earth, Na-sulfates are found on Mars as weathering products in evaporitic environments (Mangold et al., 2008; Zhu et al., 2006a), and as surface components of the Jupiter's moons, Ganymede (McCord et al., 2001), Io (Wiens et al., 1997), and Europa (Johnson, 2000; McCord et al., 1998; McCord et al., 1999). Additionally, numerous prebiotic organic compounds have

been detected on these solar bodies making them high priority candidates for biological activity (Kotler et al., 2009). Thus, with the ubiquity of Na-sulfates in the solar system, understanding their ability to preserve and relinquish bio/organic signatures, which are signatures that are organic and potentially biological in origin, is crucial in the search for extraterrestrial life.

Since the *Viking* missions (Klein, 1979; Oro, 1979), the search for life in the solar system has predominantly focused on the planet Mars (Chyba and McDonald, 1995). Unfortunately, due to the oxidizing martian atmosphere, bio/organic compounds are better preserved when protected (via substitution, inclusion, adsorption) by a mineral host to avoid degradation (Parnell et al., 2007). On Earth, organic compounds are often codeposited in sulfate salts during mineralization (Aubrey et al., 2006; Kotler et al., 2008; Richardson et al., 2008). Likewise, if life once existed on Mars, bio/organic compounds could be incorporated and preserved in the martian geological record. Sulfate minerals are a likely candidate for bio/organic preservation, since they are ubiquitous on the martian regolith, forming in evaporitic environments due to weathering of primary basaltic minerals (Squyres et al., 2004). Chemical/mineralogical models using data from SNC-type meteorites, MER rovers, and martian orbiters provide evidence that Na-sulfates are a likely constituent of evaporitic assemblages on Mars (Tosca and McLennan, 2006). Additionally, spectrometry data from the Visible and Infrared Mineralogical Mapping Spectrometer, (OMEGA) aboard the Mars *Express* Orbiter, detected signatures consistent with the presence of thenardite (Na_2SO_4) near the low-albedo region of Syrtis Major (Zhu et al., 2006a). More recently, Mangold et al. (2008) suggested that polyhydrated Na-sulfates may be a constituent in the layered sulfate

sequences of West Candor Chasma, known to contain one of the largest sequences of sulfate minerals on Mars.

In addition to Mars, several Galilean satellites have spectrometric signatures characteristic of surficial Na-sulfates. Of these satellites, the moon-sized satellite of Jupiter, Europa, is the most promising in the search for extraterrestrial life, as it likely contains liquid water, biogenic elements, and chemical disequilibria (Chela-Flores, 2006; Chyba and Phillips, 2002; Gaidos et al., 1999; Kargel et al., 2000). The surface composition of Europa is dominated by water ice with localized regions of non-ice components, consisting mostly of polyhydrated Na- and Mg-sulfate species (Fanale et al., 2001; Kargel et al., 2000; McCord et al., 1998; McCord et al., 1999; Zolotov and Shock, 2001). These sulfate minerals originate as solutes in the internal ocean, probably derived from leaching and degassing of elements on the ocean-rock interface (Fanale et al., 2001). These solutes subsequently are emplaced on the surface by cryovolcanism and impact events (Orlando et al., 2005).

Geomatrix-assisted laser desorption/ionization mass spectrometry (GALDI-MS) is a proven technique capable of characterizing bio/organic compounds associated with terrestrial sulfate minerals (Kotler et al., 2008b; Richardson et al., 2008), and possibly bio/organic compounds associated with returned samples from Mars and Europa. This technique uses a mineral matrix to aid in desorption so that organic signatures can be detected along with any bio/organic signatures present in the sample (Yan et al., 2007c). Further, the mineral matrix can stabilize organic ions to aid detection. Thus, the ability of minerals to facilitate the ionization and desorption of bio/organic compounds is a primary focus in the effectiveness of GALDI-MS. When used in conjunction with a Fourier

transform ion cyclotron resonance mass spectrometer (FTICR-MS) (Scott and Tremblay, 2002), GALDI-FTICR-MS has the ability to obtain high resolution spectra using a single laser shot, with low detection limits for chemical signatures, with little or no sample preparation (Kotler et al., 2008b; Richardson et al., 2008; Yan et al., 2007a). When coupled with imaging or mapping capability (Scott and Tremblay, 2002), GALDI-FTICR-MS can search for bio/organic signatures in heterogeneous geomatrices from both terrestrial samples (Kotler et al., 2008b; Richardson et al., 2008) and future samples returned from Mars and Europa. While FTICR-MS systems are not practical for a rover, a low power, compact laser desorption quadrupole ion trap mass spectrometer is being developed for deployment on Mars as part of the Mars Organic Molecule Analyzer (MOMA) as part of the ExoMars mission (Evans-Nguyen et al., 2008).

Previous GALDI-FTICR-MS investigations have focused on sulfate salts and halides (NaCl) acting as mineral matrices to facilitate the ionization and desorption of bio/organic compounds (fatty acids, amino acids, and proteins) (Kotler et al., 2008b; Richardson et al., 2008; Yan et al., 2007a; Yan et al., 2007c). These combinations produced inorganic and organic cluster ions (Kotler et al., 2008b; Richardson et al., 2008), deprotonated bio/organic compounds ($[M-H]^-$) (Richardson et al., 2008), and/or cation-attached peaks $[M+Na]^+$ (Yan et al., 2007a). Polycyclic aromatic hydrocarbon (PAH) compounds are also of interest due to their occurrence throughout the universe including meteorites (Kotler et al., 2009). Unlike most bio/organic compounds, PAH compounds self-ionize during laser ablation and may facilitate the detection of non-ionizing bio/organic compounds (Yan et al., 2007c).

The occurrence of thenardite (Na_2SO_4) throughout the solar system makes it a primary candidate for GALDI-FTICR-MS studies. The mineral has sufficient gas-phase basicity to abstract a proton from the aliphatic amino acid glycine, contrary to results using other sulfate salts (Richardson et al., 2008). Furthermore, thenardite taken from a terrestrial evaporitic environment showed signatures consistent with bio/organic compounds (Richardson et al., 2008). Gas-phase reactions between thenardite and stearic acid produce organic and inorganic cluster ions, similar to cluster ions observed by matrix-assisted laser desorption/ionization (MALDI), such as an accumulation of adducts (Karas and Hillenkamp, 1988a), matrix moieties (Knochenmuss et al., 1996b) and/or analyte components (Budimer et al., 2007; Ham et al., 2003a). Thenardite was also used to ascertain the limit of detection for GALDI-FTICR-MS, estimated to be approximately 3 parts per trillion based on bulk concentrations, corresponding into ~7 zeptomoles (10^{-21}) per laser shot (Richardson et al., 2008).

In this study, we evaluate the ability of thenardite to facilitate the desorption, ionization, and detection of aromatic amino acids using GALDI-FTICR-MS. Aromatic compounds were chosen because they have been proposed as primary biosignature targets in the solar system (McKay, 2007; Parnell et al., 2007; Storrie-Lombardi et al., 2001), as they readily donate electrons via multiple metabolic pathways during protein synthesis in terrestrial microorganisms (Plekan et al., 2008; Porat et al., 2004). Spectra obtained from mixing of individual aromatic amino acids (tryptophan, tyrosine and phenylalanine) with thenardite were evaluated for differences in ionization and fragmentation patterns. The effectiveness of thenardite to assist in the detection of

aromatic amino acids and other bio/organic signatures, along with its occurrence on Mars and Europa, further signifies its importance in the search for life in the solar system.

3.3. MATERIALS AND METHODS

Physical mixtures of thenardite (Fischer Scientific, Pittsburgh, PA) with phenylalanine, tyrosine, and tryptophan (Sigma-Aldrich, St. Louis, MO) were prepared following methods of Richardson et al. (2008) and Yan et al. (2007a). Approximately 1×10^{-4} mole (0.02 g) of tryptophan was added to 10g of thenardite. The mixture was then mixed for approximately 5 minutes at 70 Hz using a vortex mixer (Model 231, Fischer Scientific, Pittsburgh, PA) with two 4.5 mm zinc-plated steel ball bearings (Premium Grade BBs, Daisy Outdoor Products, Rogers, AR) to ensure a relatively homogeneous sample corresponding to a bulk concentration of ~2 ppm. The phenylalanine and tyrosine samples were produced in a similar manner to that of tryptophan.

Lower concentrations of phenylalanine, tyrosine, and tryptophan with thenardite were produced by a series of dry serial dilutions with incremental steps of 10^{-3} molar. The resulting samples had an approximate concentration of ~1 nM (~3 ppb). Vortex mixing was completed between all dilutions steps to ensure homogeneity, similar to previous methods by Richardson et al. (2008) and Yan et al. (2007a). Samples were then pressed into half inch pellets using a Beckman dye with a Carver Laboratory Press (Menomonee Falls, WI) at an approximate pressure of 3.5×10^{-7} Pa. Samples were subsequently mounted on copper discs using epoxy (Devcon 5 minute epoxy, Danvers, MA). To prevent absorption of the epoxy, the epoxy was allowed to dry for approximately 5 minutes before applying the sample pellet.

3.3.1. Instrumentation

Mass spectra were obtained using a laboratory-built imaging laser desorption FTICR-MS (McJunkin et al., 2002b; Scott et al., 2003; Scott and Tremblay, 2002) with a 7 T Oxford (Oxford, England) superconducting magnet. Instrumental parameters are similar to those previously described (Kotler et al., 2008b; Richardson et al., 2008; Yan et al., 2007a; Yan et al., 2007c). Data acquisition was accomplished using an Odyssey control and data acquisition computer system (Finnigan FT/MS, Bremen, Germany). Desorption/ionization was performed using a Nd:YAG laser (Continuum, Santa Clara, CA) operating at 355 nm with a 6 ns laser pulse and an irradiance of 1×10^8 W/cm^2, unless otherwise specified. During ionization, voltage potential between the front and back plates was maintained at 0 V, while after ionization, a trapping potential of 2 V was applied to both trap plates. A delay of 0.5 s was allowed prior to chirp excitation over the range of 50 Hz to 4 MHz (corresponding to m/z 10^5 and 26.9, respectively) with a sweep rate of 3600 Hz/μs. Ions were detected in direct mode using 128 K data points. After acquisition, data was baseline corrected, Hamming apodized, zero filled, and Fourier transformed. Pressure during analysis was $\leq 4 \times 10^{-9}$ Torr. For the given parameters, the LD-FTICR-MS has a mass error of ±0.003 Da, resolution of ~10,000), high sensitivity (≤ 400 ions for peaks with signal-to-noise ratio ~3) for m/z range <2000 Da. All spectra were acquired with single laser shots and in the positive mode unless specified otherwise. Peak identification was accomplished by systematic analysis following the method described in Kotler et al. (2008). Additional information regarding FTICR-MS can be found in the literature (Comisarow, 1993; Marshall and Hendrickson, 2002; Marshall et al., 1998).

3.4. RESULTS AND DISCUSSION

The possibility of life on Mars and Europa in conjunction with the occurrence of endogenous Na-sulfates that could potentially harbor signatures of life makes understanding the interaction between Na-sulfates and bio/organic compounds crucial for the potential applications for LDMS techniques in the search for extraterrestrial life in the solar system. A first step toward understanding the spectra is distinguishing the difference between peaks produced from inorganic ions generated from the mineral from those of the bio/organic compounds of interest. The second major step is determining if the mineral is likely to affect the types of peaks observed from the bio/organic compounds, which is the primary focus of this paper.

Positive spectra of the mineral thenardite (Fig. 3.1) by itself are dominated by a small number of peaks. The peaks represent inorganic cluster ions at m/z 164, 265, 279, and 305. These peaks are easily identified as representing inorganic ions, based on their mass defect (Kim et al., 2006; Kotler et al., 2008; McLafferty and Tureček, 1993; Sack et al., 1984). The high mass accuracy and resolution of FTICR-MS enables distinction between inorganic and organic ions. Detailed explanation and methodology for identification of peaks is found in Kotler et al. (2008) and Richardson et al. (2008). The presence of H, and some of the O, in the inorganic ions is likely the result of remnant water left behind from hydrated Na-sulfate mineral phases. Similar inorganic cluster ions have been previously reported in Na-sulfate spectra (Kotler et al., 2008b; Richardson et al., 2008; Van Vaeck et al., 1998b), including the $Na_3SO_4^+$ peak at m/z 164 observed by Van Vaeck et al. (1997). Unlike the negative mode spectra of thenardite which show

numerous inorganic cluster ions (Richardson et al., 2008), the positive mode spectrum of thenardite (Fig. 3.1) shows significantly fewer peaks.

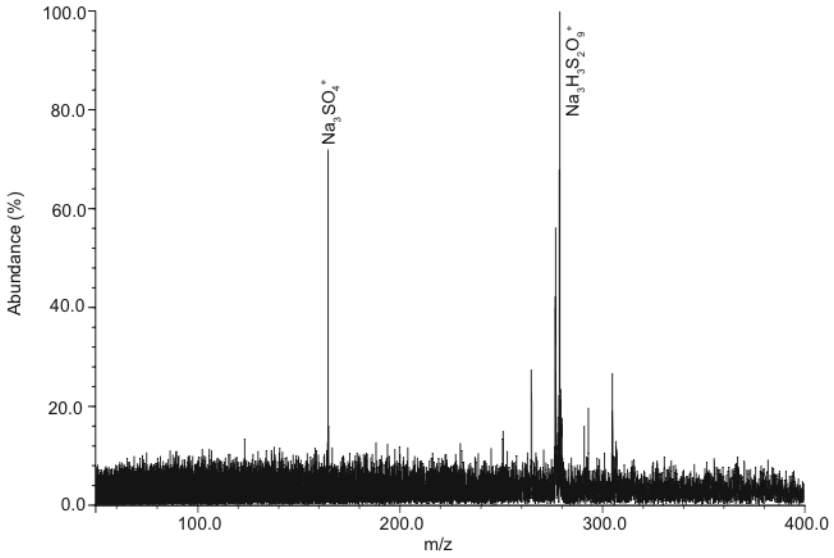

Figure 3.1. Positive ion GALDI-FTICR-MS spectrum of thenardite.

The aromatic amino acids are presented from lowest to highest molecular weight, which also corresponds with their cation affinities (i.e., Phe<Tyr<Trp). A common fragmentation occurs from the cleavage of the C_α–C_β bond (location of C_α–C_β bond in the aromatic amino acids is shown in the diagram below using Phe for illustration) for all of the aromatic amino acids (Plekan et al., 2008). The structural schemes in Figures 3.2, 3.3, and 3.4 are provided as an aid to understanding how the ions are related to the neutral

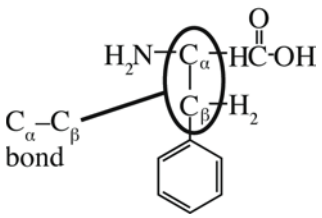

amino acid and as possible formation pathways to the observed ions. They are not necessarily indicative of the actual gas-phase structure, which can be quite complex (El Aribi et al., 2004; McLafferty and Tureček, 1993) and are beyond the scope of this paper.

The spectrum of phenylalanine alone (Fig. 3.2A) is dominated by fragmentation of the molecular backbone and the phenyl aromatic ring ion. Decarboxylation of the molecular backbone results in the peak at m/z 120. Further fragmentation is seen in the cleavage of the C_α–C_β bond of the molecular backbone resulting in the positively charged $C_2H_4NO_2^+$ fragmented backbone at m/z 74 and the phenyl ring fragment observed at m/z 91 (Fig. 3.2C). The high intensity peaks at m/z 155 and 139 in the phenylalanine spectrum (Fig. 3.2A) are due to sample contamination (<1%) of alkali ions (K^+, Na^+) and their subsequent gas-phase interactions. These contaminants may have been introduced via a salt with its own counter anion, or as a salt of phenylalanine. Regardless of the exact source of the contaminants, these cluster ions have inorganic compositions based on their high mass defects. Furthermore, systematic analysis of their isotopic distribution supports the presence of alkali elements and their subsequent interaction with the phenylalanine and thenardite moieties. Further, the peak at m/z 38.96 corresponds to singly-charged K^+ ions. Alkali element contamination has been reported in similar spectra of aromatic amino acids (Karas et al., 1985; Plekan et al., 2008; Willey et al., 1998). The high intensity of the alkali element-attached peaks reflects the ease of alkali element ionization at 355 nm, resulting in abundant alkali element desorption and subsequent high intensity peaks (Karas et al., 1985; Scott et al., 2006 ; Yan et al., 2007c), although the exact formation mechanisms of these cluster ions are highly speculative and unclear at this time.

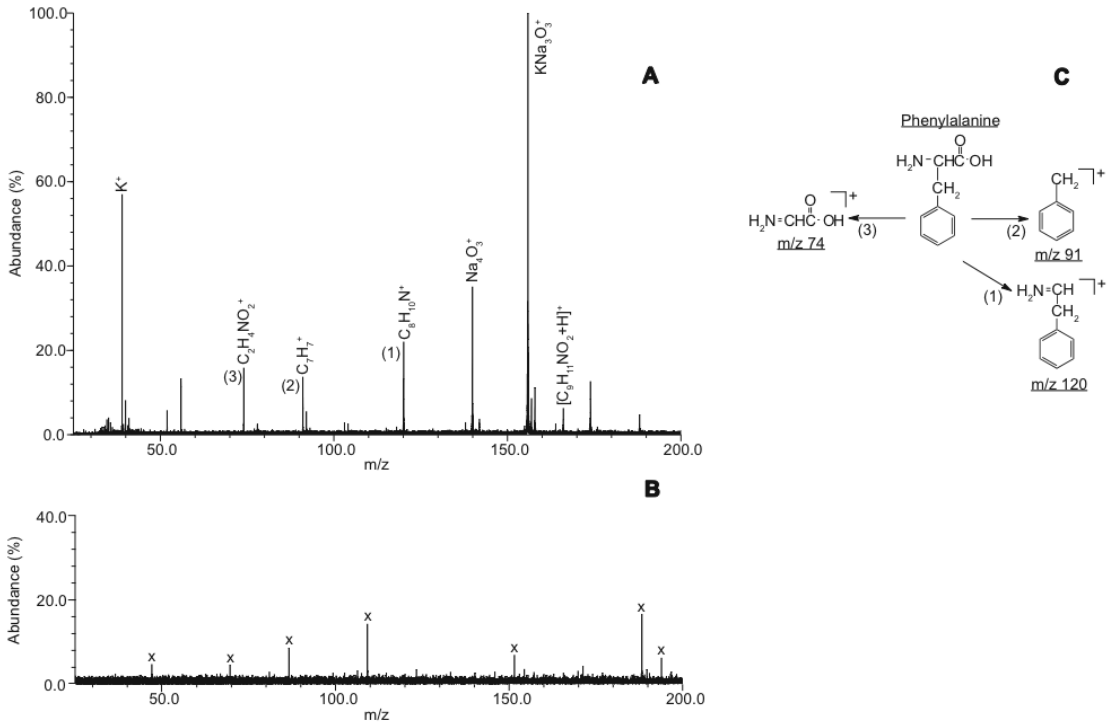

Figure 3.2. GALDI-FTICR-MS spectra showing (a) phenylalanine alone and (b) thenardite mixed with phenylalanine (3 ppb). The numbers next to the peaks on (a) correspond to the possible fragmentation ion illustrated in scheme (c). Inorganic cluster ions are designated by ×'s. Structures shown in (c) are not indicative of the actual gas-phase structure, but are shown as a reference to the neutral phenylalanine structure.

Excluding the alkali element-cluster peaks, the highest intensity peak in the phenylalanine spectrum (Fig. 3.2A) is caused by decarboxylation ($[M\text{-}COOH]^+$), contrary to studies by Plekan et al. (2008) whose major peak corresponded to breakage of the C_α–C_β bond and the subsequent formation of the molecular backbone ion. The difference in major peaks between studies is likely a function of the laser irradiance and system parameters. Major peaks corresponding to $[M\text{-}COOH]^+$ were observed using laser desorption mass spectrometry instrumentation (Karas et al., 1985) under higher laser intensities than were used in this study. High laser fluences could cause ablation at the laser-mineral interface rather than desorption (Aubriet, 2007; Aubriet et al., 2005;

Aubriet and Muller, 2008). However, the distinction between desorption and ablation processes for GALDI-FTICR-MS has not been determined because only one type of spectral signature was observed when varying the laser irradiance. The relatively high laser irradiance used in GALDI-FTICR-MS appears to be necessary for optimal ionization due to the refractory nature of the host minerals.

The absence of peaks in mixed phenylalanine-thenardite spectra implies that there are competitive gas-phase reactions. This competition results in the self-ionized peaks of phenylalanine being completely suppressed. However, there is also an absence of cation-attached peaks of phenylalanine, which would be expected due to the presence of thenardite. The absence of cation-attached peaks associated with phenylalanine may also be the result of the low binding energy of Na^+ with the phenyl ring as well as with the carbonyl oxygen and the nitrogen of the amine group (Dunbar, 2000; Ryzhov et al., 2000). Binding energies associated with the aromatic amino acids tend to decrease with decreasing polarization of the aromatic ring, although the stability of Na^+ chelation with phenylalanine is largely controlled by the carbonyl oxygen and/or amine nitrogen (Ryzhov et al., 2000). It follows that cation affinity associated with tryptophan will be greater than tyrosine and even more so than phenylalanine. This is further supported by collision-induced dissociation experiments showing that Na^+ tends to form stronger bonds with phenol than with benzene rings (Armentrout and Rodgers, 2000), which is contradictory to studies by Ryzhov et al. (2000) and Dunbar (2000) that suggest Na^+ binds to phenol and benzene rings with equal strength. Even though phenylalanine is less prone to cationization than tyrosine or tryptophan, cation attachment can occur when the laser intensity is near the optimized peak height irradiances of singly-charged alkali

element ions (Karas et al., 1985). At these irradiances, the alkali element ions and cation-attached peaks have comparable peak heights, but at higher intensities, alkali element ion formation dominates, while cation-attached abundances decrease (Karas et al., 1985). This observation is concurrent with the peak heights of the singly-charged K^+ ions and alkali element-attached inorganic cluster ions in Figure 3.2A. Thus, the absence of Na-attachment peaks in Figure 3.2B could reflect both the low cation binding energy of phenylalanine and the typical laser intensity used in this study, while the absence of self-ionized peaks in Figure 3.2B may result from thenardite suppressing the self-ionization mechanisms of phenylalanine. The exact mechanisms are still unclear, but could reflect the suppression of ion formation or that the self-ionization occurs, but is subsequently neutralized in the desorption plume due to their interaction with desorption products from thenardite.

The major peak of the tyrosine spectrum (Fig. 3.3A) is observed at m/z 107 ($C_7H_7O^+$), which is consistent with previous tyrosine spectra (Plekan et al., 2008; Vorsa et al., 1999). The $C_7H_7O^+$ ions arise from fragmentation of the C_α–C_β bond and the concomitant loss of the H^+ ion from the attached hydroxyl group (Fig. 3.3C). The additional loss of the O from the $C_7H_7O^+$ ion leads to the $C_7H_7^+$ fragment ion (m/z 91). Fragmentation of the molecular backbone (Fig. 3.3C) is observed by successive cleaving of the amine group ([M-NH_2]) and the carboxyl group ([M-COOH]) at m/z 165 and 136, respectively. This fragmentation is consistent with previous tyrosine spectra (Vorsa et al., 1999). Both fragments are less than 10% of the major peak and comparable in intensity to the molecular ion at m/z 182.

Structurally, tyrosine is identical to phenylalanine with the addition of a hydroxyl group bonded to the aromatic ring. Although this hydroxyl group is located far from the C_α–C_β bond, the tyrosine spectrum is much different than the phenylalanine spectrum. This dichotomy results from the ionization energy potentials and the preferential organization of the positive charge after cleavage of the C_α–C_β bond. For tyrosine, the lowest ionization energy is attributed to the removal of the π-electron from the phenol functional group, this differs from phenylalanine where the lowest ionization energy corresponds to removal of the amine-group electron or the phenyl-group electron (Campbell et al., 1992; McLafferty and Tureček, 1993). As a result, the positive charge in tyrosine is transferred to the C_β fragment (phenol ring) (Plekan et al., 2008; Willey et al., 1998). Conversely, for phenylalanine the relocation of the positive charge is dominated by the C_α fragment. This preferential charge localization in tyrosine along with the subsequent hydroxyl deprotonation from the phenol group leads to the formation of the $C_7H_7O^+$ major peak. The presence of this peak suggests that thenardite does not significantly affect the $C_7H_7O^+$ formation mechanism. Conversely, the self-ionization peaks in the phenylalanine spectrum are suppressed and absent when phenylalanine is associated with thenardite.

Unlike the corresponding phenylalanine spectrum, the spectrum of tyrosine mixed with thenardite (Fig. 3.3B), is virtually devoid of inorganic cluster ions, although inorganic cluster ions were observed in other spectra from the same sample. This discrepancy is not unusual considering the single shot technique and the heterogeneity of the sample. Additionally, it is possible that inorganic cluster ion formation may be affected by the relative amount of organic constituent present in a particular shot.

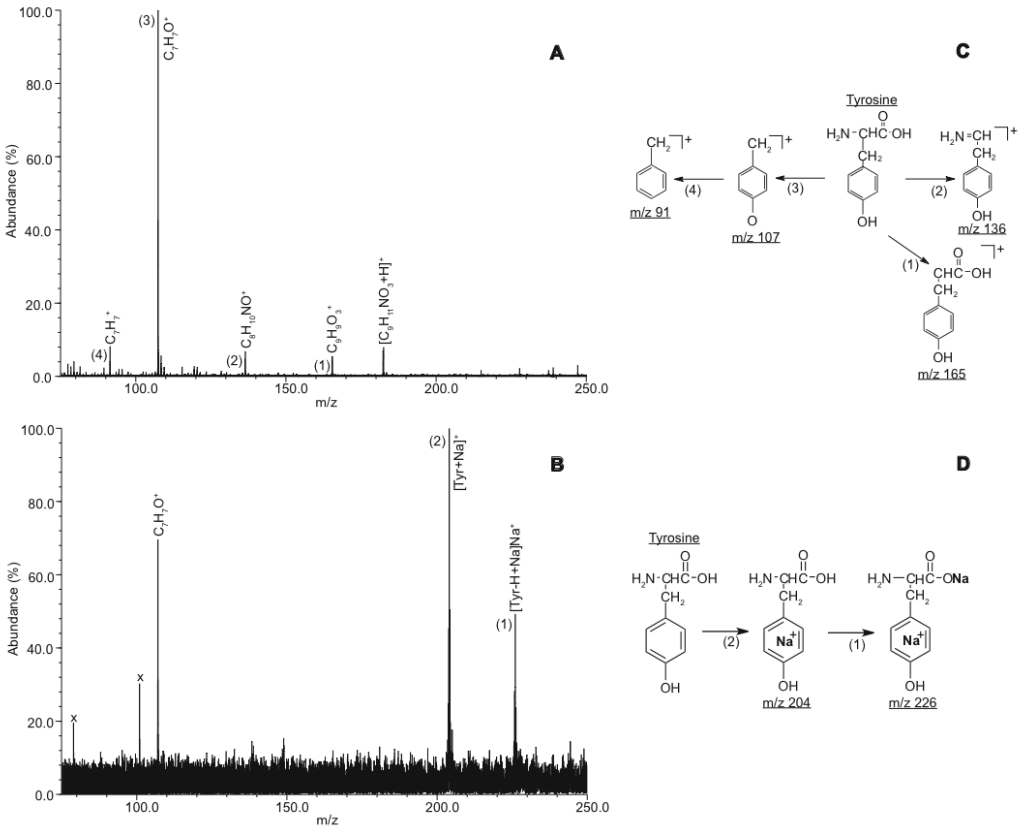

Figure 3.3. GALDI-FTICR-MS spectra showing (a) tyrosine alone and (b) thenardite mixed with tyrosine (3 ppb). The numbers next to the peaks on (a) correspond to the possible fragmentation ion illustrated in scheme (c). Likewise values on (b) correspond to the possible fragmentation ion illustrated in scheme (d). Inorganic cluster ions are designated by ×'s. Structures shown in (c) and (d) are not indicative of the actual gas-phase structure, but are shown as a reference to the neutral tyrosine structure.

However, only a small number of peaks are typically observed in the spectra, which are either from tyrosine fragmentation or cation attachment between thenardite and tyrosine (Fig. 3.3D). An exception is found in the peaks at m/z 78 and 100, which represent inorganic cluster ions based on their mass defect, similar to peaks found in previous spectra of Na-sulfates (Richardson et al., 2008; Van Vaeck et al., 1998b). It is likely that the presence of the organic analyte affects the production of the inorganic peaks from thenardite, possibly through alterations of the desorption process or through competitive gas-phase reactions.

The major peak in spectra from the tyrosine mixed with thenardite samples (Fig. 3.3B) corresponds to Na^+ binding to the π-electron from the aromatic ring of tyrosine (Fig. 3.3D). This Na-π bond is likely centered across the face of the aromatic ring with chelation by the phenol ring as well as the amine nitrogen and carbonyl oxygen (Ryzhov et al., 2000). An additional sodium exchanges with the hydrogen of the carboxyl group to form the alkaline carboxylate salt, either in the condensed phase or in a gas-phase reaction, leading to formation of $[M-H+Na]Na^+$ ions observed at m/z 226 with a peak height roughly half that of the single cation-attached peak. An ion with two alkali metals attached is sometimes referred to as a double-cation attached ion (Tomlinson et al., 1999; Lou et al., 2007), which is a slight misnomer because only one of the alkali metals is providing the charge for the singly-charged ion.

The structure of tryptophan is characterized by the indole functional group: benzene ring attached to an N-heterocyclic five-member ring (pyrrole). The major peak (m/z 130) of the tryptophan spectrum (Fig. 3.4A) is attributed to the dehydroindole ion ($C_9H_8N^+$). This major peak is consistent with previous studies of tryptophan mass spectra (Junk and Svec, 1963; Plekan et al., 2008; Vorsa et al., 1999; Wilson et al., 2006). Fragmentation of the molecular backbone (Fig. 3.4C) is evident as loss of the amine group ($[M-NH_2]$) at m/z 188, similar to previous observations using laser desorption mass spectrometry (Gogichaeva et al., 2007; Karas et al., 1985; Wilson et al., 2006), and time of flight-secondary ion mass spectrometry techniques (Vorsa et al., 1999). Additional fragmentation of the molecular backbone is seen at m/z 159, corresponding to decarboxylation.

Figure 3.4B shows a spectrum of thenardite mixed with tryptophan. The major peak in the spectrum, as with the tryptophan spectrum, corresponds to the dehydroindole ion at m/z 130. Simple cation attachment $[M+Na]^+$ is observed at m/z 227, corresponding to a Na^+ ion attaching to the indole functional group (Fig. 3.4D). Further gas-phase reactions between tryptophan and thenardite leads to the formation of the double cation-attached ion ($[M-H+Na]Na^+$) observed at m/z 249 (Fig. 3.4D). This peak is roughly 80% of the major peak and slightly less abundant than the $[M+Na]^+$ peak.

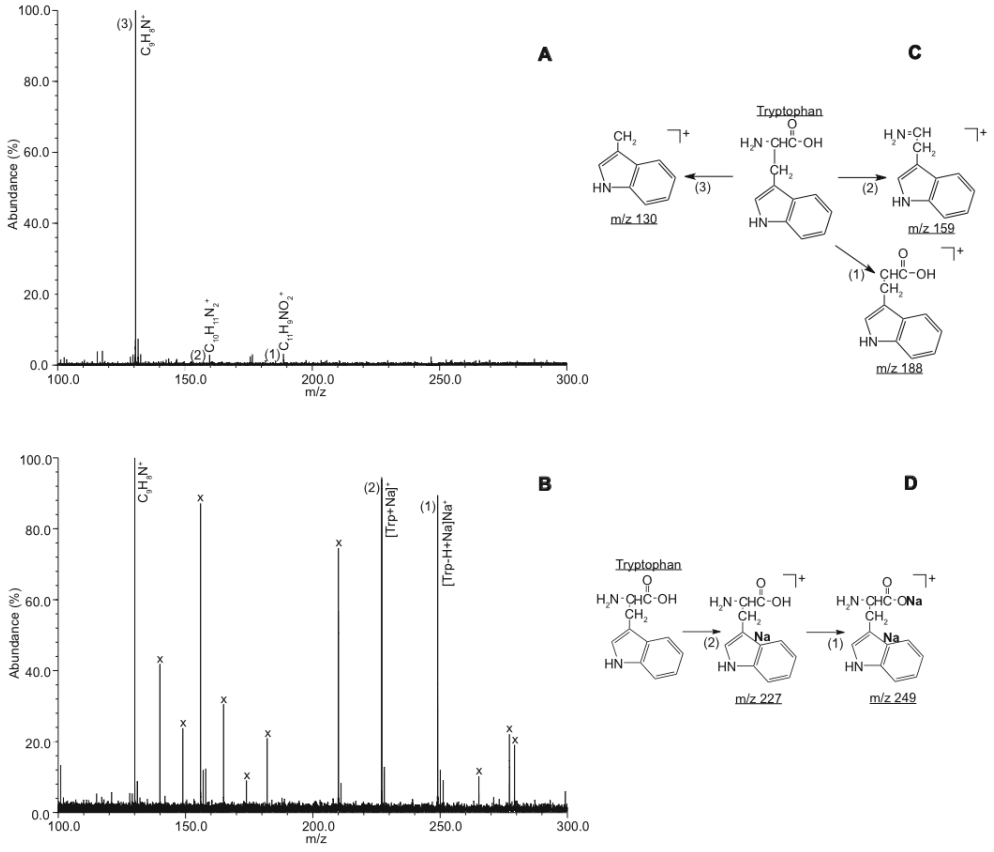

Figure 3.4. GALDI-FTICR-MS spectra showing (a) tryptophan alone and (b) thenardite mixed with tryptophan (3 ppb). The numbers next to the peaks on (a) correspond to the possible fragmentation ion illustrated in scheme (c). Likewise values on (b) correspond to the possible fragmentation ion illustrated in scheme (d). Inorganic cluster ions are designated by ×'s. Structures shown in (c) and (d) are not indicative of the actual gas-phase structure, but are shown as a reference to the neutral tryptophan structure.

As previously mentioned, Na^+ has the strongest affinity to bind with tryptophan, evidenced by the presence and high abundance of both the single and double cation-attached peaks in Figure 3.4B. The formation of the double cation-attached peak (m/z 249) is accomplished via a multiple step process (Fig. 3.4D). Initially, a Na^+ ion attaches to the π-electron of the indole aromatic ring. This attachment is likely offset to the side of the pyrrole ring face, rather than the benzene ring, because of differences in binding energies between the two regions of the indole group. This offset position above the pyrrole ring, results in cation chelation to the nitrogen from the amine group, the oxygen from the carbonyl group, and the π-electrons from the pyrrole group (Ryzhov et al., 2000). Secondly, another Na^+ from thenardite replaces the H^+ ion from the carboxyl group, either in the desorption plume or in the gas phase, leading to the formation of the $[M+Na-H]Na^+$ ion (Yan et al., 2007c). Comparison of the tyrosine and tryptophan spectra, with and without thenardite present, suggests that cation-attachment competes with and suppresses the self-ionization mechanisms and some related fragmentation pathways. However, fragment peaks related to the aromatic side chains of tyrosine and tryptophan are still observed in the presence of thenardite.

Other minerals can also provide cations to function in a similar manner to thenardite for ionizing bio/organic compounds. Sodium ions from the mineral halite (NaCl) participates in the formation of cation-attached peaks associated with the amino acids histidine, threonine, and cysteine (Yan et al., 2007c). These results are not surprising considering the ease with which Na^+ ionizes and its affinity to interact with bio/organic compounds in the desorption plume or gas phase (Liu et al., 2001); however, it is interesting to note that high concentrations of salts, similar to the minerals halite and

thenardite, suppress ion formation in MALDI (Goheen et al., 1997; Yao et al., 1998a). Cation attachment to histidine (Yan et al., 2007c) is not surprising, considering the aromaticity and the high alkali affinity of histidine (Kish et al., 2003). Thus, cation-attachment mechanisms of histidine with halite are likely similar to that described above for tyrosine and tryptophan in the presence of thenardite. Because threonine and cysteine are aliphatic amino acids, the formation of their cation-attached peaks is likely different than their aromatic counterparts. Regardless of the formation mechanisms, the occurrence of cation-attached peaks associated with different Na-salt geomatrices (halide and sulfate) suggests that Na^+ ionization and subsequent gas-phase interactions are common regardless of the anion or oxyanion moiety.

3.5. CONCLUSIONS

Pure samples of the aromatic amino acids (phenylalanine, tyrosine, and tryptophan) all produce ions through self-ionization mechanism(s) and produce similar fragmentation patterns when thenardite is absent. In all spectra, the fragmentation of the molecular backbone is observed by loss of the carboxyl group. Spectra from tyrosine and tryptophan show additional loss of the amine group. Further, fragmentation is observed in aromatic side chains, which accounts for the major peaks in the tyrosine and tryptophan spectrum, which is consistent with ionization potentials between the aromatic ring and the molecular backbone.

Of the aromatic amino acids used in this study, tyrosine and tryptophan associated with thenardite are observed to undergo cationization. The cation attachment results from the high affinity of the aromatic side chain for bind with alkali metal ions. Substitution of the carboxyl hydrogen by Na leads to formation of “double cation-

attached" ions. In contrast, phenylalanine shows no evidence of Na^+ interaction, a consequence of system parameters (e.g., laser intensity, wavelength) and/or lower alkali element-binding energy. In addition, the presence of thenardite suppresses all of the self-ionized peaks that are definitive for the presence of phenylalanine, leaving only fragment peaks common to all three aromatic amino acids studied. However, the ability of cation attachment to out compete and suppress the majority of the self-ionized peaks for tyrosine and tryptophan associated with thenardite makes interpretation of spectra for these aromatic amino acids less complicated.

The effectiveness of thenardite, and other Na-related geomatrices, for detection of bio/organic compounds is a product of analyte-matrix interactions and competitive gas-phase reactions. Understanding these types of Na-sulfate mineral and bio/organic compound interactions has astrobiological implications because terrestrial Na-sulfate mineral deposits are known to harbor bio/organic compounds; therefore, the presence of these minerals on Mars and Europa represent a prime opportunity to search for signs of life using LDMS instruments on rovers.

3.6. ACKNOWLEDGMENTS

The authors acknowledge support by the National Aeronautics and Space Agency (NASA) Exobiology Program (NNX08AP59G). CDR would also like to thank Montana Space Grant Consortium for support. Research performed at the Idaho National Laboratory under DOE Idaho Operations Office Contract DE-AC07-05ID14517.

3.7. REFERENCES

Allwood, D.A., Dreyfus, R.W., Perera, I.K. and Dyer, P.E., 1997. Optical absorption of matrix compounds for laser-induced desorption and ionization (MALDI). Applied Surface Science, 110: 154-157.

Armentrout, P.B. and Rodgers, M.T., 2000. An Absolute Sodium Cation Affinity Scale: Threshold Collision-Induced Dissociation Experiments and Ab Initio Theory. J. Phys. Chem., 104(A): 2238-2247.

Aubrey, A. et al., 2006. Sulfate minerals and organic compounds on Mars. Geology, 34(5): 357-360.

Aubriet, F., 2007. Laser-induced Fourier transform ion cyclotron resonance mass spectrometry of organic and inorganic compounds: methologies and aplications. Anal Bioanal Chem, 389: 1381-1396.

Aubriet, F., Carre, V. and Muller, J.F., 2005. Laser desorption and laser ablation Fourier transform mass spectrometry for the analysis of pollutants in complex matrices. Spectroscopy Europe, 17: 14-22.

Aubriet, F. and Muller, J., 2008. Laser ablation mass spectrometry of inorganic transition metal compounds. Additional knowledge for the understanding of ion formation. American Society for Mass Spectrometry, 19: 488-501.

Bezabeh, D.Z., Allen, T.M., McCauley, E.M., Kelly, P.B. and Jones, A.D., 1997. Negative ion laser desorption ionization time-of-flight mass spectrometry of nitrated polycyclic aromatic hydrocarbons. Journal of the American Society for Mass Spectrometry, 8(6): 630-636.

Botta, O. and Bada, J.L., 2002. Extraterrestrial organic compounds in meteorites. Surveys in Geophysics, 23(5): 411-467.

Bowden, S. and Parnell, J., 2007. Intracrystalline lipids within sulfates from the Haughton impact structure-Implications of survival of lipids on Mars. Icarus, 187: 422-429.

Budimer, N., Blais, J.C., Fournier, T. and Tabet, J.C., 2007. Desorption/ionization on porous silicon mass spectrometry (DIOS) of model cationized fatty acids. Journal of Mass Spectrometry, 42: 42-48.

Campbell, S., Beauchamp, J., Rempe, M. and Lichtenberger, D., 1992. Correlations of lone pair ionization energies with proton affinities of amino acids and related compounds. Site specificity or protonation. International Journal of Mass Spectrometry and Ion Processes, 117: 83-99.

Chela-Flores, J., 2006. The sulphur dilemma: are there biosignatures on Europa's icy and patchy surface? International Journal of Astrobiology, 5: 17-22.

Chen, Y., Chen, H., Aleksandrov, A. and Orlando, T., 2008. Roles of water, acidity, and surface morhology in surface-assisted laser desorption ionization of amino acids. Journal of Mass Spectrometry, C 112: 6953-6960.

Chevrier, V., Mathe, P., Rochette, P. and Gunnlaugsson, H., 2006. Magnetic study of an Antarctic weathering profile on basalt: Implications for recent weathering on Mars. Earth and Planetary Science Letter, 244(3-4): 501-514.

Chevrier, V. and Mathe, P.E., 2006. Mineralogy and evolution of the surface of Mars: A review. Planetary and Space Science, 55(3): 289-314.

Chyba, C. and McDonald, G., 1995. The origin of life in the solar system: current issues. Annual Review of Earth and Planetary Sciences, 23: 215-249.

Chyba, C. and Phillips, C., 2002. Europa as an abode of life. Origins of Life and Evolution of Biospheres, 32: 47-67.

Clark, B.C. et al., 2005. Chemistry and mineralogy of outcrops at Meridiani Planum. Earth and Planetary Science Letters, 240: 74-94.

Comisarow, M.B., 1993. Fundamental aspects of FT-ICR and applications to chemistry. Hyperfine Interactions, 81: 171-178.

Cushing, G.E., Titus, T.N., Wynne, P.R. and Christensen, P.R., 2007. Themis observes possible cave skylights on Mars. Geophysical Research Letters, 34(L17201): Doi:10.1029/2007/2007GL030709.

Dale, M.J., Jones, A.C., Pollard, S.J.T. and Langridgesmith, P.R.R., 1994. Direct determination of polycyclic aromatic-hydrocarbons in environmental matrices using laser-desorption laser photoionization time-of-flight mass-spectrometry. Analyst, 119(4): 571-578.

Drost, C. et al., 2006. Remotely sensed cave detection on Earth and Mars, 37th Annual Lunar and Planetary Science Conference, League City, TX.

Dunbar, R., 2000. Complexation of Na+ and K+ to aromatic amino acids: A density functional computational study of cation-π interactions. Journal of Physical Chemistry, 104: 8067-8074.

El Aribi, H., Orlova, G., Hopkinson, A. and Siu, K., 2004. Gas-phase fragmentation reactions of protonated aromatic amino acids: concomitant and consecutive neutral eliminations and radical cation formation. J. Phys. Chem., A(108): 3844-3853.

Elsila, J.E., de Leon, N.P. and Zare, R.N., 2004. Factors affecting quantitative analysis in laser desorption/laser ionization mass spectrometry. Analytical Chemistry, 76(9): 2430-2437.

Evans-Nguyen, T., Becker, L., Doroschenko, V. and Cotter, R., 2008. Development of a low power, high mass range mass spectrometer for Mars surface analysis. International Journal of Mass Spectrometry, 278: 170-177.

Fanale, F.P. et al., 2001. An experimental estimate of Europa's "ocean" composition independent of Galileo orbital remote sensing. Journal of Geophysical Research, 106(E7): 14595-14600.

Farmer, V., 1974. The infrared spectra of minerals. Mineralogical Society, London.

Fernandez-Lima, F.A., Ponciano, C.R. and da Silveira, E.F., 2008. UV laser-induced desorption mechanism analyzed through two-layer alkali halide samples. Journal of Mass Spectrometry, 43(5): 587-593.

Forti, P., 2005. Genetic processes of cave minerals in volcanic environments: An overview. Journal of Cave and Karst Studies, 67(1): 3-13.

Gaidos, E., Nealson, K. and Kirschvink, J., 1999. Life in ice-covered oceans. Science, 284: 1631-1633.

Gianotto, A.K. et al., 2004. Hydration of alumina cluster anions in the gas phase. Journal of the American Chemical Society, 126(26): 8275-8283.

Gogichaeva, N.V., Williams, T. and Alterman, M.A., 2007. MALDI TOF/TOF tandem mass spectrometry as a new tool for amino acid analysis. Journal American Society of Mass Spectrometry, 18: 279-284.

Goheen, S.C., Wahl, K.L., Campbell, J.A. and Hess, W.P., 1997. Mass spectrometry of low molecular mass solids by matrix-assisted laser desorption/ionization. Journal of Mass Spectrometry, 32: 820-828.

Haglund, R.F., 1996. Microscopic and mesoscopic aspects of laser-induced desorption and ablation. Applied Surface Science, 96-8: 1-13.

Ham, J.E., Durham, B. and Scott, J.R., 2003a. Comparison of laser desorption and matrix-assisted laser desorption/ionization for ruthenium and osmium trisbipyridine complexes using Fourier transform mass spectrometry. Journal of the American Society for Mass Spectrometry, 14: 393-400.

Hankin, S.M. and John, P., 1999. Laser time-of flight mass analysis of PAHs on single diesel particulates. Analytical Chemistry, 71(6): 1100-1104.

Hanton, S.D. and Parees, D.M., 2005. Extending the solvent-free MALDI sample preparation method. Journal of the American Society for Mass Spectrometry, 16(1): 90-93.

Hill, C. and Forti, P., 1997. Cave minerals of the world, 2nd National Speleological Society, Huntsville, AL.

Hughes, S.S., Smith, R., Hackett, W. and Anderson, S., 1999. Mafic volcanism and environmental geology of the eastern Snake River Plain. In: S.S. Hughes and G.

Thackray (Editors), Guidebook to the geology of eastern Idaho. Idaho Museum of Natural History, Pocatello, Idaho, pp. 143-168.

Johnson, R.E., 2000. Sodium at Europa. Icarus, 143: 429-433.

Junk, G. and Svec, H., 1963. The mass spectra of the a-amino acids. Journal of the American Chemical Society, 85: 839.

Karas, M., Bachmann, D. and Hillenkamp, F., 1985. Influence of the wavelength in high-irradiance ultraviolet laser desorption mass spectrometry of organic molecules. Analalytical Chemistry, 57: 2935-2939.

Karas, M. and Hillenkamp, F., 1988a. Laser desorption ionization of proteins with molecular masses exceeding 10000 daltons. Analytical Chemistry, 60: 2299-2301.

Karas, M. and Kruger, R., 2003. Ion formation in MALDI: The cluster ionization mechanism. Chemical Reviews, 103(2): 427-439.

Kargel, J.S. et al., 2000. Europa's crust and ocean: origin, composition, and the prospects for life. Icarus, 148: 226-265.

Karlo, J.H., Jorgenson, D.B. and Shineldecker, C.L., 1980. Sulfate minerals in Snake River Plain volcanoes. Northwest Science, 54(3): 178-182.

Kim, J. and Kang, W., 2000. Use of graphite plate for homogeneous sample preparation in matrix/surface-assisted laser desorption and ionization of polypropyleneglycol and polystyrene. Bulletin of the Korean Chemical Society, 21(4): 401-404.

Kim, S., Rodgers, R.P. and Marshall, A.G., 2006. Truly "exact" mass: Elemental composition can be determined uniquely from molecular mass measurement at similar to 0.1 mDa accuracy for molecules up to similar to 500 Da. International Journal of Mass Spectrometry, 251: 260-265.

Kish, M., Ohanessian, G. and Wesdemiotis, C., 2003. The Na+ affinities of a-amino acid: Side-chain substituent effects. International Journal of Mass Spectrometry, 227: 509-524.

Klein, H., 1979. Viking mission and the search for life on Mars. Reviews of Geophysics, 17: 1655-1662.

Knochenmuss, R., Dubois, F., Dale, M.J. and Zenobi, R., 1996a. The matrix suppression effect and ionization mechanisms in matrix-assisted laser desorption/ionization. Rapid Communications in Mass Spectrometry, 10(8): 871-877.

Kotler, J.M., Hinman, N.W., Yan, B., Stoner, D.L. and Scott, J.R., 2008. Glycine identification in natural jarosites using laser-desorption Fourier transform mass spectrometry: Implications for the search for life on Mars. Astrobiology, 8: 253-266.

Kotler, J.M., Richardson, C.D., W., H.N. and Scott, J.R., 2009. The stellar stew: distribution of extraterrestrial organics in the universe. In: V.A. Basiuk (Editor), From simple molecules to primitive life. American Scientific Publishers, Valencia, CA, pp. in press.

Kovalenko, L.J. et al., 1992. Microscopic organic-analysis using 2-step laser mass-spectrometry - Application to meteoritic acid residues. Analytical Chemistry, 64(6): 682-690.

Kujawinski, E.B., Hatcher, P.G. and Freitas, M.A., 2002. High-resolution Fourier transform ion cyclotron resonance mass spectrometry of humic and fulvic acids: Improvements and comparisons. Analytical Chemistry, 74: 413-419.

Kuntz, M., Anderson, S., Champion, D., Lanphere, M. and Grunwald, D., 2002. Tension cracks, eruptive fissures, dikes, and faults related to late Pleistocene–Holocene basaltic volcanism and implications for the distribution of hydraulic conductivity in the eastern Snake River Plain, Idaho. In: P. Link and L. Mink (Editors), Geology, hydrogeology, and environmental remediation. Idaho National Engineering and Environmental Laboratory, eastern Snake River Plain, Idaho. Geological Society of America Special Paper 353, pp. 111-133.

Kuntz, M., Champion, D., Spiker, E. and Lefebvre, R., 1986. Contrasting magma types and steady-state, volume-predictable volcanism along the great rift, Idaho. GSA bulletin, 97: 579-594.

Kuntz, M., Covington, H. and Schorr, L., 1992. An overview of basalitc volcanism of the eastern Snake River Plain, Idaho. In: P. Link, M. Kuntz and L. Platt (Editors), Regional geology of eastern Idaho and western Wyoming. Geological Society of America memoir, pp. 227-267.

Kuntz, M.E., 1989. Geology of the Craters of the Moon lava field, Idaho. In: K.L. Ruebelmann (Editor), Snake River Plain-Yellowstone Volcanic Province. American Geophysical Union, Washington D.C., pp. 51-56.

Lane, M., 2007. Mid-infrared emission spectroscopy of sulfate and sulfate-bearing minerals. American Mineralogist, 92: 1-18.

Leeman, W., Vitaliano, C. and Prinz, M., 1976. Evolved lavas from the Snake River Plain: Craters of the Moon National Monument, Idaho. Contributions to Mineralogy and Petrology, 56: 35-60.

Li, J., Lowenstein, T.K., Brown, C.B., Ku, T. and Luo, S., 1996. A 100 ka record of water tables and paleoclimates from salt cores, Death Valley, California Palaeogeography, Palaeoclimatology, Palaeoecology, 123: 179-203.

Limbach, P.A., Grosshans, P.B. and Marshall, A.G., 1993. Experimental-determination of the number of trapped ions, detection limit, and dynamic-range in Fourier-

transform ion-cyclotron resonance mass-spectrometry. Analytical Chemistry, 65(2): 135-140.

Liu, J., Tseng, K. and Lebrilla, C.B., 2001. A new external ionization multisample MALDI source for Fourier transform mass spectrometry. International Journal of Mass Spectrometry, 204: 23-29.

Lyons, R., 2004. Understanding Digital Signal Processing. Prentice Hall, Upper Saddle River, NJ.

Macha, S.F., Limbach, P.A. and Savickas, P.J., 2000. Application of nonpolar matrices for the analysis of low molecular weight nonpolar synthetic polymers by matrix-assisted laser desorption/ionization time-of-flight mass spectrometry. Journal of the American Society for Mass Spectrometry, 11(8): 731-737.

Mangold, N. et al., 2008. Spectral and geological study of the sulfate-rich region of West Candor Chasma, Mars. Icarus, 194: 519-543.

Marshall, A.G. and Hendrickson, C.L., 2002. Fourier transform ion cyclotron resonance detection: principles and experimental configurations. International Journal of Mass Spectrometry, 215(1-3): 59-75.

Marshall, A.G., Hendrickson, C.L. and Jackson, G.S., 1998. Fourier transform ion cyclotron resonance mass spectrometry: A primer. Mass Spectrometry Reviews, 17: 1-35.

McCord, T.B. et al., 1998. Salts on Europa's surface detected by Galileo's near infrared mapping spectrometer. Science, 280: 1242-1245.

McCord, T.B., Hansen, G.B. and Hibbitts, C.A., 2001. Hydrates salt minerals on Ganymede's surface: Evidence of an ocean below. Science, 292: 1523-1525.

McCord, T.B. et al., 1999. Hydrated salt minerals on Europa's surface from the Galileo near-infrared mapping spectrometer (NIMS) investigation. Journal of Geophysical Research, 104: 11827-11851.

McHenry, L., 2009. Element mobility during zeolitic and argillic alteration of volcanic ash in a closed-basin lacustrine environment: Case study Olduvai Gorge, Tanzania. Chemical Geology, 265: 540-552.

McJunkin, T.R. and Scott, J.R., 2006. Fuzzy logic classification of imaging laser desorption Fourier transform mass spectrometry data. arXiv:cs.AI/0611085.

McJunkin, T.R., Tremblay, P.L. and Scott, J.R., 2002. Automation and control of an imaging internal laser desorption Fourier transform mass spectrometer (I^2LD-FTMS). Journal of the Association for Laboratory Automation, 7: 76-83.

McKay, C.P., 2007. An approach to searching for life on Mars, Europa, and Enceladus. Space Science Reviews, 135: 49-54.

McLafferty, F.W. and Tureček, F., 1993. Interpretation of Mass Spectra. University Science Books, Sausalito, CA, 225-282 pp.

McLennan, S.M. et al., 2005. Provenance and diagenesis of the evaporite-bearing Burns formation, Meridiani Planum, Mars. Earth and Planetary Science Letters, 240(1): 95-121.

Morris, R.V. et al., 2000. Mineralogy, composition, and alteration of Mars Pathfinder rocks and soils: Evidence from multispectral, elemental, and magnetic data on terrestrial analogue, SNC meteorite, and Pathfinder samples. Journal of Geophysical Research-Planets, 105(E1): 1757-1817.

Müller, L.A., 1927. Absorption spectra of the alkali halides in aqueous solutions and in vapors. Ann. Phys., 82: 39-66.

Navarro-Gonzalez, R. et al., 2006. The limitations on organic detection in Mars-like soils by thermal volatilization-gas chromatography-MS and their implications for the Viking results. Proceedings of the National Academy of Sciences of the United States of America, 103(44): 16089-16094.

Ohno, H., Igarashi, M. and Hondoh, T., 2006. Characteristics of salt inclusions in polar ice from Dome Fuji, East Antarctica. Geophysical Research Letter, 33: L08501.1-L08501.5.

Orlando, T.M., McCord, T.B. and Grieves, G.A., 2005. The chemical nature of Europa surface material and the relation to a subsurface ocean. Icarus, 177: 528-533.

Oro, J., 1979. Viking mission and the question of life on Mars- introduction. Journal of Molecular Evolution, 14: 3-4.

Parnell, J. et al., 2007. Searching for Life on Mars: Selection of Molecular Targets for ESA's Aurora ExoMars Mission. Astrobiology, 7: 578-604.

Pastor, S.J. and Wilkins, C.L., 1997. Analysis of hydrocarbon polymers by matrix-assisted laser desorption/ionization Fourier transform mass spectrometry. Journal of the American Society for Mass Spectrometry, 8(3): 225-233.

Peck, S.B., 1974. Unusual mineralogy of the Crystal Pit Spatter Cone, Craters of the Moon National Mounument, Idaho. NSS Bulletin, 36(1): 19-24.

Peterson, S.B., Nelson, W., Madu, B. and Shurvell, H.F., 2007. Meridianiite: A new mineral species observed on Earth and predicted to exist on Mars. American Mineralogist, 92: 1756-1759.

Plekan, O., Feyer, V., Richter, R., Coreno, M. and Prince, K.C., 2008. Valence photoionization and photofragmentation of aromatic amino acids. Molecular Physics, 106: 1143-1153.

Poels, K., Van Vaeck, L. and Gijbels, R., 1998. Microprobe speciation analysis of inorganic solids by Fourier transform laser mass spectrometry. Analytical Chemistry, 70: 504-512.

Porat, I., Waters, B.W., Teng, Q. and Whitman, W.B., 2004. Two biosynthetic pathways for aromatic amino acids in the archaeon *Methanococcus maripaludis*. Journal of Bacteriology, 186: 4940-4950.

Raczyńska, E.D., Gal, J.F., Maria, P.C., Zientara, K. and Szelag, M., 2007. Application of FT-ICR-MS for the study of proton-transfer reactions involving biomolecules. Analytical and Bioanalytical Chemistry, 389(5): 1365-1380.

Rankin, A.M., Wolff, E.W. and Martin, S., 2002. Frost flowers: Implicatoins for tropospheric chemistry adn ice core interpretation. Journal Geophysical Research, 107: 4683.

Reid, M., 1995. Processes of mantle enrichment and magmatic differentiation in the eastern Snake River Plain: Th isotope evidence. Earth and Planetary Science Letters, 131: 239-254.

Richardson, C., Hinman, N., McJunkin, T., Kotler, J. and Scott, J., 2008. Exploring biosignatures associated with thenardite by geomatrix-assisted laser desorption/ionization Fourier transform ion cyclotron resonance mass spectrometry (GALDI-FTICR-MS). Geomicrobiology Journal, 25(7): 432-440.

Richardson, C., Hinman, N. and Scott, J., 2009. Effect of thenardite on the direct dectection of aromatic amino acids: Implications for the search for life in the solar system. International Journal of Astrobiology, 8(4): 291-300.

Rodgers, R.P., Lazar, A.C., Reilly, P.T.A., Whitten, W.B. and Ramsey, J.M., 2000. Direct determination of soil surface bound polycyclic aromatic hydrocarbons in petroleum-contaminated soils by real time aerosol mass spectrometry. Analytical Chemistry, 72(20): 5040-5046.

Rodier, C., Sternberg, R., Raulin, F. and Vidal-Madjar, C., 2001. Chemical derivatization of amino acids for in situ analysis of Martian samples by gas chromatography. Journal of Chromatography A, 915(1-2): 199-207.

Rodriquez-Navarro, C., Doehne, E. and Sebastian, E., 2000. How does sodium sulfate crystalllize? Implications for the decay and testing of building materials. Cement and Concrete Research, 30: 1527-1534.

Ryzhov, V., Dunbar, R.C., Cerda, B. and Wesdemiotis, C., 2000. Cation-pi effects in teh complexation of Na+ adn K+ with Phe, Tyr, and Trp in the gas phase. American Society of Mass Spectrometry, 11: 1037-1046.

Sack, T.M., Lapp, R.L., Gross, M.L. and Kimble, B.J., 1984. A Method for the Statistical Evaluation of Accurate Mass Measurement Quality. International Journal of Mass Spectrometry and Ion Processes, 61(2): 191-213.

Sakimoto, S., Gregg, T., Hughes, S.S. and Chadwick, J., 2003. Re-assessing plains-style volcanism on Mars, Sixth International Conference on Mars, pp. 3197.pdf.

Scott, J.R. et al., 2007. Searching for biosignatures as signs of life using GALDI-FTMS. Journal of the Idaho Academy of Science: (in press).

Scott, J.R., McJunkin, T.R. and Tremblay, P.L., 2003. Automated analysis of mass spectral data using fuzzy logic classification. Journal of the Association for Laboratory Automation (JALA), 8(2): 61-63.

Scott, J.R., Schürch, S., Moore, S. and Wilkins, C.L., 1997. Evaluation of MALDI-FTMS for analysis of peptide mixtures generated by ladder sequencing. International Journal of Mass Spectrometry and Ion Processes, 160(1-3): 291-302.

Scott, J.R. and Tremblay, P.L., 2002. Highly reproducible laser beam scanning device for an internal source laser desorption microprobe Fourier transform mass spectrometer. Review of Scientific Instruments, 73(3): 1108-1116.

Scott, J.R., Yan, B. and Stoner, D.L., 2006 Spatially correlated spectroscopic analysis of microbe-mineral interactions. Journal of Microbiological Methods 67: 381-384.

Soltzberg, L.J. and Patel, P., 2004. Small molecule matrix-assisted laser desorption/ionization time-of-flight mass spectrometry using a polymer matrix. Rapid Communications in Mass Spectrometry, 18(13): 1455-1458.

Speir, J.P. and Amster, I.J., 1992. Substrate-assisted laser desorption of neutral peptide molecules. Analytical Chemistry, 64(9): 1041-1045.

Speir, J.P., Gorman, G.S. and Amster, I.J., 1993. Fe^{+} chemical ionization of peptides. Journal Of The American Society For Mass Spectrometry, 4(2): 106-110.

Spencer, R.J., 2000. Sulfate minerals in evaporite deposits. In: C.N. Alpers, J.L. Jambor and D.K. Nordstrom (Editors), Sulfate minerals: Crystallography, geochemistry, and environmental significance. Mineralogical Society of America, Washington, D. C., pp. 173-192.

Squyres, S.W. et al., 2004. The Opportunity Rover's Athena Science Investigation at Meridiani Planum, Mars. Science, 306(5702): 1698-1703.

Stearns, H.T., 1963. Geology of the Craters of the Moon, Idaho. Craters of the Moon Natural History Association, Caldwell, Idaho.

Storrie-Lombardi, M.C., Hug, W.F., McDonald, G.D., Tsapin, A.I. and Nealson, K.H., 2001. Hollow cathode ion lasers for deep ultraviolet Raman spectroscopy and fluorescence imaging. Review of Scientific Instruments, 72(12): 4452-4459.

Stout, M.Z. and Nicholls, J., 1977. Mineralogy and petrology of Quaternary lavas from the Snake River Plain, Idaho. Canadian Journal of Earth Sciences, 14: 2140-2156.

Stout, M.Z., Nicholls, J. and Kuntz, M.A., 1994. Petrological and mineralogical variations in 2500-2000 yr B.P. lava flows, Craters of the Moon lava field, Idaho. Journal of Petrology, 35(6): 1681-1715.

Stump, M.J. et al., 2002. Matrix-assisted laser desorption mass spectrometry. Applied Spectroscopy Reviews, 37(3): 275-303.

Tanaka, K. et al., 1988. Protein and polymer analyses up to m/z 100,000 by laser ionization time-of-flight mass spectrometry. Rapid Communications in Mass Spectrometry, 2(8): 151-153.

Tomlinson, M.J., Scott, J.R., Wilkins, C.L., Wright, J.B. and White, W.E., 1999. Fragmentation of an alkali metal-attached peptide probed by collision-induced dissociation Fourier transform mass spectrometry and computational methodology. Journal of Mass Spectrometry, 34(9): 958-968.

Tosca, N.J. and McLennan, S.M., 2006. Chemical divides and evaporite assemblages on Mars. Earth and Planetary Science Letters, 241: 21-31.

Trimpin, S., Rouhanipour, A., Az, R., Rader, H.J. and Mullen, K., 2001. New aspects in matrix-assisted laser desorption/ionization time-of-flight mass spectrometry: A universal solvent-free sample preparation. Rapid Communications in Mass Spectrometry, 15(15): 1364-1373.

Van Vaeck, L., Adriaens, A. and Adams, F., 1998a. Microscopical speciation analysis with laser microprobe mass spectrometry and static secondary ion mass spectrometry. Spectrochimica Acta Part B-Atomic Spectroscopy, 53(2): 367-378.

Van Vaeck, L. and Gijbels, R., 1990. Potential and limitations for inorganic and organic micro-analysis. Fresenius Journal of Analytical Chemistry, 337: 755-765.

Vassallo, A. and Finnie, K., 1992. Infrared emission spectroscopy of some sulfate minerals. Applied Spectroscopy, 46: 1477-1482.

Vermillion-Salsbury, R.L. and Hercules, D.M., 2002. 9-aminoacridine as a matrix for negative mode matrix-assisted laser desorption/ionization. Rapid Communications in Mass Spectrometry, 16(16): 1575-1581.

Vorsa, V., Kono, T., Willey, K. and Winograd, N., 1999. Femtosecond photoionization of ion beam desorbed aliphatic and aromatic amino acids: fragmentation via alpha-cleavage reactions. Journal of Physical Chemistry, B(103): 7889-7895.

Weast, R.C. (Editor), 1984. Handbook of Chemistry and Physics. CRC, Boca Raton.

Wiedemann, H. and Smykatz-Kloss, W., 1981. Thermal studies of thenardite. Thermochimica Acta, 50: 17-29.

Wiens, R.C. et al., 1997. Sputtering products of sodium sulfate: Implications for Io's surface adn for sodium-bearing molecules in the Io torus. Icarus, 128(2): 386-397.

Willey, K., Vorsa, V., Braun, R. and Winograd, N., 1998. Postionization of molecules desorbed from surfaces by keV Ion bombardment with femtosecond laser pulses. Rapid Communications in Mass Spectrometry, 12: 1253-1260.

Wilson, K.R. et al., 2006. Thermal vaporization of biological nanoparticles: fragment-free vacuum ultraviolet photoionization mass spectra of Tryptophan, Phenylalanine-Glycine-Glycine, and B-Carotene. Journal Physical Chemistry, A(110): 2106-2113.

Wu, H.P., Su, C.L., Chang, H.C. and Tseng, W.L., 2007. Sample-first preparation: A method for surface-assisted laser desorption/ionization time-of-flight mass spectrometry analysis of cyclic oligosaccharides. Analytical Chemistry, 79(16): 6215-6221.

Wyrick, D., Ferrill, D., Morris, A., Colton, S. and Sims, D., 2004. Distribution, morphology, and origins of martian pit crater chains. Journal of Geophysical Research, 109: E06005.

Yalcin, T., Wallace, W.E., Guttman, C.M. and Li, L., 2002. Metal powder substrate-assisted laser desorption/ionization mass spectrometry for polyethylene analysis. Analytical Chemistry, 74(18): 4750-4756.

Yan, B., McJunkin, T.R., Stoner, D.L. and Scott, J.R., 2005. Mineral identification in basalts using automated mass spectral data analysis. Geochimica et Cosmochimica Acta, 69(10): A797-A797.

Yan, B., McJunkin, T.R., Stoner, D.L. and Scott, J.R., 2006. Validation of fuzzy logic method for automated mass spectral classification for mineral imaging. Applied Surface Science, 253(4): 2011-2017.

Yan, B., Stoner, D.L., Kotler, J.M., Hinman, N.W. and Scott, J.R., 2007a. Detection of biosignatures by geomatrix-assisted laser desorption/ionization (GALDI) mass spectrometry. Geomicrobiology Journal, 24: 379-385.

Yan, B., Stoner, D.L. and Scott, J.R., 2007b. Direct LD-FTMS detection of mineral-associated PAHs and their influence on the detection of other organics. Talanta, 72: 634-641.

Yao, J., Scott, J.R., Young, M.K. and Wilkins, C.L., 1998a. Importance of matrix : analyte ratio for buffer tolerance using 2,5-dihydroxybenzoic acid as a matrix in matrix-assisted laser desorption/ionization Fourier transform mass spectrometry and matrix-assisted laser desorption/ionization time of flight. Journal of The American Society for Mass Spectrometry, 9: 805-813.

Zhu, M., Xie, H., Guan, H. and Smith, R., 2006. Mineral and lithologic mapping of martian low albedo regions using OMEGA data, Lunar and Planetary Science XXXVII pp. 2173.pdf.

Zimmermann, R., Van Vaeck, L., Davidovic, M., Beckmann, M. and Adams, F., 2000. Analysis of polycyclic aromatic hydrocarbons (PAH) adsorbed on soot particles by Fourier transform laser microprobe mass spectrometry (FT LMMS): Variation of the PAH patterns at different positions in the combustion chamber of an incineration plant. Environmental Science & Technology, 34(22): 4780-4788.

Zolotov, M.Y. and Shock, E.L., 2001. Composition and stability of salts on the surface of Europa and their oceanic origin. Journal of Geophysical Research, 106(E12): 32815-32827.

CHAPTER 4: SECONDARY SULFATE MINERALIZATION AND BASALTIIC CHEMISTRY OF CRATERS OF THE MOON NATIONAL MONUMENT, IDAHO: A VIEW INTO THE MARTIAN SUBSURFACE

C. Doc Richardson [a], Nancy W. Hinman [a], Lindsay J. McHenry [b], J. Michelle Kotler [a], Jill R. Scott [*c]

[a] Geosciences Department, University of Montana, 32 Campus Dr., Missoula, MT 59812, USA

[b] Department of Geosciences , University of Wisconsin-Milwaukee, P.O Box 413, 2200 E. Kenwood Blvd., WI 53201, USA

[c] Chemical Sciences, Idaho National Laboratory, 1765 N. Yellowstone Hwy., Idaho Falls, ID 83415, USA

Short Title: SECONDARY SULFATE MINERALS AT CRATERS OF THE MOON NATIONAL MONUMENT, ID.

4.1. ABSTRACT

Secondary deposits associated with the basaltic caves of Craters of the Moon National Monument (COM) in southern Idaho were examined using X-ray powder diffraction (XRD), X-ray fluorescence spectrometry (XRF), Fourier transform infrared spectrometry (FTIR), and Fourier transform ion cyclotron resonance mass spectrometry (FTICR-MS). Good agreement was found between XRD, FTIR, and FTICR-MS for mineral characterization. The secondary mineral assemblages are dominated by Na-sulfate minerals (thenardite, mirabilite) with a small fraction of the deposits containing minor concentrations of Na-carbonate minerals. The assemblages are found as white, efflorescent deposits in small cavities along the cave walls and ceilings and as localized mounds on the cave floors. Formation of the deposits is likely due to direct and indirect

physiochemical leaching of meteoritic water through the overlying basalts. Whole rock data from the overlying basaltic flows are characterized by their extremely high iron concentrations, making them good analogs for martian basalts. Understanding the physiochemical pathways leading to secondary mineralization at COM is also important because lava tubes and basaltic caves are present on Mars.

Keywords: Craters of the Moon National Monument, thenardite, Mars, secondary sulfate mineralization, FTIR, XRD, FTICR-MS

4.2. INTRODUCTION

Basaltic caves and lava tubes are widespread on Earth, offering stable physicochemical conditions for the formation and preservation of secondary minerals. Unfortunately, detailed investigations regarding the minerogenetic mechanisms of secondary cave deposits in basaltic environments have been limited (Forti, 2005; Hill and Forti, 1997), even though these minerals provide valuable insight into past aqueous activity and any associated biological activity during mineral formation. Recently, basaltic caves and lava tubes have been observed on Mars (Cushing et al., 2007; Wyrick et al., 2004). These subsurface features could intercept groundwater and provide adequate physiochemical conditions for the mineralization and subsequent preservation of secondary minerals on Mars. Additionally, these stable environments are ideal locations to search for evidence of past biological activity, as they offer protection from the harsh oxidizing martian atmosphere. Thus, investigating the formation of secondary

mineral assemblages in terrestrial basaltic caves is imperative in the search for past evidence of aqueous activity and associated biological activity in the subsurface of Mars.

In this study, we identify and characterize the secondary minerals found within the basaltic subsurface of Craters of the Moon National Monument (COM), while comparing the basaltic chemical signatures of COM to that of Mars. Secondary Na-sulfate (thenardite; Na_2SO_4), found at COM, is typically found in non-marine environments such as evaporitic salt flats (sabkhas, playas), fumarolic exhalations (Hill and Forti, 1997), and subsurface Antarctic ice (Ohno et al., 2006). Recently, Na-sulfates have been found on Mars in evaporitic environments (Mangold et al., 2008; McLennan et al., 2005; Zhu et al., 2006) and have also been suggested to be a constituent of the martian regolith based on chemical/mineralogical modeling (Tosca and McLennan, 2006). The occurrence of thenardite and polyhydrated sulfate minerals (e.g., gypsum, kieserite) on Mars indicates the past existence of water on the planet. Therefore, the presence of sulfate speleogenesis at COM offers an excellent opportunity to investigate similar formational mechanisms and physiochemical processes that may occur in the subsurface of Mars.

4.3. SITE DESCRIPTION

The lava flows at COM (43.417° N; 113.518 ° W) collectively cover 1,600 km^2 along the northern flank of the Eastern Snake River Plain (ESRP) in southern Idaho (Kuntz et al., 1992). Radiocarbon dating of underlying carbonized vegetation has constrained the basaltic flows between 15 ka and 2.1 ka, representing eight eruptive periods (Kuntz et al., 1986; Kuntz et al., 1992; Reid, 1995). These eruptive events originated along the Great Rift, a tensional feature that extends approximately 85 km,

running parallel to the basin and range fault systems (Fig. 4.1), suggesting that the Great Rift may be a extension of basement faulting allowing the ascent of COM lavas (Kuntz et al., 2002; Leeman et al., 1976). Unlike the majority of the basaltic flows in the ESRP, which are olivine tholeiites (Hughes et al., 1999), chemical compositions of the COM basalts are slightly more evolved (Kuntz et al., 1986; Stout and Nicholls, 1977; Stout et al., 1994) with elevated Fe and alkali-elements and depleted alkali-earth elements (Hughes et al., 1999). Since all basaltic flows in the ESRP are thought to originate from a single parent magma, the variance likely reflects extensive crustal assimilation or magma fractionation (Kuntz et al., 1986; Kuntz et al., 1992; Leeman et al., 1976).

Of the 60 cumulative flows that comprise COM, the young Blue Dragon flow (~2.1 ka) contains the majority of the accessible caves and lava tubes. These features likely reflect the younger age of the flow because they have had less time to undergo gravitational collapse.

4.4. Sample Collection and Analytical Methods

4.4.1. Mineral Collection

Samples of the secondary deposits were collected biannually between June 2006 and October 2008 from several cave locations within the Blue Dragon flow. Distances between these caves ranged from several hundred meters to approximately two kilometers. Deposits were carefully transferred to glass vials, making sure no extraneous material or contamination was introduced. Observations were noted and compared to previous visits to determine any physical alterations or changes in mineral abundances.

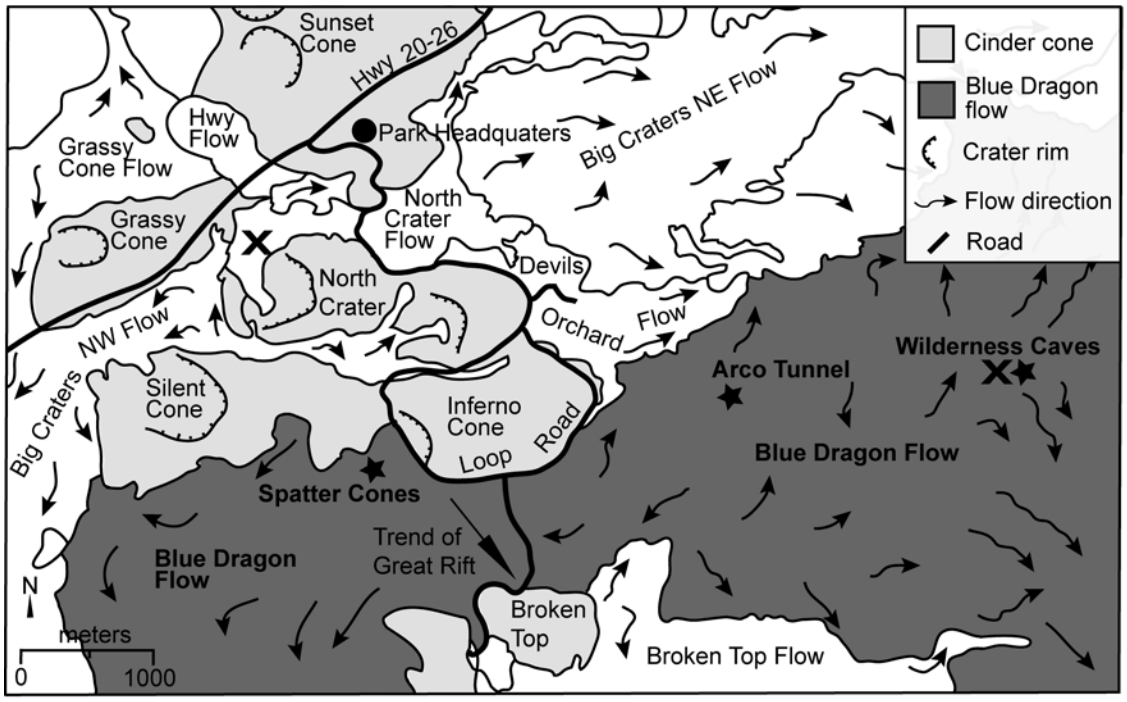

Figure 4.1. Map of COM lava field showing extent of Blue Dragon flow. Location of Arco Tunnel, Wilderness Caves and spatter cones are also shown (indicated by ★'s). Location of basaltic samples used for whole rock analyses are indicated by ×'s. Map modified from Kuntz (1989).

4.4.2. X-ray Powder Diffraction

Samples were ground into a fine powder with a corundum mortar and pestle, before being mounted on glass slides for X-ray powder diffraction (XRD) studies for mineral characterization. Analyses were performed using a Philips APD 3720 X-ray diffractometer with a step size of 0.01 °2θ with a scan rate of 0.24 °2θ/min. Spectral features were compared to published mineral patterns from the Joint Committee on Powder Diffraction Standards (JCPDS).

4.4.3. Fourier Transform Infrared Spectroscopy

Attenuated total reflectance Fourier transform infrared spectroscopy (FTIR) spectra were obtained using a Thermo Nicolet Nexus 670 FTIR spectrometer (Madison,

WI). Spectra were collected with an average of 100 scans with a resolution of 4 cm^{-1}. All spectra were measured in absorbance between 4000 cm^{-1} and 500 cm^{-1}.

4.4.4. Fourier Transform Ion Cyclotron Resonance-Mass Spectrometry Instrumentation and Parameters

Fourier transform ion cyclotron resonance-mass spectrometry (FTICR-MS) spectra of the mineral deposits were obtained using a laboratory-built imaging laser desorption FTICR-MS (McJunkin et al., 2002b; Scott et al., 2003; Scott and Tremblay, 2002) with a 7 T Oxford (Oxford, England) superconducting magnet. Parameters have been previously described (Kotler et al., 2008b; Richardson et al., 2008; Richardson et al., 2009; Yan et al., 2007a; Yan et al., 2007b). All spectra were acquired with single laser shots in both positive and negative mode. Peaks were identified by systematic analysis following procedures previous described in Kotler et al. (2008).

4.4.5. X-ray Fluorescence

Bulk compositions of the COM basalts were analyzed by X-ray fluorescence (XRF). One gram of finely ground sample powder was combined with 10 g of flux (50:50 LiT:LiM with integrated LiBr non-wetting agent) and ~1 g of an oxidizer (ammonium nitrate). The mixture was fused in a platinum crucible in a Claise M4 fluxer using a predetermined 21-min fusion routine (high temperature ~1050 °C) before being analyzed using a Bruker S4 Pioneer WD-XRF (Madison, WI). The instrument was calibrated for major and minor elements using 11 USGS rock standards. More detailed methods are reported in (McHenry, 2009). Because of difficulties with sulfur loss during fusion, a separate pressed pellet was prepared for XRF analysis for sulfur. The sample was powdered using a tungsten carbide shatterbox, and then ten grams of sample was mixed with a wax binder (in the shatterbox) for 30 s. The powder was pressed into a

40 mm pellet using a semiautomatic press, where it was held at 30 tons for one minute. The pressed pellet was then analyzed using the Bruker S4 Pioneer, using a calibration curve derived from six USGS rock standards with published sulfur concentrations prepared using the same method.

4.5. RESULTS

4.5.1. Mineral Deposits

The caves and lava tubes of the Blue Dragon flow host a majority of the secondary sulfate deposits found at COM. Field observations and past reports indicate that secondary minerals are found throughout the flow within caves, lava tubes, and beneath spatter cones (Karlo et al., 1980; Peck, 1974). Their presence in the Blue Dragon flow likely results from the young age and morphological characteristics of the flow, rather than chemical and mineralogical differences between them and the older flows (Stout et al., 1994). The caves and lava tubes of the Blue Dragon flow are concentrated in a few locations (Wilderness Caves, Cave Trail caves) and vary in size from small and shallow to >1 km in length. Extent of the Blue Dragon flow and locations of caves used in this study can be seen in Figure 4.1. Secondary sulfate minerals occur in caves of all sizes. The more extensive caves (e.g., Arco Tunnel) maintain cold conditions (< 10 °C, ~ 75% relative humidity) year round and associated lower-temperature secondary minerals (e.g., mirabilite).

The secondary deposits are found in small cavities on the ceiling and walls and as localized mounds on the cave floors (Fig. 4.2A, 4.3A). Floor deposits are found intermittently dispersed as localized, efflorescent, white, powdery mounds, with thicknesses ranging from ~ 1 cm to ~ 10 cm in depth. These deposits are not a direct

alteration product of the weathering basalts, as the interface between the authigenic minerals and the cave floors is quite abrupt, showing no evidence of basaltic replacement or mixing of basaltic minerals (plagioclase, diopside, olivine). Likewise, the floor deposits do not seem to form directly as precipitates from liquid water, as the precipitates are not found in the deepest spots on the cave floor or as uniform coatings in the lowest areas of the cave floor. In addition to the floor deposits, secondary deposits are found within small (< 2 cm diameter) cavities and cracks on the ceilings and walls (Fig. 4.2A). These deposits are found in the same caves, but are less frequent than the floor deposits. No spatial correlation is observed between ceilings deposits and their floor counterparts.

The secondary sulfate deposits appear to be a seasonal feature. Observations made between October and June of 2007 and 2008 showed significant differences in the amount of each representative deposit. In October, fewer mineral deposits were found and were general smaller in abundance. Conversely, in June, the deposits were more abundant and larger. It appears that the formation of sulfate minerals fluctuates on an annual basis, dissolving during wet months and reprecipitating when dry. Changes in temperature and relative humidity within the caves also appear to be important, especially for the Na-sulfate minerals. Mirabilite ($Na_2SO_4 \cdot 10H_2O$), the hydrous, low-temperature Na-sulfate, was observed during June visits when the cave temperatures and relative humidity were more conducive for mirabilite formation and preservation. For example,

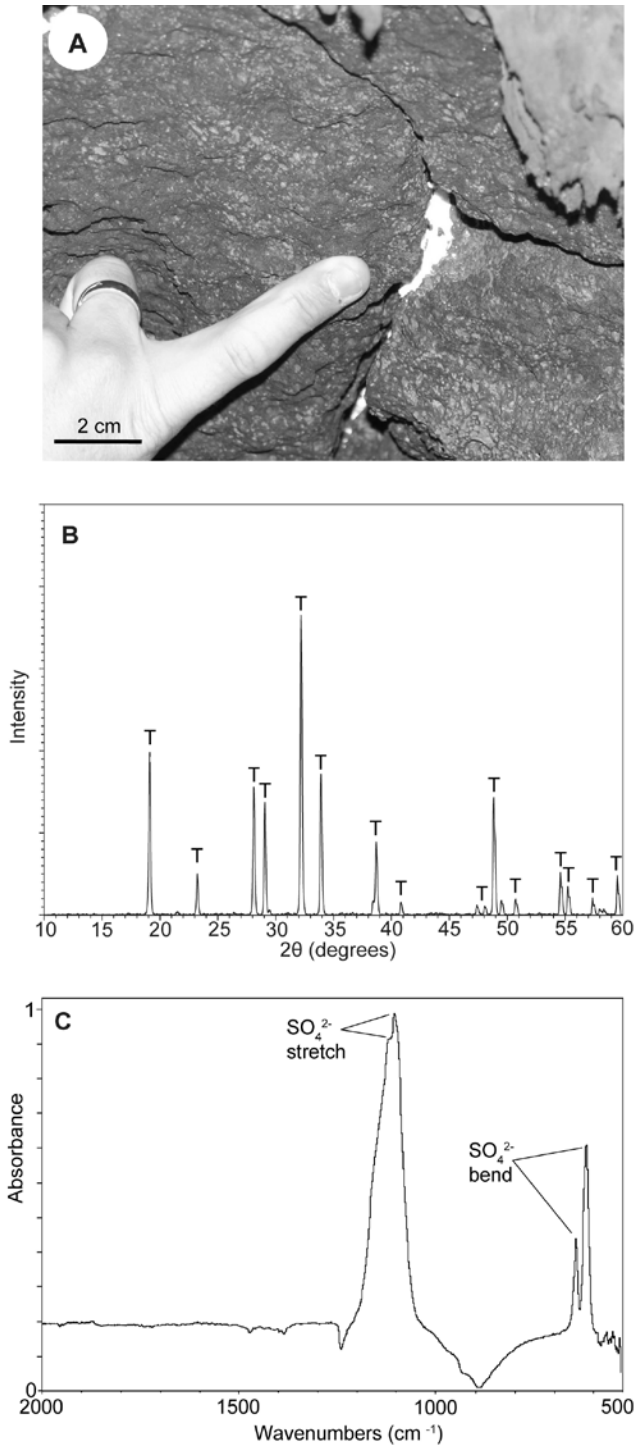

Figure 4.2. (A) Photograph of secondary deposit within a ceiling cavity taken in a cave from the Blue Dragon flow (B) Background corrected XRD of corresponding deposit demonstrating the sample consists entirely of thenardite. (C) FTIR spectrum from same deposit confirming the sample is dominated by thenardite with no evidence of Na-carbonates. Sample is representative of a majority of the secondary sulfate deposits found in the subsurface of COM.

temperature and relative humidity of a unnamed cave in the Wilderness Caves area was recorded to be ~ 8 °C and 73%, respectively. Conversely, in October, the cave was slightly warmer (~ 15 °C) and drier (67% relative humidity) and thenardite was present instead of mirabilite. The dehydration-rehydration between Na-sulfate species occurs with slight changes in temperature and relative humidity, as the efflorescent susceptibility of mirabilite make it extremely vulnerable to dehydration, occurring within minutes depending on air temperature and relative humidity (Rodriquez-Navarro et al., 2000), which is consistent with the conversion of mirabilite to thenardite and vice versa with only slight changes in cave temperature and relative humidity between October and June visits.

4.5.2. Secondary Mineral Identification

Secondary deposits at COM are dominated by Na-sulfate minerals (thenardite, mirabilite) with minor concentrations of Na-carbonate minerals (i.e., trona, natron) (Table 4.1). The bulk XRD spectrum shown in Figure 4.2B is representative of a majority of the secondary deposits analyzed. Peak assignments show the sample is composed entirely of thenardite with no evidence of any other mineral constituent, further supported by the FTIR spectrum shown in Figure 4.2C. The FTIR spectrum shows three dominant bands at 1109 cm^{-1}, 639 cm^{-1} and 621 cm^{-1}, corresponding to a SO_4^{2-} ν3 symmetric stretch and a ν4 double bend, respectively. The symmetric stretch at 1109 cm^{-1} has an associated ν3 stretch at 1129 cm^{-1}. These double bands are consistent with synthetic samples of thenardite observed in this study and with previously reported spectra of thenardite (Farmer, 1974; Lane, 2007; Vassallo and Finnie, 1992). No bands corresponding to the carbonate oxyanion were observed in this particular sample.

Although all samples consist primarily of thenardite or mirabilite depending on cave conditions, approximately 50% of the samples analyzed also have minor concentrations of Na-carbonate minerals (trona, natron). Evidence of Na-carbonates can be seen in a representative XRD spectrum in Figure 4.3B, which along with thenardite has numerous peaks attributed to trona and/or natron. As with the XRD spectrum in Figure 4.3B, the FTIR spectrum (Fig. 4.3B) shows prominent absorbance bands consistent with carbonate and sulfate moieties. The doublet bands of sulfate near 1169 cm^{-1}, 1130 cm^{-1}, 637 cm^{-1}, and 614 cm^{-1} are reminiscent of thenardite, while additional bands suggest the presence of Na-carbonate species. The most prominent bands of the carbonate anion are seen at 1691 cm^{-1}, 1451 cm^{-1} and 847 cm^{-1}, with minor bands at 1764 cm^{-1},1032 cm^{-1}, 875 cm^{-1}, and 680 cm^{-1}. Exact carbonate species identification using FTIR was unobtainable, as bands of various Na-carbonate and bicarbonate species often overlap, making accurate identification difficult.

Table 4.1. Mineral assemblages secondary deposits as determined by XRD, FTIR, and FTICR-MS.

		XRD			FTIR			FTICR-MS[b]	
	Cave Location[a]	Na-sulfate	burkeite	Na-carbonate	Na-sulfate	burkeite	Na-carbonate	Na-sulfate	Na-carbonate
Floor deposits									
071010.1A	WC	XXX	-	-	XXX	-	-	XXX	-
70604.1A	WC	XX	-	X	XX	+	X	XXX	+
070604.3A	WC	XXX	-	+	XXX	-	+	XXX	+
071010.1B	WC	XX	X	+	XX	X	X	XX	X
COM-781	AT	XXX	-	-	XXX	-	-	XXX	-
070605.5a	AT	XX	X	+	XX	+	X	XX	+
Ceiling and wall deposits									
071010.1A	WC	XXX	-	-	XXX	-	-	XXX	-
080607.3a	AT	XXX	-	-	XXX	-	-	XXX	+
070605.5a	AT	XX	X	+	XX	+	X	XX	X

XXX=abundant, XX= common, X = between common and rare, + = rare, - = not detected

[a] AT= Arco Tunnel, WC= Wilderness Caves.

[b] FTICR-MS identification was based on positive and negative spectra.

In addition to sulfate and carbonate species, several peaks in the XRD spectrum (Fig. 4.3B) are attributed to the presence of the carbonate-sulfate salt burkeite ($Na_6CO_3(SO_4)_2$). FTIR spectral features in Figure 4.3C support the presence of burkeite, by the characteristic band at 1764 cm^{-1} due to a ν3 bend of CO_3, which is not characteristic of the mentioned Na- carbonate or Na-sulfate species (Farmer, 1974; Lane, 2007). Other CO_3 and SO_4 spectral bands characteristic of burkeite are seen (at 1128 cm^{-1}, ν3 stretch of SO_4; at 637 cm^{-1} and 614 cm^{-1} due to ν4 bend of SO_4; at 1477 cm^{-1} due to ν3 of CO_3; and at 875 cm^{-1} due to ν2 of CO_3), although these bands also correspond to Na-sulfate and Na-carbonate species. Thus definitive evidence of the presence of burkeite is difficult using FTIR spectra when sulfate and carbonate minerals are also present in the sample, however its presence is also supported by the XRD spectra.

4.5.3. Chemical Identification using FTICR-MS

In addition to XRD and FTIR, mineral deposits were characterized using imaging FTICR-MS (Table 4.1). This technique has been used successfully in previous studies of synthetic and natural sulfate minerals (Kotler et al., 2008b; Richardson et al., 2008; Richardson et al., 2009; Yan et al., 2007a), demonstrating its ability to characterize inorganic minerals at a microscopic level. Imaging mass spectrometry is a useful technique for micron-scale identification of compounds and minerals, especially compared to more conventional methods that tend to have problems identifying individual mineral species in heterogeneous mixtures (Van Vaeck et al., 1998). Mass spectrometry techniques yield signals composed of a combination of mineral moieties, including adduct ions formed during the desorption and ionization process. These adduct ions, consisting of one or two intact analyte molecules and a stable ion, allow specific

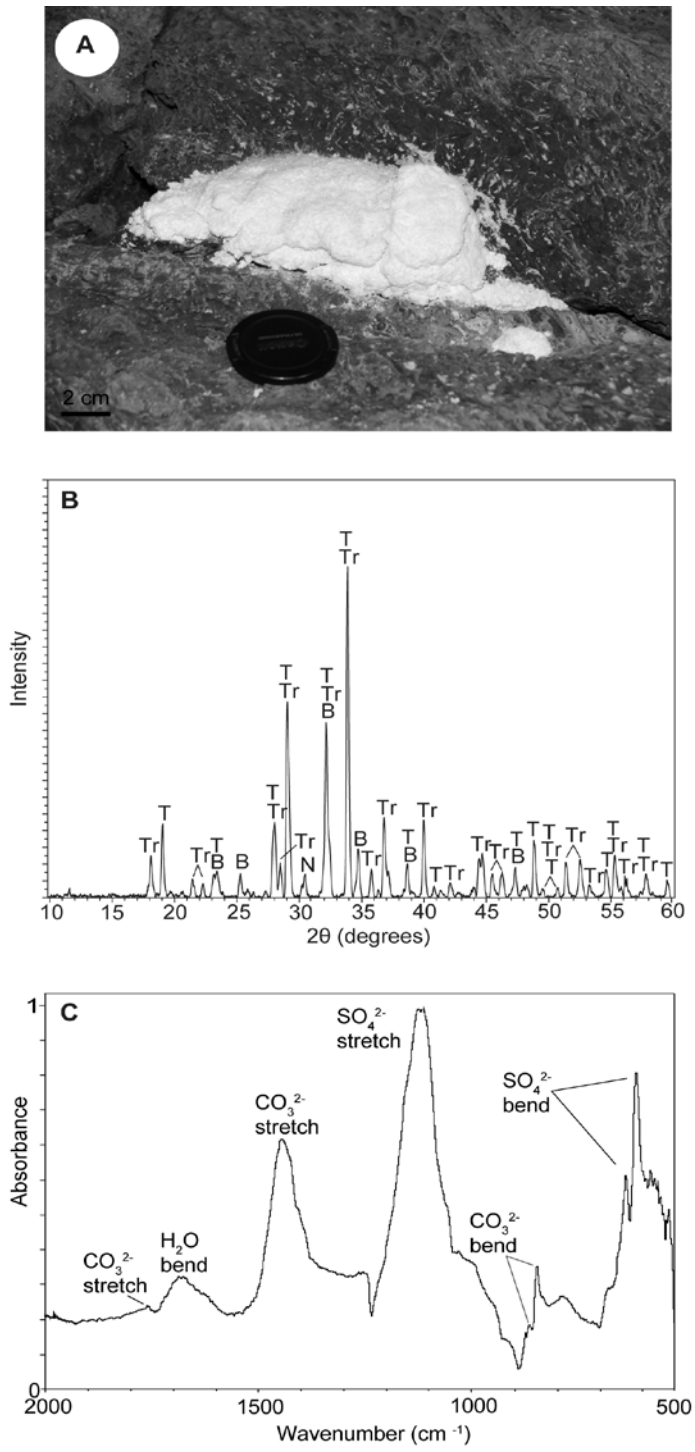

Figure 4.3. (A) Photograph of a secondary floor deposit in a cave within the Blue Dragon flow, (B) Background corrected XRD of corresponding deposit demonstrating the sample is dominated by Na-sulfate with minor concentrations of Na-carbonate minerals and possibly double salt burkeite (thenardite = T; burkeite = B; trona = Tr; natron = N. (C) FTIR spectrum from same deposit confirming the sample is dominated by thenardite with peaks corresponding to Na-carbonates and burkeite.

and accurate identification of the molecule (Poels et al., 1998; Van Vaeck and Gijbels, 1990). Previous mass spectrometry studies involving Na-sulfate species have shown that corresponding adduct ions can be easily and accurately identified by deductive reasoning rather than relying on reference spectra (Poels et al., 1998). Similar studies identifying minerals have also shown that the fingerprints can be determined without specific reference spectra (Poels et al., 1998; Yan et al., 2006).

Figure 4.4 shows the positive and negative mode FTICR-MS spectra of a representative secondary deposit. The sample appears to be dominated by Na-sulfate moieties, consistent with XRD and FTIR analyses. Peaks were identified following the detailed procedures of Kotler et al. (2008) and were systematically compared to a suite of synthetic reference samples. The major peaks in the positive spectrum (Fig. 4.4A) are clearly attributed to Na-sulfate ions, with the exception of peaks at m/z 130, 175, 225, 310, and 393, which contain carbonate adduct ions. Generally, these peaks are less abundant than peaks consisting entirely of Na-sulfate ions. No peaks in the spectrum consist entirely of Na-carbonate constituents, possibly reflecting the lower concentration of carbonate minerals in the sample. Peaks at m/z 62, 110, 165, and 227 are comprised of Na-sulfate ions and have been identified in previous mass spectrometry studies of Na_2SO_4 (Poels et al., 1998; Richardson et al., 2009; Van Vaeck et al., 1998).

The negative mode spectrum of the secondary deposit (Fig. 4.4B) shows similar adduct ions to those observed in the positive mode spectrum. The major peaks in the spectrum are dominated by Na-sulfate adduct ions, while peaks at m/z 166 and 351 contain the carbonate moiety. Peaks consisting entirely of Na-sulfate adduct ions have been previously reported in Na_2SO_4 studies (Poels et al., 1998; Van Vaeck et al., 1998).

As with the positive spectrum, the negative spectrum suggests that the sample consists of Na-sulfate with a minor amount of Na-carbonates. Quantification of the oxyanions is difficult using laser desorption mass spectrometry (LDMS) practices, as the abundance of the ions in the spectrum is not only dependent on the amount of the substance in the sample, but also by its ionization efficiency (Yan et al., 2006) and subsequent gas-phase interactions between the ions (Richardson et al., 2009). The general consistency between the FTICR-MS spectra and the bulk analyses of the XRD and FTIR results between each sample results confirm that imaging laser desorption FTICR-MS is a useful technique for the direct fingerprinting of heterogeneous mineral assemblages (Yan et al., 2006).

4.6. DISCUSSION

XRF whole-rock compositions of the COM basalts (Table 4.2) prove they are an excellent analog for geochemical and mineralogical studies of martian secondary mineral formations. COM basalts are very high in Fe by Earth standards (Kuntz, 1989), and thus, are more comparable to martian basalts than other traditional terrestrial analogs (e.g., Hawaii, Antarctica; (Chevrier et al., 2006; Morris et al., 2000)). Whole-rock chemical comparisons between these environments can be seen in Table 4.2. Although COM and the martian basalts have similar Fe concentrations, they differ substantially in other potentially important elements as do other terrestrial analogs. COM basaltic chemistries are higher in Al, Ti, Na, and K and lower in Mg, Ca, and S than their martian counterparts, which is consistent with previous studies of COM basalts (Hughes et al., 1999; Kuntz et al., 1986; Stout et al., 1994). Despite these differences, the COM basalts are closer to martian basaltic compositions than previously and frequently used terrestrial basalts that suffer from the same limitations but have lower Fe concentrations.

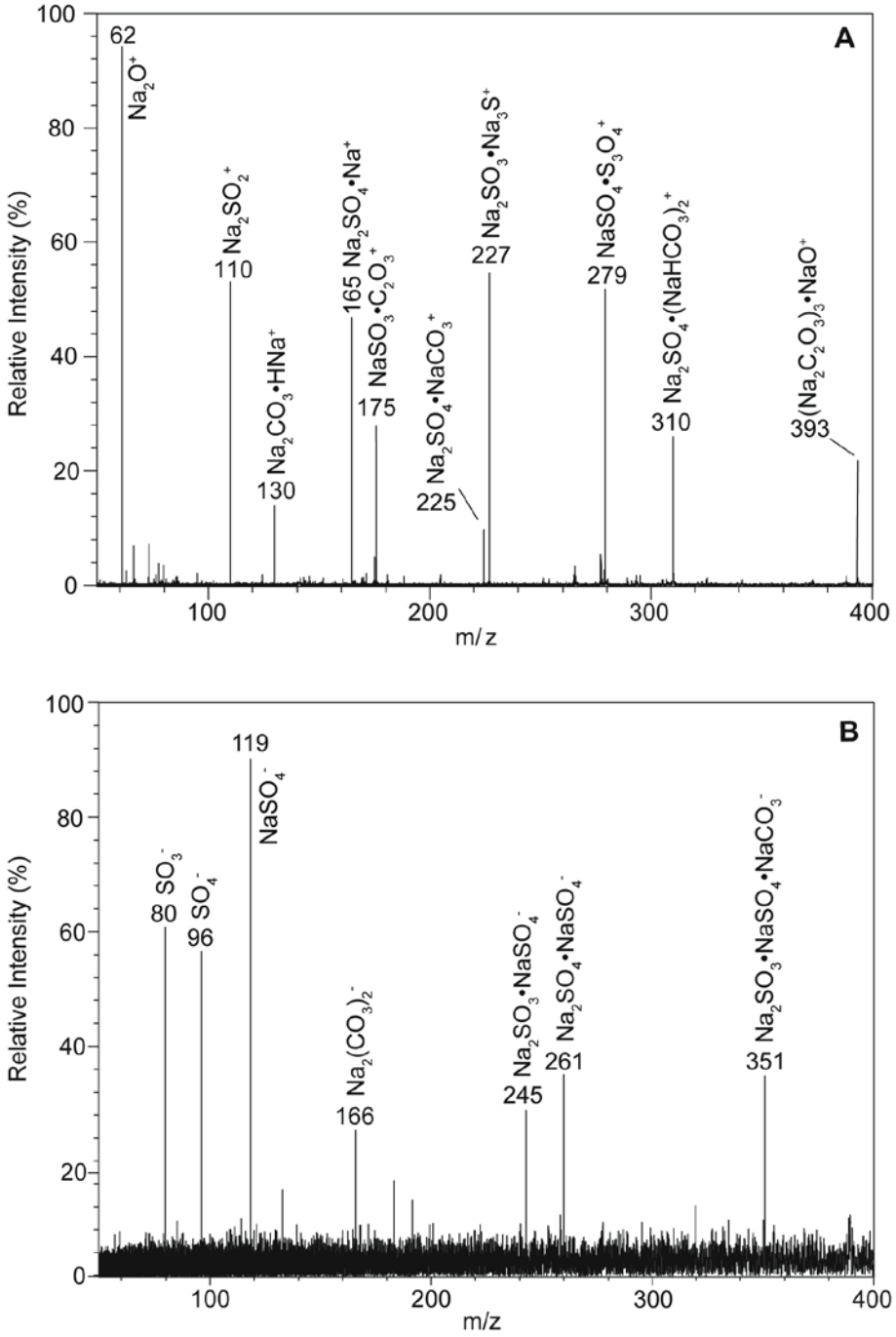

Figure 4.4. Laser desorption FTICR-MS spectra of secondary sulfate deposits from floor deposit within a cave in the Wilderness Caves area. (A) Positive mode spectrum and corresponding (B) negative mode spectrum.

If the basaltic emplacement of COM is indeed analogous to Mars, then lava tubes and caves should be a common feature across the martian landscape and a potentially pristine environment for the preservation of secondary minerals. Lava tubes have been putatively observed by martian orbiters (Drost et al., 2006; Wyrick et al., 2004), in addition to recent observations by the Thermal Emission Imaging System aboard the Mars Odyssey Orbiter, which confirmed the existence of several potential cave openings, along the side of Arsia Mons, the southernmost flank of the Tharsis shield volcanoes (Cushing et al., 2007). Morphological characteristics of these volcanic plains closely resemble the plains-style volcanism found in the ESRP in size, volume, and shape of the basaltic shields (Sakimoto et al., 2003).

Table 4.2. Comparison of COM, Hawaii, and Mars basaltic compositions

	COM flows				Hawaii	Mars Basalts		
Oxide	BD1 [a]	NC [a]	BD2 [b]	BC [b]	MK [c]	Spirit [d]	Sherg [e]	Merid [f]
SiO_2	47.8	48.7	49.0	51.3	49.7	45.4	51.3	38.1
TiO_2	3.0	2.7	2.9	2.5	2.8	0.5	0.9	0.9
Al_2O_3	12.5	12.7	13.4	14.2	17.4	10.9	6.8	6.0
Fe_2O_3T	17.1	16.9	15.3	14.6	12.0	20.0	19.4	19.6
MnO	0.2	0.3	0.2	0.3	0.2	0.4	0.5	0.3
MgO	3.3	3.1	3.3	2.9	3.9	11.9	9.3	7.4
CaO	7.0	6.7	6.9	6.4	6.6	7.4	9.6	4.5
Na_2O	3.1	2.9	3.6	3.6	4.3	2.7	1.4	1.1
K_2O	1.9	2.1	2.0	2.2	1.9	0.1	0.2	0.6
P_2O_5	-	1.8	1.8	1.6	0.9	0.5	0.7	1.0
Cr_2O_3	-	-	-	-		0.6	0.2	0.2
Cl	-	-	-	-		0.1		0.4
SO_3	0.02	-	-	-	0.1	1.2	0.1	21.0
Total	96.0	97.9	-	99.5	99.7	-	100.3	-

[a] Blue Dragon (BD1) and North Crater (NC) Flows, COM. This study.
[b] Blue Dragon(BD2) and Big Crater (BC) flows, COM. From Stout et al. (1994).
[c] Average unaltered Hawaiitic tephra from Mauna Kea (MK). From Morris et al. (2000).
[d] MER Spirit analysis of Adirondack (RAT). From Gellert et al. (2004).
[e] Shergotty meteorite, calculated volatile free. From Lodders (1998).
[f] MER Opportunity analysis of McKittrick (RAT). From Rieder et al. (2004).

The evaporitic assemblages on Mars consist primarily of secondary Mg-, Ca-, and Fe-bearing sulfate minerals and silica; however, spectroscopic signatures suggestive of

minor concentrations of Na-sulfate species have been observed from several evaporitic environments on Mars (Mangold et al., 2008; McLennan et al., 2005; Zhu et al., 2006). Na-sulfates may be more abundant within the secondary assemblages on Mars, as spectroscopic signatures of Mg-, Ca-, and Na-bearing sulfate minerals are sufficiently similar to prevent precise mineral identification (Mangold et al., 2008). Furthermore, chemical/mineralogical modeling suggests that Na-sulfates could form through primary basaltic weathering on Mars (Tosca and McLennan, 2006). The general lack of Na-sulfate and Na-carbonates on Mars could also reflect differences in environmental conditions, as terrestrial thenardite is typically an evaporitic mineral from neutral to alkaline non-marine environments (Spencer, 2000), while Mg and Fe-sulfates, which are common on Mars, are more typical of acidic environments (Chevrier and Mathe, 2006; Clark et al., 2005; Hill and Forti, 1997). This difference is unlikely related to variations in the availability of water, as jarosite and thenardite are both highly soluble and representative of arid conditions. Thenardite also has a solubility that is between the Mg-sulfates of epsomite and kieserite (Spencer, 2000), both observed on Mars (Chevrier and Mathe, 2006; Peterson et al., 2007).

4.7. MINERAL FORMATION

Previous hypotheses have suggested that the secondary sulfate deposits are the result of fumarolic activity during basaltic emplacement (Stearns, 1963), by influx of brine-type groundwater (Peck, 1974), or a combination of the two (Karlo et al., 1980). These hypotheses seem unlikely as no volcanic activity has occurred in over 2000 years, and field observations imply that the deposits are a seasonal feature. Likewise, evidence of brine-type groundwater infiltration and subsequent mineral precipitation was not

observed in any of the caves. The secondary sulfate deposits more likely form from the primary weathering of the overlying basaltic host.

PHREEQC modeling software was used to understand the progression of secondary minerals that would precipitate from the aqueous leaching of the major basaltic minerals. Minerals used in the modeling were based on XRF data and subsequent CIPW-NORM modal analysis (only the major minerals were used in the modeling, mineral dissolution equations are shown in Figure 4.5). PHREEQC input files are shown in Appendix C. These models show that when calcite reaches oversaturation and precipitates out, it reduces the Ca concentrations leading the Mg/Ca ratio in the residual solution to increase. Consequently, this leads to shifts in the saturation indices (SI) of epsomite and gypsum (Figure 4.5). The SI values of mirabilite are unaffected by the precipitation of calcite. Since the secondary deposits at COM are dominated by mirabilite and thenardite, Na-sulfate may be among the first constituents to precipitate out of solution. These chemical divides may help explain the lack of gypsum in the secondary deposits. Similar mineral fractionation trends have been described by Eugster (1980). The absence of Mg-sulfate in the secondary deposits based on these models is perplexing but may be due to the increased precipitation of dolomite and magnesite.

The abrupt contact between the sulfate mounds and the basaltic floor, in addition to the absence of intermixing between the sulfate mounds and the authigenic basaltic minerals further supports that secondary mineralization occurs via precipitation rather than direct mineralogical replacement. The fact that some of the sulfate minerals are found as mounds on the floor is interesting, and may suggest a biogenic activity in their formation, either through biooxidation of basaltic sulfidic minerals or through alteration

of bat guano. The lack of associated gypsum, nitrate, and phosphate minerals makes the latter possibility unlikely, as these are the most common minerals formed through alteration and leaching of bat guano (Forti, 2005; Hill and Forti, 1997). Additionally, the occurrence of thenardite in wall and ceiling cavities (Fig. 4.2) make any interaction and associated mineralization via bat guano unlikely.

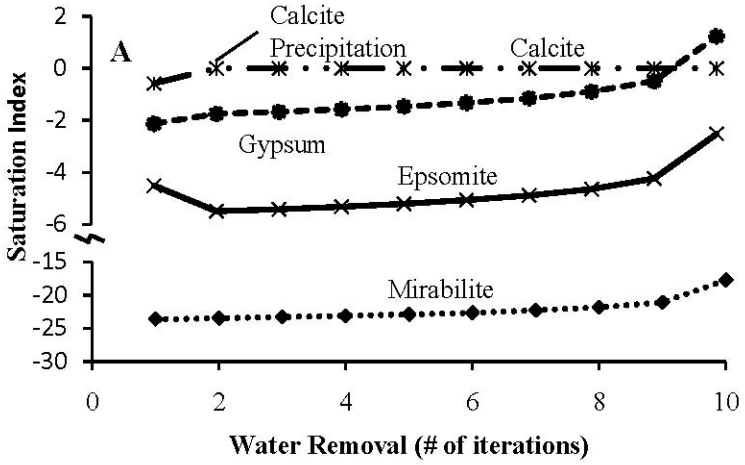

Figure 4.5. Saturation indices for calcite, gypsum, epsomite and mirabilite as a function of the systematic evaporation of water using PHREEQC modeling software. Mineral dissolution formulas were based on PHREEQC database equations. Basaltic minerals and equations used in modeling are: Diopside, $CaMgSi_2O_6 = Ca^{2+} + Mg^{2+} + 2H_2O + 2SiO_2$; Fayalite, $Fe_2SiO_4 + 4H^+ = SiO_2 + 2Fe^{2+} + 2H_2O$; Ilmenite, $FeTiO_3 + 2H^+ + H_2O = Fe^{2+} + Ti(OH)_4$; Quartz, $SiO_2 = SiO_2$; Pyrite, $FeS_2 + H_2O = 0.25H^+ + 0.25SO_4^{2-} + Fe^{2+} + 1.75HS^-$, Plagioclase, $Na_{0.6}Ca_{0.4}Al_{1.4}Si_{2.6}O_8 + 5.6H^+ = 0.6Na^+ + 0.4Ca^{2+} + 1.4Al^{3+} + 2.8H_2O + 2.6SiO_2$.

4.8. CONCLUSION

COM basalts offer an excellent analog to martian basalts, as they have elevated Fe concentrations compared to traditional terrestrial analogs. Although secondary sulfate minerals on the evaporitic regions of Mars consist primarily of Mg-, Ca-, and Fe-bearing sulfate minerals, recent spectroscopic data have shown the presence of Na-sulfate minerals. Secondary precipitates within the basaltic subsurface of the Holocene COM

basaltic flows are dominated by Na-sulfates (thenardite, mirabilite) with minor concentrations of Na-carbonates (trona, natron). The deposits are found in cavities along the ceiling and walls of the caves and as localized efflorescent mounds on the cave floors. The occurrence of Na-sulfate and Na-carbonate minerals in the subsurface of COM suggests that similar mineral assemblages could occur in the subsurface of Mars. The formation of secondary sulfate minerals within the subsurface of COM is likely the result of leaching of overlying basaltic host rock, through abiotic and possible biotic physiochemical pathways.

4.9. ACKNOWLEDGEMENTS

The authors acknowledge support by the National Aeronautics and Space Agency (NASA) Exobiology Program (NNX08AP59G) and the Wisconsin Space Grant Consortium. Research performed at the Idaho National Laboratory under DOE Idaho Operations Office Contract DE-AC07-05ID14517. CDR would also like to thank Dawn Knipe and Katherine LeCloux for their help in the field and the laboratory, respectively.

4.10. REFERENCES

Chevrier, V., Mathe, P., Rochette, P., Gunnlaugsson, H., 2006. Magnetic study of an Antarctic weathering profile on basalt: Implications for recent weathering on Mars. Earth and Planetary Science Letter 244 (3-4), 501-514.

Chevrier, V., Mathe, P.E., 2006. Mineralogy and evolution of the surface of Mars: A review. Planetary and Space Science 55 (3), 289-314.

Clark, B.C., Morris, R.V., McLennan, S.M., Gellert, R., Jolliff, B., Knoll, A.H., Squyres, S.W., Lowenstein, T.K., Ming, D.W., Tosca, N.J., A., Y., Christensen, P.R., Gorevan, S., Bruckner, J., Calvin, W., Dreibus, G., Farrand, W., Klingelhoefer, G., Waenke, H., Zipfel, J., Bell III, J.F., Grotzinger, J., McSceen, H.Y., Rieder, R., 2005. Chemistry and mineralogy of outcrops at Meridiani Planum. Earth and Planetary Science Letters 240, 74-94.

Cushing, G.E., Titus, T.N., Wynne, P.R., Christensen, P.R., 2007. Themis observes possible cave skylights on Mars. Geophysical Research Letters 34 (L17201), Doi:10.1029/2007/2007GL030709.

Drost, C., Wynne, J., Chapman, M., Kargel, J., Titus, T., Toomey, R., 2006. Remotely sensed cave detection on Earth and Mars, 37th Annual Lunar and Planetary Science Conference, League City, TX.

Eugster, 1980. Geochemistry of evaporitic lacustrine deposits. Ann. Rev. Earth Planet Sci 8, 35-63

Farmer, V., 1974. The infrared spectra of minerals. Mineralogical Society, London.

Forti, P., 2005. Genetic processes of cave minerals in volcanic environments: An overview. Journal of Cave and Karst Studies 67 (1), 3-13.

Gellert, R., Rieder, R., Anderson, R., Bruckner, J., Clark, B., Dreibus, G., Eonomou, T., Klingelhofer, G., Lugmair, G., Ming, D., Squyres, S., d'Uston, C., Wanke, H., Yen, A., Zipfel, J., 2004. Chemistry of rocks and soils in Gusev Crater from the Alpha Particle X-ray Spectrometer. Science 305, 829-832.

Hill, C., Forti, P., 1997. Cave minerals of the world, 2nd National Speleological Society, Huntsville, AL.

Hughes, S.S., Smith, R., Hackett, W., Anderson, S., 1999. Mafic volcanism and environmental geology of the eastern Snake River Plain. In: Hughes, S.S., Thackray, G. (Eds.), Guidebook to the geology of eastern Idaho. Idaho Museum of Natural History, Pocatello, Idaho, pp. 143-168.

Karlo, J.H., Jorgenson, D.B., Shineldecker, C.L., 1980. Sulfate minerals in Snake River Plain volcanoes. Northwest Science 54 (3), 178-182.

Kotler, J.M., Hinman, N.W., Yan, B., Stoner, D.L., Scott, J.R., 2008. Glycine identification in natural jarosites using laser-desorption Fourier transform mass spectrometry: Implications for the search for life on Mars. Astrobiology 8, 253-266.

Kuntz, M., Anderson, S., Champion, D., Lanphere, M., Grunwald, D., 2002. Tension cracks, eruptive fissures, dikes, and faults related to late Pleistocene–Holocene basaltic volcanism and implications for the distribution of hydraulic conductivity in the eastern Snake River Plain, Idaho. In: Link, P., Mink, L. (Eds.), Geology, hydrogeology, and environmental remediation. Idaho National Engineering and Environmental Laboratory, eastern Snake River Plain, Idaho. Geological Society of America Special Paper 353, pp. 111-133.

Kuntz, M., Champion, D., Spiker, E., Lefebvre, R., 1986. Contrasting magma types and steady-state, volume-predictable volcanism along the great rift, Idaho. GSA bulletin 97, 579-594.

Kuntz, M., Covington, H., Schorr, L., 1992. An overview of basalitc volcanism of the eastern Snake River Plain, Idaho. In: Link, P., Kuntz, M., Platt, L. (Eds.),

Regional geology of eastern Idaho and western Wyoming. Geological Society of America memoir, pp. 227-267.

Kuntz, M., 1989. Geology of the Craters of the Moon lava field, Idaho. In: Ruebelmann, K.L. (Editor), Snake River Plain-Yellowstone Volcanic Province. American Geophysical Union, Washington D.C., pp. 51-56.

Lane, M., 2007. Mid-infrared emission spectroscopy of sulfate and sulfate-bearing minerals. American Mineralogist 92, 1-18.

Leeman, W., Vitaliano, C., Prinz, M., 1976. Evolved lavas from the Snake River Plain: Craters of the Moon National Monument, Idaho. Contributions to Mineralogy and Petrology 56, 35-60.

Lodders, K., 1998. A survey of shergottite, nakhlite and chassigny meteorites whole-rock compositions. Meteoritics and Planetary Science 33, A183-A190.

Mangold, N., Gendrin, A., Gondet, B., LeMouelic, S., Quantin, C., Ansan, V., Bibring, J., Langevin, Y., Masson, P., Neukum, G., 2008. Spectral and geological study of the sulfate-rich region of West Candor Chasma, Mars. Icarus 194, 519-543.

McHenry, L., 2009. Element mobility during zeolitic and argillic alteration of volcanic ash in a closed-basin lacustrine environment: Case study Olduvai Gorge, Tanzania. Chemical Geology 265, 540-552.

McJunkin, T.R., Tremblay, P.L., Scott, J.R., 2002. Automation and control of an imaging internal laser desorption Fourier transform mass spectrometer (I^2LD-FTMS). Journal of the Association for Laboratory Automation (JALA) 7, 76-83.

McLennan, S.M., Bell, J.F., Calvin, W.M., Christensen, P.R., Clark, B.C., de Souza, P.A., Farmer, J., Farrand, W.H., Fike, D.A., Gellert, R., Ghosh, A., Glotch, T.D., Grotzinger, J.P., Hahn, B., Herkenhoff, K.E., Hurowitz, J.A., Johnson, J.R., Johnson, S.S., Jolliff, B., Klingelhofer, G., Knoll, A.H., Learner, Z., Malin, M.C., McSween, H.Y., Pocock, J., Ruff, S.W., Soderblom, L.A., Squyres, S.W., Tosca, N.J., Watters, W.A., Wyatt, M.B., Yen, A., 2005. Provenance and diagenesis of the evaporite-bearing Burns formation, Meridiani Planum, Mars. Earth and Planetary Science Letters 240 (1), 95-121.

Morris, R.V., Golden, D.C., Bell, J.F., Shelfer, T.D., Scheinost, A.C., Hinman, N.W., Furniss, G., Mertzman, S.A., Bishop, J.L., Ming, D.W., Allen, C.C., Britt, D.T., 2000. Mineralogy, composition, and alteration of Mars Pathfinder rocks and soils: Evidence from multispectral, elemental, and magnetic data on terrestrial analogue, SNC meteorite, and Pathfinder samples. Journal of Geophysical Research-Planets 105 (E1), 1757-1817.

Ohno, H., Igarashi, M., Hondoh, T., 2006. Characteristics of salt inclusions in polar ice from Dome Fuji, East Antarctica. Geophysical Research Letter 33, L08501.1-L08501.5.

Peck, S.B., 1974. Unusual mineralogy of the Crystal Pit Spatter Cone, Craters of the Moon National Mounument, Idaho. NSS Bulletin 36 (1), 19-24.

Peterson, S.B., Nelson, W., Madu, B., Shurvell, H.F., 2007. Meridianiite: A new mineral species observed on Earth and predicted to exist on Mars. American Mineralogist 92, 1756-1759.

Poels, K., Van Vaeck, L., Gijbels, R., 1998. Microprobe speciation analysis of inorganic solids by Fourier transform laser mass spectrometry. Analytical Chemistry 70, 504-512.

Reid, M., 1995. Processes of mantle enrichment and magmatic differentiation in the eastern Snake River Plain: Th isotope evidence. Earth and Planetary Science Letters 131, 239-254.

Richardson, C., Hinman, N., Scott, J., 2009. Effect of thenardite on the direct dectection of aromatic amino acids: Implications for the search for life in the solar system. International Journal of Astrobiology 8 (4), 391-400.

Richardson, C., Hinman, N., McJunkin, T., Kotler, J., Scott, J., 2008. Exploring biosignatures associated with thenardite by geomatrix-assisted laser desorption/ionization Fourier transform ion cyclotron resonance mass spectrometry (GALDI-FTICR-MS). Geomicrobiology Journal 25 (7), 432-440.

Rieder, R., Gellert, R., Anderson, R.C., Bruckner, J., Clark, B.C., Dreibus, G., Economou, T., Klingelhoefer, G., Lugmair, G.W., Ming, D.W., Squyres, S.W., d'Uston, C., Waenke, H., Yen, A., Zipfel, J., 2004. Chemistry of rocks and soils at Meridiani Planum from the Alpha Particle X-ray Spectrometer. Science 306, 1746-1749.

Rodriquez-Navarro, C., Doehne, E., Sebastian, E., 2000. How does sodium sulfate crystalllize? Implications for the decay and testing of building materials. Cement and Concrete Research 30, 1527-1534.

Sakimoto, S., Gregg, T., Hughes, S.S., Chadwick, J., 2003. Re-assessing plains-style volcanism on Mars, Sixth International Conference on Mars, pp. 3197.pdf

Scott, J.R., McJunkin, T.R., Tremblay, P.L., 2003. Automated analysis of mass spectral data using fuzzy logic classification. Journal of the Association for Laboratory Automation (JALA) 8 (2), 61-63.

Scott, J.R., Tremblay, P.L., 2002. Highly reproducible laser beam scanning device for an internal source laser desorption microprobe Fourier transform mass spectrometer. Review of Scientific Instruments 73 (3), 1108-1116.

Spencer, R.J., 2000. Sulfate minerals in evaporite deposits. In: Alpers, C.N., Jambor, J.L., Nordstrom, D.K. (Eds.), Sulfate minerals: Crystallography, geochemistry, and

environmental significance. Mineralogical Society of America, Washington, D. C., pp. 173-192.

Stearns, H.T., 1963. Geology of the Craters of the Moon, Idaho. Craters of the Moon Natural History Association, Caldwell, Idaho.

Stout, M.Z., Nicholls, J., 1977. Mineralogy and petrology of Quaternary lavas from the Snake River Plain, Idaho. Canadian Journal of Earth Sciences 14, 2140-2156.

Stout, M.Z., Nicholls, J., Kuntz, M.A., 1994. Petrological and mineralogical variations in 2500-2000 yr B.P. lava flows, Craters of the Moon lava field, Idaho. Journal of Petrology 35 (6), 1681-1715.

Tosca, N.J., McLennan, S.M., 2006. Chemical divides and evaporite assemblages on Mars. Earth and Planetary Science Letters 241, 21-31.

Van Vaeck, L., Adriaens, A., Adams, F., 1998. Microscopical speciation analysis with laser microprobe mass spectrometry and static secondary ion mass spectrometry. Spectrochim Acta B 53, 367-378.

Van Vaeck, L., Gijbels, R., 1990. Potential and limitations for inorganic and organic micro-analysis. Fresenius Journal of Analytical Chemistry 337, 755-765.

Vassallo, A., Finnie, K., 1992. Infrared emission spectroscopy of some sulfate minerals. Applied Spectroscopy 46, 1477-1482.

Wyrick, D., Ferrill, D., Morris, A., Colton, S., Sims, D., 2004. Distribution, morphology, and origins of martian pit crater chains. Journal of Geophysical Research 109, E06005.

Yan, B., McJunkin, T.R., Stoner, D.L., Scott, J.R., 2006. Validation of fuzzy logic method for automated mass spectral classification for mineral imaging. Applied Surface Science 253 (4), 2011-2017.

Yan, B., Stoner, D.L., Kotler, J.M., Hinman, N.W., Scott, J.R., 2007a. Detection of biosignatures by geomatrix-assisted laser desorption/ionization (GALDI) mass spectrometry. Geomicrobiology Journal 24, 379-385.

Yan, B., Stoner, D.L., Scott, J.R., 2007b. Direct LD-FTMS detection of mineral-associated PAHs and their influence on the detection of other organics. Talanta 72, 634-641.

Zhu, M., Xie, H., Guan, H., Smith, R., 2006. Mineral and lithologic mapping of martian low albedo regions using OMEGA data, Lunar and Planetary Science XXXVII, pp. 2173.pdf.

CHAPTER 5: BIOLOGICAL ACTIVITY IN THE MINERALIZATION OF SECONDARY DEPOSITS WITHIN THE BASATLIC SUBSURFACE OF CRATERS OF THE MOON NATIONAL MONUMENT: IMPLICATIONS FOR THE SEARCH FOR LIFE ON MARS.

C. Doc Richardson [a], Nancy W. Hinman [a], Lindsay J. McHenry [b], Jill R. Scott [*c]

[a] Geosciences Department, University of Montana, 32 Campus Dr., Missoula, MT 59812, USA

[b] Department of Geosciences , University of Wisconsin-Milwaukee, P.O Box 413, 2200 E. Kenwood Blvd., WI 53201, USA

[c] Chemical Sciences, Idaho National Laboratory, 1765 N. Yellowstone Hwy., Idaho Falls, ID 83415, USA

[*] Address correspondence to Jill R. Scott, Chemical Sciences, Idaho National Laboratory, 1765 North Yellowstone Hwy, Idaho Falls, ID 83415, United States. Phone: +1 (208) 526-0429. Fax: +1 (208) 526-8541. Email: jill.scott@inl.gov

Short Title: Biogenic mineralization at Craters of the Moon National Monument

5.1 ABSTRACT

Evidence of microbial activity associated with the mineralization of secondary Na-sulfate minerals (thenardite, mirabilite) in the basaltic subsurface of Craters of the Moon National Monument (COM), Idaho was examined by laser desorption mass spectrometry, infrared spectroscopy and sulfur isotopic fractionation. Peaks suggestive of bio/organic compounds were observed in the secondary Na-sulfate deposits by Fourier

transform mass spectrometry (FTICR-MS), suggesting biological involvement in the formation of the deposits. These secondary Na-sulfate minerals form by aqueous leaching of Na ions and biooxidation of Fe-sulfide minerals in the overlying basalt rock. With the chemical composition of the COM basalts being similar to their martian counterparts, the occurrence of biological activity in the formation of sulfate minerals at COM has direct implications for the search for life on Mars. Additionally, the presence of caves on Mars suggests the importance of these environments as a possible location for the growth and preservation of microbial activity. Thus, understanding the physiochemical pathways of abiotic and biotic mineralization in the COM basaltic subsurface and similar basaltic settings is imperative into the search for extinct or even extant life in the martian subsurface.

Kewords: Thenardite, Mars, Craters of the Moon National Monument, bio/organic compounds, FTICR-MS

5.2. INTRODUCTION

Lava tubes and caves are a common feature in terrestrial basaltic settings, offering unique physiochemical conditions for the biogenic growth of secondary minerals. These stable conditions lead to the formation and preservation of secondary mineral deposits that may subsequently harbor bio/organic compounds, which are define as chemical compounds produced by living organisms or derived from other biogenic organic compounds. Understanding the abiotic and biotic physiochemical processes in terrestrial caves may provide valuable insight into the presence of life elsewhere in the solar system. Lava tubes and caves on Mars would represent ideal locations in searching for

past evidence of aqueous and biological activity, as these subsurface environments would offer protection from radiolytic degradation and diurnal temperature fluctuations (Boston et al., 2001; Leveille and Datta, 2007, 2009). In this research, it is necessary to conduct geomicrobiological and geochemical investigations of terrestrial basaltic caves to help elucidate similar abiotic and possibly biotic physiochemical processes on Mars.

Due to the thin atmosphere and weak magnetic field, the upper few meters of the martian surface is constantly bombarded with ultraviolet radiation (Benner et al., 2000; Martinez-Frias et al., 2006) and high-energy galactic cosmic particles (Badhwar, 2004; Parnell et al., 2007). As a result, the martian surface is considered an inhospitable environment for life, contrary to the martian subsurface which may provide more favorable physiochemical conditions for the growth and preservation bio/organic compounds (Boston et al., 2001). Thus, the martian subsurface may offer the most stable environment and the best chance to observe evidence of extinct or even extant life.

This study investigates the role of microbial activity in the formation of secondary Na-sulfate deposits found within the basaltic subsurface of Craters of the Moon National Monument (COM), Idaho. Due to the high-Fe content of the COM basalts, they are an excellent analog to the Fe-rich martian basalts, especially when compared to more traditional terrestrial analogs (Richardson et al., 2009a). The importance of Na-sulfate minerals has been made clear to the astrobiological community since their discovery in several planetary bodies throughout the solar system. Recently, Na-sulfates have been observed as weathering products in the martian regolith (Mangold et al., 2008; Zhu et al., 2006), and they are a major surficial component on the icy moon of Europa (Fanale et al., 2001; Kargel et al., 2000; McCord et al., 1998; 1999; Zolotov

and Shock, 2001). Additionally, anhydrous Na-sulfate (thenardite) is a proven host mineral in the direct detection of bio/organic compounds using laser desorption Fourier transform ion cyclotron resonance-mass spectrometry (FTICR-MS) (Richardson et al., 2008; Richardson et al., 2009b). The role of microbial activity in the mineralization of Na-sulfates in the basaltic subsurface of COM, and the ability of these minerals to assist in the direct detection of bio/organic compounds has significant implications for the search for life on Mars, especially considering future laser desorption mass spectrometry (LDMS) instruments, like Mars Organic Molecule Analyzer which will search for similar bio/organic compounds as a part of the upcoming ExoMars mission.

5.2.1. COM as a Martian Analog

COM is located along the northern flank of the Eastern Snake River Plain in southern Idaho. It is composed of more than 60 individual Holocene-aged basaltic flows (Kuntz et al., 1986; 1992; Reid, 1995). COM basalts are enriched in silica, iron and alkali-elements relative to basaltic flows elsewhere in the Eastern Snake River Plain (Hughes et al., 1999). These differences are putatively agreed to reflect larger degrees of crustal assimilation and/or fractionation (Leeman et al., 1976).

Mineralogical and bulk chemical comparisons between COM and martian basalts show similar compositions (Hughes et al., 1999; Richardson et al., 2009a). These two regions are marked with extremely high Fe concentrations, especially when compared to other terrestrial basaltic chemistries. However, COM basalts are slightly higher in Al, P, Ti, Na, and K and lower in alkali-earth elements and S than their martian counterparts (Hughes et al., 1999; Kuntz et al., 1986; Richardson et al., 2009a). Despite these differences, COM basalts are still closer in chemical composition to martian basalts than

other frequently used terrestrial analogs, which suffer similar variations but also have much lower Fe concentrations.

5.2.2. Occurrence of Subsurface Features on Mars

Lava tubes and caves are widely considered to be a common feature on Mars due to the weak martian gravity and their occurrence in terrestrial basaltic environments (Leveille and Datta, 2009). Lava tubes and related features have now been observed by martian orbiters (Drost et al., 2006; Wyrick et al., 2004). Imagery from Mars *Odyssey*, Mars *Global Surveyor*, Mars *Express*, and Mars *Reconnaissance* Orbiters have observed such subsurface features as collapsed lava tubes, lave tube pits, and hollow lava tube conduits (Leveille and Datta, 2009; Wyrick et al., 2004). Additionally, thermal imaging has observed caves measuring between 100 m to 250 m in diameter (Cushing et al., 2007). These caves are located in the Tharsis shield volcano region, which is considered to be morphologically and topographically similar to the basaltic shields of the Eastern Snake River Plain (Sakimoto et al., 2003).

5. 3. METHODOLOGY AND ANALYTICAL TECHNIQUES

5.3.1. Mineral Collection

Samples of the secondary deposits were collected biannually between June 2006 and October 2008. Approximately 10 g of the deposits were carefully transferred to glass containers, making sure no extraneous material or contamination was introduced. Unfortunately, due to safety regulations, COM park officials did not grant access into the two spatter cones, named Crystal Pit or Snow Cone Pit. As a result, all samples from these spatter cones were obtained through subsampling from the mineral archive located

at COM Park Headquarters, these samples were originally collected by the Environmental Science and Research Foundation (Morris et al., 1995).

5.3.2. Fourier Transform Infrared Spectroscopy

Attenuated Fourier transform infrared spectroscopy (FTIR) spectra were obtained using a Thermo Nicolet Nexus 670 FTIR spectrometer (Madison, WI). Spectra were collected using an average of 100 scans with a resolution of 4 cm^{-1}. All spectra were measured in absorbance between 4000 cm^{-1} and 500 cm^{-1}.

5.3.3. FTICR-MS Instrumentation and Parameters

Spectra of the secondary sulfate deposits were obtained using a laboratory-derived FTICR-MS (McJunkin et al., 2002; Scott et al., 2003; Scott and Tremblay, 2002) equipped with a 7 T Oxford (Oxford, England) superconducting magnet. Instrument parameters have been previously described (Kotler et al., 2008; Richardson et al., 2008; 2009b; Yan et al., 2007a; 2007b). All spectra were acquired using single laser shots in both the positive and negative mode. Peak identification was accomplished by systematic analysis following Kotler et al. (2008).

5.3.4. Sulfur Isotopes

Evidence of sulfur fractionation between the secondary deposits and the host basalts was obtained using a continuous flow stable isotope ratio mass spectrometer by DPRA-Zymax Industries (Escondido, CA). Eleven secondary mineral samples, from the three sampling locations, were analyzed and compared to two host basalts taken from Wilderness Caves area and on the flank of Crystal Pit Spatter Cone, respectively. These basalt samples bound the eastern and western boundary of the sampling area in the Blue

Dragon flow (Fig 5.1). Sulfur isotope ratios are reported in the conventional δ-notation, expressed as ‰ deviation relative to Vienna Canyon Diablo Troilite (VCDT).

5.4. RESULTS

5.4.1. Description of Subsurface Features at COM

Of the 60 basaltic flows that compose COM, the young Blue Dragon flow (~ 2.1 ka) contains the majority of the accessible lava tubes and caves found in the Eastern Snake River Plain. Their abundance is due to the young age of the flow, as it has had less time to undergo gravitational collapse. As a result the Blue Dragon flow hosts a majority of the secondary sulfate deposits found at COM; likely the result of its morphological characteristics rather than any chemical differences between adjacent COM flows (Richardson et al., 2009a; Stout et al., 1994).

Within the Blue Dragon flow three locations were chosen for mineral sampling, these locations where chosen based on mineral occurrence, mineral abundance, cave accessibility and lack of public access. The extent of the Blue Dragon flow and cave locations used in this study are shown in Figure 5.1. Wilderness Caves area is a collection of roughly six small lava tubes and caves covering an area nearly 200 meters in diameter. Approximately two kilometer to the west of the Wilderness Caves area is the branching lava tunnel of Arco Tunnel. Cumulatively, Arco tunnel extends for over a kilometer while maintaining a relatively shallow depth (<30 m). The final sampling location comes from the two hollow magma chambers located within adjacent spatter cones (Crystal Pit, and Snow Cone Pit). These spatter cones are approximately two and half kilometers west of Arco Tunnel on the western boundary of the Blue Dragon flow. These magma chambers are only accessible through narrow > 20-meter vertical throats

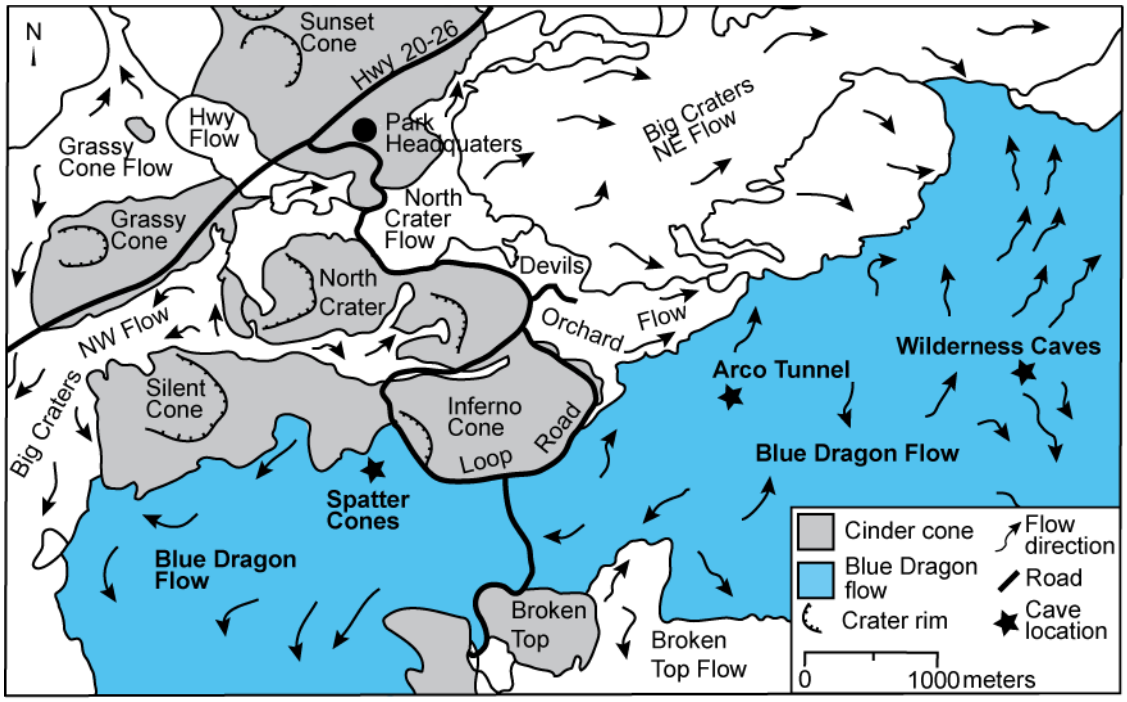

Figure 5.1. Map of COM lava field showing cave locations in Blue Dragon flow. Map modified from Kuntz (1989) with permission of American Geophysical Union.

(Morris et al., 1995; Peck, 1974). The hollow magma chambers of Crystal and Snow Cone Pit are only two of three such formations known to the authors worldwide (Morris et al., 1995; Stefansson, 1992), as similar magma chambers are inaccessible due to lava infill, weathering and/or ice plugs.

5.4.2. Description of Secondary Deposits

Secondary Na-sulfate deposits from Wilderness Caves area and Arco Tunnel are found in small cavities on the ceilings and walls and as mounds on the floors. Floor deposits are found intermittently dispersed as localized, efflorescent, white, powdery mounds. These deposits appear to be a seasonal feature, as the size and amount of each representative mineral deposit fluctuates on a semi-annual basis. It appears these deposits fluctuate throughout the year, dissolving during wetter months, and

reprecipitating during drier times of the year. A more detailed description of the secondary deposits can be found in Richardson et al. (2009a).

4.3. Evidence of Microbial Activity

The secondary deposits found in the subsurface of COM are dominated by Na-sulfate minerals (thenardite, mirabilite) with approximately 50% of the deposits containing minor concentrations of Na-carbonate minerals (trona, natron) (Richardson et al., 2009a). These secondary deposits were investigated for chemical and isotopic biological signatures. Biological activity associated with mineral deposits can be inferred through various methods including chemical or isotopic signatures, which can be preserved in the minerals (Boston et al., 2001; Leveille and Datta, 2007). Such bio/organic compounds would suggest direct or indirect biological involvement in the mineralization of the Na-sulfate deposits at COM. It must be noted that other mechanisms of bio/organic compounds interaction with the secondary deposits can not be overlooked. Although unlikely, emplacement and delivery of these bio/organic compounds to the secondary deposits may be due to plant detritus moving downward through the basalts, organic aerosols, and post-depositional interaction with cave animals. To the authors' knowledge, no investigation of biogenic activity related to Na-sulfate mineralization in volcanic settings has been conducted. However, evidence of biological activity, such as fossilized remnants and FTICR-MS spectra containing peaks suggestive of bio/organic compounds, has been observed in Na-sulfate minerals in several evaporitic settings (Dongyan et al., 1998; Richardson et al., 2008).

Mineral deposits were investigated for microbial evidence using geomatrix assisted laser desorption/ionization (GALDI) (Yan et al., 2007a). This technique uses a

mineral matrix to assist in the desorption and ionization of bio/organic compounds with little to no sample preparation. The ability of minerals to facilitate in the desorption and ionization of bio/organic compounds is a primary focus in previous studies of GALDI-FTICR-MS as a viable technique for bio/organic compound detection (Kotler et al., 2008; Richardson et al., 2008; Richardson et al., 2009b; Yan et al., 2007a; Yan et al., 2007b). Previous studies using synthetic and natural thenardite have shown the ability of thenardite to assist in the ionization and detection of bio/organic compounds (Richardson et al., 2008; Richardson et al., 2009b).

In order to accurately identify any associated bio/organic compounds in the COM secondary deposits, a suite of FTICR-MS spectra was compiled, composed of inorganic thenardite, Na-carbonate (trona, natron), and physical combinations between these Na-sulfate and Na-carbonate minerals. This inorganic suite of minerals was based on previous XRD, FTIR and FTICR-MS spectra of COM secondary deposits by Richardson et al. (2009a).

The positive and negative mode FTICR-MS spectra of the Na-sulfate standards obtained from this study are identical to previously reported spectra (Richardson et al., 2009a; Richardson et al., 2008; Richardson et al., 2009b). All spectra of the Na-sulfate and Na-carbonate minerals (not shown) have peaks with mass defects (i.e., the number after the decimal point) suggestive of inorganic constituents. Common non-hydrogen elements associated with bio/organic compounds have mass defects near 0.00 amu (e.g., ^{12}C at 12.000 amu, ^{16}O at 15.995 amu). Hydrogen with an elemental mass of 1.008 amu tends to dominate the mass defects of bio/organic compounds because there are usually twice as many hydrogen atoms as other elements. Hence, it is necessary to have

sufficient mass accuracy and resolution to distinguish between peaks related to inorganic and organic ions. Distinguishing between an inorganic and organic ion based on the peak's mass defect is easily accomplished when the ion has a m/z (mass-to-charge) less than 400, as the m/z begins to rise above this value, organic ions tend to accumulate hydrogen atoms causing the mass defect to appear to contain inorganic elements.

Figure 5.2 is a representative negative mode spectrum from a secondary deposit collected from a wall cavity inside Arco Tunnel. The inorganic peaks observed in the spectra have been reported in previous studies of Na-sulfate spectra (Poels et al., 1998; Richardson et al., 2009a; Richardson et al., 2008; Van Vaeck et al., 1998). Among the inorganic peaks, two distinctive peaks at m/z 183.081 and 339.040 have mass defects suggestive of bio/organic compounds. These peaks are related to bio/organic compounds due to (1) absence of the peaks in the inorganic Na-sulfate and Na-carbonate standards, (2) mass defects suggestive of bio/organic elements, and (3) isotopic distributions (expanded regions in Fig. 5.2), which correspond to the theoretical isotopic distribution of the suggestive bio/organic formulas. The bio/organic related peaks are an example of complex cluster ions, similar to that reported for glycine with jarosite (Kotler et al., 2008), and stearic acid with thenardite (Richardson et al., 2008). Using a systematic procedure based on the mass defects and isotopic distributions outlined by Kotler et al. (2008), the most likely composition for the peaks at m/z 183 and 339 are $C_8H_{16}SONa^-$ and $C_{10}H_{20}S_3O_5Na^-$, respectively. The occurrence of these complex cluster ions is not unusual, as they often form due to complex reactions in the laser desorption plume or in the gas phase (Budimir et al., 2007; Karas et al., 1985; Knochenmuss et al., 1996). These reactions lead to ions larger than the expected molecular ion due to formation of adducts

from the addition of matrix components and/or analyte species (Budimir et al., 2007; Ham et al., 2003; Karas and Kruger, 2000; Knochenmuss et al., 1996). The exact identification of the original bio/organic compound was unobtainable as it is quite difficult to ascertain without undertaking a systematic experiment using a variety of bio/organic compound/thenardite combinations.

As with the negative spectra, a number of complex bio/organic or organic cluster ions are seen in the positive spectra of the secondary deposits (Table 5.1). A comprehensive list of these positive and negative mode peaks and their suggestive chemical formulas is shown in Table 5.1. Approximately 30% of these suggestive formulas have C:H:O ratios that resemble ratios observed in lipids, sugars and/or amino acids. Unfortunately, many of the suggestive formulas seen in Table 5.1 have suggestive formulas that may result from gas-phase reactions in the desorption plume. These gas-phase reactions can lead to unusual chemical formulas. Similar gas phase reactions have been observed in previous FTICR-MS studies using thenardite (Richardson et al. 2008). A representative positive mode spectrum (Fig. 5.3) shows several high mass peaks, most of which are easily identified as inorganic based on their high mass defects, their occurrence in the inorganic standard spectra, and their occurrence in previously reported thenardite spectra (Poels et al., 1998; Richardson et al., 2009b; Van Vaeck et al., 1998). Close inspection reveal that the peaks at m/z 141.052, 170.044 and 181.039 have mass defects suggestive of bio/organic compounds and are absent in the inorganic standard spectra. Peak identification in the positive spectra was more difficult as the minor isotopic peaks were less distinct (i.e., low abundance) due to poor S/N. This is not uncommon as thenardite interactions often produce elevated background noise in the

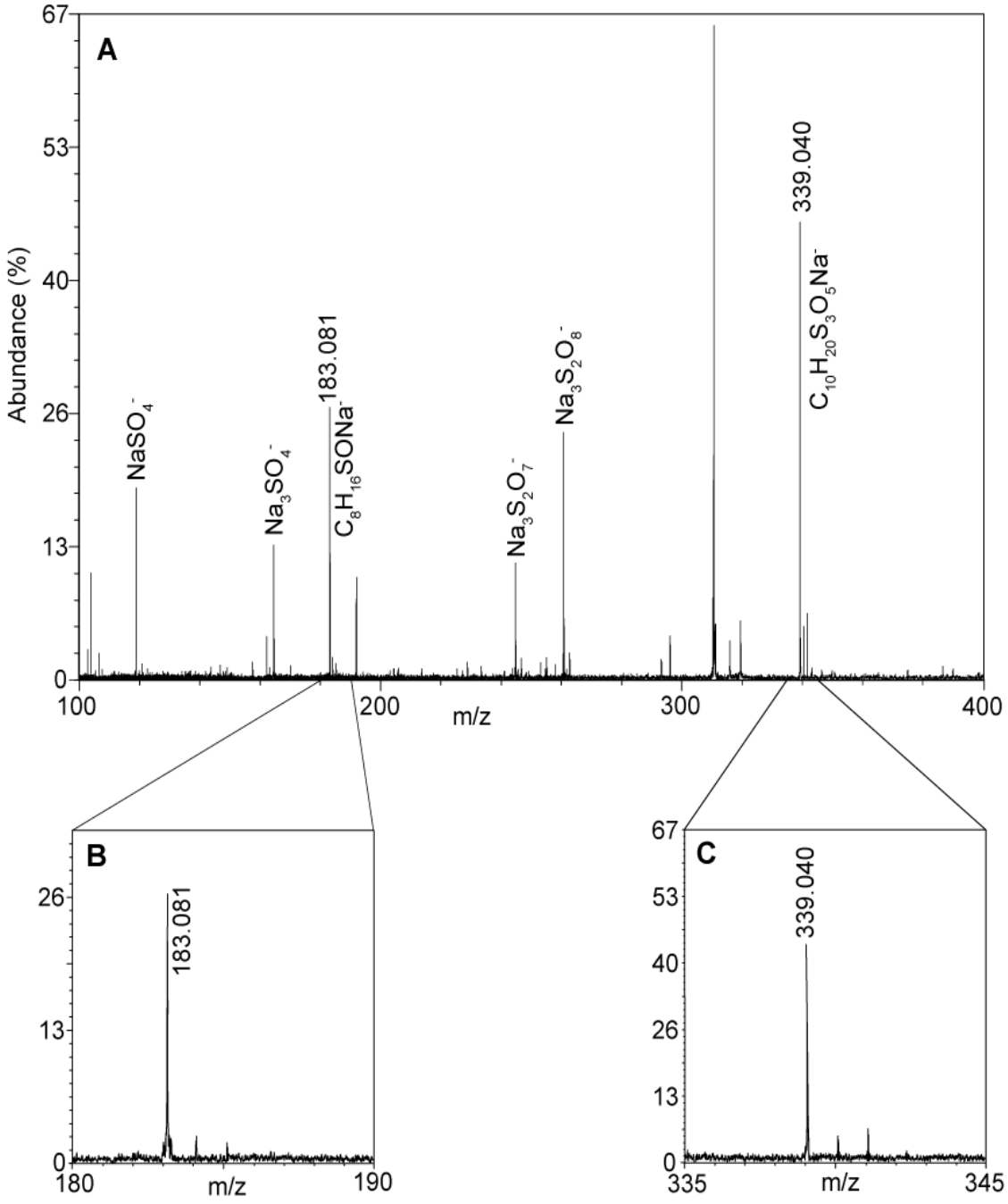

Figure 5.2. (A) Negative mode laser desorption ion FTICR-MS spectrum of a secondary sulfate deposits from a wall cavity inside Arco Tunnel. Peaks at (B) m/z 183 and (C) m/z 339 have mass defects and isotopic distributions suggestive of bio/organic cluster ions.

positive mode (Richardson et al., 2009b). However, peak identification was obtained by comparing the observed mass defects with theoretical mass defects. Using this method, the peak at m/z 141.052 was found to have only one likely composition with a theoretical weight of 141.053, corresponding to a formula of $C_5H_{10}O_3Na^+$. Precise identification of the peaks at m/z 170.044 and 181.039 were unobtainable as several likely formulas could account for these mass defects (Formulas are shown in Table 5.1). However, these peaks are clearly related to bio/organic compounds due to their mass defects and their absence in the Na-sulfate, Na- carbonate and physical mixture standard spectra. Additional evidence of associated bio/organic compounds in the secondary deposits was investigated using FTIR techniques. Even though FTIR does not have the sensitivity and

Table 5.1. Suggestive chemical formulas for bio/organic peaks associated with the secondary sulfate deposits observed in the laser desorption FTICR-MS spectra.

m/z	Positive Mode Bio/organic Peaks	Cave Location
113.022	$C_3H_6O_3Na^+$	AT, SC
130.098	$C_7H_{14}O_2^+$, $C_5H_{12}N_3O^+$	CP
136.098	$C_4H_{10}SNa_2^+$, $C_4H_8O_5^+$, $C_6H_9SNa^+$,	CP
141.053	$C_5H_{10}O_3Na^+$	WC, SC
163.026	$C_5H_9O_3Na_2^+$, $C_5H_9NO_3S^+$,	WC, CP
170.044	$C_4H_9NO_4Na^+$, $C_4H_{10}O_7^+$, $C_6H_{11}O_2SNa^+$	WC, CP
181.037	$C_5H_{11}NSO_4^+$, $C_6H_8NO_4Na^+$, $C_6H_{13}S_2O_2^+$	WC, CP
186.052	$C_5H_{11}O_5Na^+$	AT, WC, SC
223.007	$C_4H_8O_9Na^+$, $C_5H_7NO_6Na^+$, $C_5H_{12}S_2O_4Na^+$	CP
233.071	$C_9H_{15}NSO_4^+$, $C_6H_{14}N_2O_6Na^+$	CP
m/z	**Negative Mode Bio/organic Peaks**	**Cave Location**
136.009	$C_3H_6SNO_3^-$, $C_3H_6O_3Na_2^-$, $C_2H_4N_2O_5^-$	AT, SC
161.047	$C_4H_{10}O_5Na^-$, $C_6H_9O_5^-$	CP
163.046	$C_5H_9NO_5^-$, $C_5H_{11}NSNa_2^-$	WC, CP
183.081	$C_8H_{16}SONa^-$	AT, CP
187.047	$C_5H_{10}NO_5Na^-$	AT, WC, SC, CP
191.055	$C_5H_{10}O_6Na^-$, $C_7H_{11}O_6^-$, $C_{10}H_9NO_3^-$, $C_7H_{13}NO_3S^-$	AT, WC, SC, CP
281.008	$C_5H_{10}N_2O_8SNa^-$, $C_6H_{14}O_3N_3S_3Na^-$	AT, WC, CP
339.041	$C_{10}H_{20}S_3O_5Na^-$	AT, SC, CP
390.260	$C_{18}H_{39}O_7Na^-$	CP

Arco Tunnel= AT; Wilderness Caves= WC; Snow Cone Pit= SC; Crystal Pit= CP.

resolution as FTICR-MS, several bands were observed to support the presence of organic compounds. Representative spectra are shown in Figures 5.4A,B.

The inorganic bands in Figure 5.4A are representative of thenardite; a more detailed description of these bands can be found in Richardson et al. (2009a). Evidence of organic-related bands can be seen at 559 cm^{-1}, 545 cm^{-1}, 536 cm^{-1} and a double band at 2111 cm^{-1}. These bands are all consistent with bonding vibrations of organic functional groups. The double band at 2111 cm^{-1} correlates to a C–C triple bond or a C–N triple bond stretch, while the bands at 559 cm^{-1}, 545 cm^{-1} and 536 cm^{-1} are characteristic of stretching and rocking of singly-bonded C–compounds (Smith, 1999). Unfortunately, direct identification of organic compounds was unsuccessful as the major of organic characteristic bands (> 2500 cm^{-1}) were not observed.

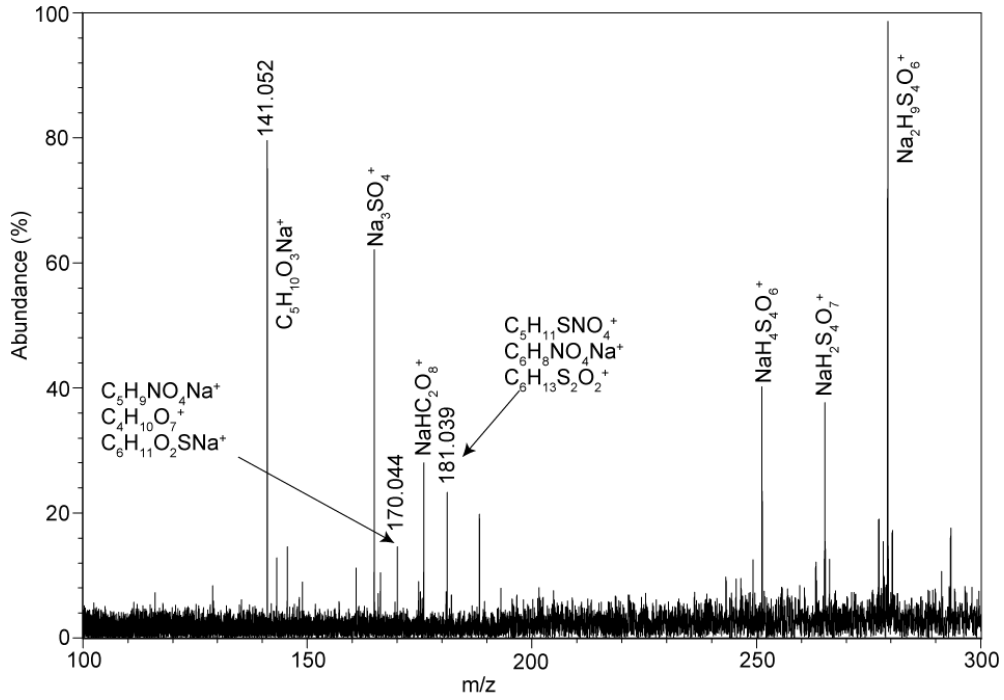

Figure 5.3. Positive mode laser desorption FTICR-MS spectrum of a secondary sulfate deposit from a floor deposit within a cave in the Wilderness Caves area.

The prominent bands seen in figure 5.4B result from a combination of sulfate and carbonate oxyanions similar to that observed by Richardson et al. (2009a). In addition to the major inorganic bands, several bands are suggestive to be representative of organic compounds. These bands at 536 cm^{-1} and 580 cm^{-1} are representative of singly-bonded organic compounds (Smith, 1999), similar to those observed in figure 5.4A. Additionally, the band at 785 cm^{-1} is reminiscent of a C–H stretch associated with aromatic organic compounds (Coates, 2000).

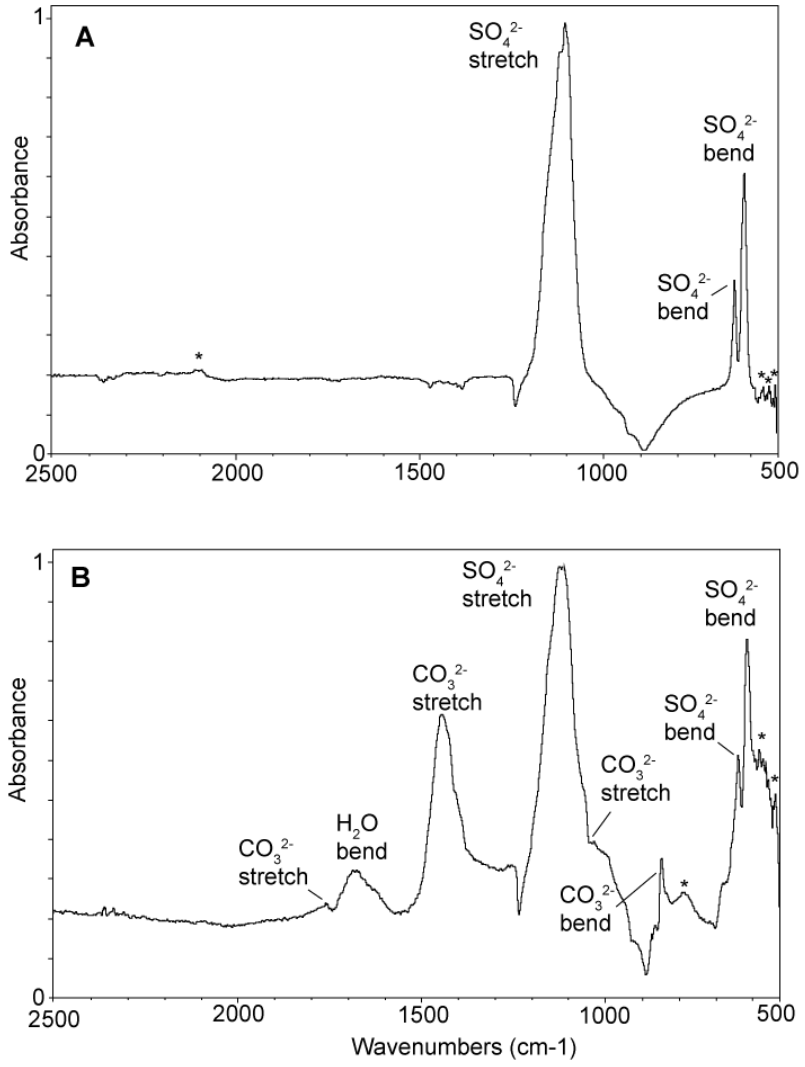

Figure 5.4. Representative FTIR spectra of secondary deposits, (A) spectrum is dominated by sulfate oxyanion, while (B) has additional bands corresponding to carbonate oxyanion. Both spectra show bands suggestive of organic bonding (indicated by *).

5.4.4. Sulfur Fractionation

The oxidation of sulfidic minerals to sulfate through a series of intermediate species represents an important energy-yielding pathway for chemolithoautrophic microorganisms. Sulfur compounds are among the most energy-rich inorganic compounds available to microbes (Douglas, 1995). Unfortunately little is known regarding the direct sulfur isotope fractionation associated with biologically mediated oxidation of natural sulfide minerals (Canfield, 2001), especially in reference to the formation of secondary minerals in basaltic environments. FeS_2 is one of the most abundant metal sulfide minerals in basaltic rocks and, therefore, is likely fundamental in biological weathering of basaltic rocks. Biologically mediated oxidation of sulfidic minerals results in progressively more depleted ^{34}S isotope ratios in the secondary minerals, as microbes preferential metabolize the lighter ^{32}S isotope. As a result, wide ranges of sulfur isotope fractionation values during bacterial sulfide oxidation have been observed in laboratory experiments (Balci et al., 2007; Kaplan and Rittenberg, 1964; Toran and Harris, 1989). In contrast, abiotic oxidation of sulfide minerals is considered to be a unidirectional process producing negligible sulfur isotope fractionation with $\partial^{34}S$ values being indistinguishable from the parent sulfide minerals (Balci et al., 2007; Canfield, 2001; Haubrich and Tichomirowa, 2002; Rye et al., 1992). However, sulfide oxidation is highly variable and is poorly understood. Fractionation of sulfide to sulfate is accomplished via multiple oxidation steps, with fractionation values having a high range of values. Canfield (2001) summarized the various oxidation steps for both abiotic and biotic pathways, although most of these reported values where done in controlled laboratory environments. These values are shown in Table 5.2.

Table 5.2. Summary of fractionation values during sulfur compound oxidation. Modified from Canfield (2001).

General Reaction	Fractionation ‰
Biotic	
$H_2S \rightarrow S^0$	-1 to 1
$H_2S \rightarrow SO_4^{2-}$	0 to -19
$S^0 \rightarrow SO_4^{2-}$	0
$S_2O_3^{2-} \rightarrow SO_4^{2-}$	-0.4
Abiotic	
$H_2S \rightarrow S^0, S_2O_3^{2-}, SO_4^{2-}$	4 to 5
$SO_3^{2-} \rightarrow SO_4^{2-}$	0.4

S^0, $S_2O_3^{2-}$, SO_3^{2-} are intermediate species.

Additionally the pathways of sulfide oxidation can form several intermediate compounds (S^0, $S_2O_3^{2-}$, $S_4O_6^{2-}$, SO_3^{2-}), in which any these intermediate compounds may be undergo oxidation, reduction, and/or disproportionation (Canfield 2001). Thus, an accurate propagation of either biotic or abiotic sulfide oxidation can be highly variable, which can depend on environmental conditions, mineralogy, type of electron acceptor, and the oxidizing microorganism involved.

Sulfur fractionation between the COM host basalts and the secondary minerals is shown in Figure 5.5. The greatest fractionation difference between the host basalt and the secondary deposits is 4.5 ‰, with several additional values exceeding 3.5 ‰. These small but significant differences may imply biological oxidation as inorganic fractionation of sulfidic minerals generally do not exceed 3 ‰ (Lefticariu et al., 2006; Taylor and Wheeler, 1994). Although, laboratory experiments have shown that biological oxidation of H_2S to SO_4^{2-} can yield fractionation values reaching up to 10 to 18‰ (Canfield, 2001). One possible explanation of the lack of substantial ^{34}S fractionation may be explained by preferential oxidation of ^{34}S by disproportionation of metastable intermediate sulfur species (Canfield, 2001). During disproportionation

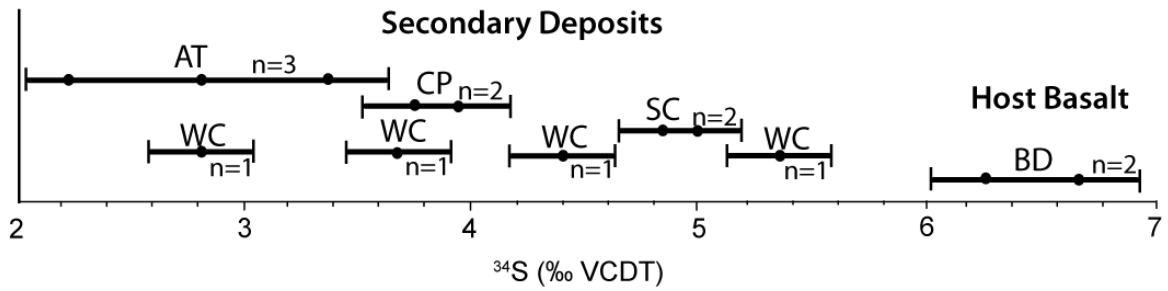

Figure 5.5. Picture illustrating the depletion of ^{34}S (‰VCDT) in the secondary deposits relative to the overlying host basalts. The two host basaltic samples were collected from the eastern and western boundary of the sampling area. Length of each box represents standard deviation of the measurement. BD- Blue Dragon flow; AT= Arco Tunnel; WC= Wilderness Caves; SC= Snow Cone Pit; CP= Crystal Pit.

processes, microorganisms show no preferential uptake between the sulfur isotopes, resulting in enriched ^{34}S values in sulfate products (Bottcher et al., 2001; Habicht et al., 1998; Smock et al., 1998). Thus, the presence of disproportionating bacteria may cause ^{34}S values to remain near the host basaltic values. Even though, the fractionation observed in the secondary deposits may suggestive a biological oxidation in their formation, it still is possible that these fractionation values may be due to abiotic processes.

No correlation with the cave location or from within the cave can be seen regarding sulfur fractionation, this lack of spatial correlation may imply that a similar oxidative pathway occurs throughout the sampling area and microbial oxidation processes are ubiquitous between these locations.

5.5. DISCUSSION

Several previous hypotheses have tried to explain the unusual occurrence of secondary sulfate deposits within the basaltic subsurface of COM. Stearns (1963) suggested a fumarolic origin, which can explain the isolated jarosite deposits found in

Crystal Pit (Peck, 1974) and Snow Cone Pit (Morris et al., 1995), but fails to explain the formation of more soluble and low temperature secondary minerals (i.e., mirabilite, thenardite, burkeite) (Richardson et al., 2009a). Peck (1974) hypothesized that the deposits were formed through groundwater leaching followed by subsequent deposition in open cavities on the cave floors. Although groundwater is a factor in the formation of the secondary sulfates, its influence is more related to weathering of the overlying basalt and subsequent physiochemical transport. A combination of fumarolic activity and subsequent groundwater leaching and redeposition was introduced as a third possible scenario for mineral precipitation (Karlo et al., 1980), although this hypothesis still suffers the same limitations as its predecessors. Furthermore, none of these hypotheses were further explored using detailed analytical techniques or subsequent field observations.

Alternatively, the secondary sulfate deposits could form from a combination of abiotic and biotic physiochemical weathering of the overlying basalt (Fig. 5.6). The Na-rich secondary deposits are consistent with the elevated alkali concentrations of COM basalts (Richardson et al., 2009a; Stout et al., 1994). Thus leaching could be a plausible source for the sodium cation, as Na leaching is a source for Na-rich speleothems in other basaltic cave settings (Forti, 2005). The source of the sulfur is more questionable since the overlying basalts have a sulfur concentration of 0.02% (Richardson et al., 2009a). Regardless, a potential sulfur source could be sulfide minerals located within the basaltic glass substrate, as sulfur concentrations in basaltic glass are shown to positively correlate with increasing overall Fe-content in the basalt (Czamanske and Moore, 1977). This could be a possible source, considering that glass percentages in the Blue Dragon flow

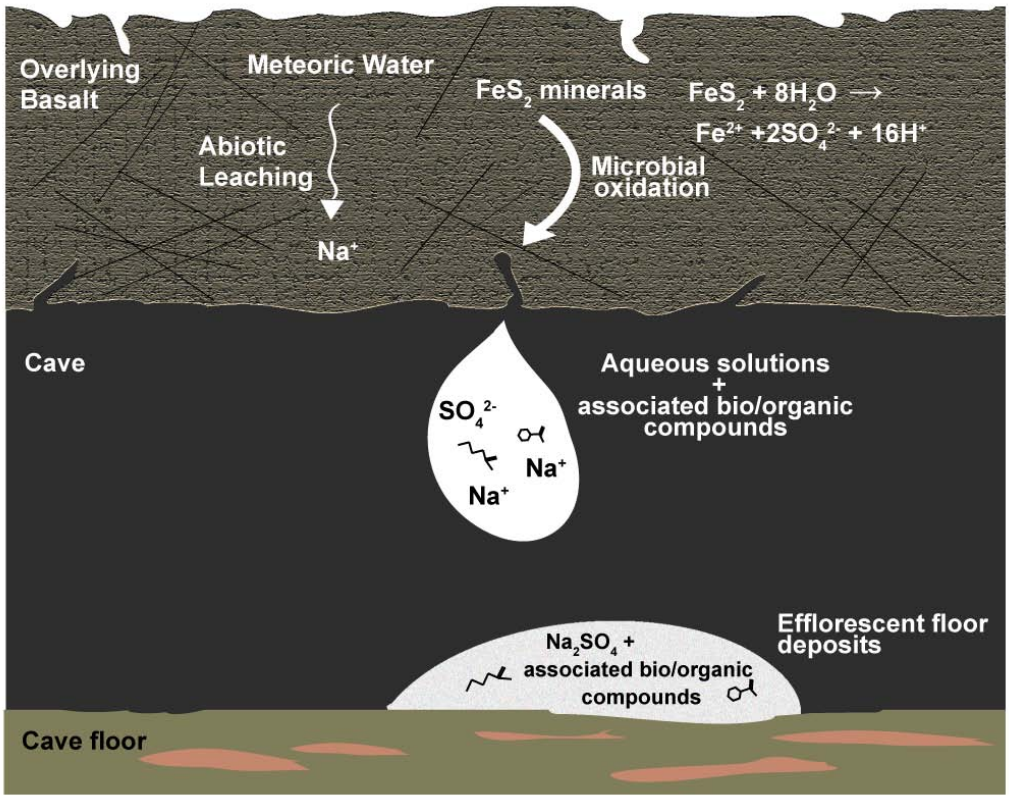

Figure 5.6. Schematic showing the biotic and abiotic weathering of the overlying basalts at COM, and the subsequent mineralization of secondary Na-sulfate minerals on the cave floors.

reach up to 25 % by volume, and COM flows are marked with extremely high Fe concentrations (Stout et al., 1994). Thus, it is possible that the glass substrate could provide a source for the sulfur. Additionally, endolithic microorganisms are commonly found within glass substrates in basalts (Cousins et al., 2009; Thorseth et al., 1995), and subsequent biological weathering has been observed by textural and chemical signatures (Fisk et al., 1998; Thorseth et al., 1995). FTICR-MS and FTIR spectra implies that the secondary deposits are associated with a variety of suggestive bio/organic compounds, implying a biogenic influence during the formation of the secondary sulfate deposits at

COM. Thus meteoritic leaching, possibly through fractures in the basaltic glass, along with biological oxidation of reduced sulfur may account for the needed sodium and sulfate ions to induce precipitation (Fig. 5.6).

5.6. CONCLUSIONS

The secondary sulfate deposits in the subsurface of COM are products of biogenic and abiogenic weathering and subsequent precipitation. Peaks suggestive of bio/organic compounds observed in the FTICR-MS spectra imply the secondary sulfate deposits directly or indirectly formed through biological activity, which is further supported by field observations, infrared spectroscopy and sulfur fractionation. The effectiveness of natural Na-sulfate minerals in the ionization/desorption of associated bio/organic compounds further implicates the importance of Na-sulfate minerals in future LDMS instruments like the Mars Organic Molecular Analyzer aboard the upcoming ExoMars rover. The occurrence of biological activity associated with the formation of secondary minerals in the lava tubes and caves of COM, in addition to the chemical and morphological similarities between the COM and martian basalts, offers further reasons as to the importance of the subsurface as an auspicious environment in the search for life on Mars.

5.7. ACKNOWLEDGEMENTS

The authors acknowledge support by the National Aeronautics and Space Administration (NASA) Exobiology Program (NNX08AP59G). Research performed at the Idaho National Laboratory under DOE Idaho Operations Office Contract DE-AC07-05ID14517. CDR would also like to thank Dawn Knipe, J. Michelle Kotler, and Doug Owen for their valuable insight and assistance.

5.8. REFERENCES

Badhwar, G., 2004. Martian radiation environment. Space Science Reviews 110, 131-142.

Balci, N., Shanks III, W.C., Mayer, B. and Mandernack, K.W., 2007. Oxygen and sulfur isotope systematics of sulfate produced by bacterial and abiotic oxidation of pyrite. Geochimica et Cosmochimica Acta 71, 3796-3811.

Benner, S., Devine, K., Matveeva, L. and Powell, D., 2000. The missing organic molecules on Mars. Proc. Natl. Acad. Sci 97, 2425-2430.

Boston, P., Spilde, M., Northup, D., Melim, L., Soroka, D., Kleina, L., Lavoie, K., Hose, L., Mallory, L., Dahm, C., Crossey, L. and Schelble, R., 2001. Cave biosignatures suites: microbes, minerals, and Mars. Astrobiology 1, 25-55.

Bottcher, M., Thamdrup, B. and Vennemann, T., 2001. Oxygen and sulfur isotop fractionation during anaerobic bacterial disproportionation of elemental sulfur. Geochimica et Cosmochimica Acta 65(10), 1601-1609.

Budimir, N., Blais, J.C., Fournier, T. and Tabet, J.C., 2007. Desorption/ionization on porous silicon mass spectrometry (DIOS) of model cationized fatty acids. Journal of Mass Spectrometry 42, 42-48.

Canfield, D.E., 2001. Biogeochemistry of sulfur isotopes. Reviews in Mineralogy and Petrology 43, 607-636.

Coates, J., 2000. Interpretation of infrared spectra, a practical approach. In: R. Meyers (Editor), Encyclopedia of analytical chemistry. John Wiley & Sons Ltd, Chichester, UK, pp. 10815-10837.

Cousins, C., Smellie, J., Jones, A. and Crawford, I., 2009. A comparative study of endolithic microborings in basaltic lavas from a transitional subglacial–marine environment. International Journal of Astrobiology 8, 37-49.

Cushing, G.E., Titus, T.N., Wynne, P.R. and Christensen, P.R., 2007. Themis observes possible cave skylights on Mars. Geophysical Research Letters 34(L17201), Doi:10.1029/2007/2007GL030709.

Czamanske, G. and Moore, J., 1977. Composition and phase chemistry of sulfide globules in basalt from the Mid-Atlantic Ridge rift valley near 37°N lat. Geological Society of America Bulletin 88(4), 587-599.

Dongyan, W., Zhenmin, L., Xiaolin, D. and Shaokang, X., 1998. Biomineralization of mirabilite deposits of Barkol Lake, China. Carbonates & Evaporites 13, 86-89.

Douglas, S., 1995. Mineralogical footprints of microbial life. American Journal of Science 305, 503-525.

Drost, C., Wynne, J., Chapman, M., Kargel, J., Titus, T. and Toomey, R., 2006. Remotely sensed cave detection on Earth and Mars, 37th Annual Lunar and Planetary Science Conference, League City, TX.

Fanale, F.P., Li, Y.-H., De Carlo, E., Farley, C., Sharma, S.K., Horton, K. and Granahan, J.C., 2001. An experimental estimate of Europa's "ocean" composition independent of Galileo orbital remote sensing. Journal of Geophysical Research 106(E7), 14595-14600.

Fisk, M., Giovanoni, S. and Thorseth, I., 1998. Alteration of oceanic volcanic glass: textural evidence of microbial activity. Science 281, 978-980.

Forti, P., 2005. Genetic processes of cave minerals in volcanic environments: An overview. Journal of Cave and Karst Studies 67(1), 3-13.

Habicht, K., Canfield, D. and Rethmeier, J., 1998. Sulfur isotope fractionation during bacterial reduction and disproportionation of thiosulfate and sulfide. Geochimica et Cosmochimica Acta 62, 2585-2595.

Ham, J.E., Durham, B. and Scott, J.R., 2003. Comparison of laser desorption and matrix-assisted laser desorption/ionization for ruthenium and osmium trisbipyridine complexes using Fourier transform mass spectrometry. Journal of the American Society for Mass Spectrometry 14, 393-400.

Haubrich, F. and Tichomirowa, M., 2002. Sulfur and oxygen isotope geochemistry of acid mine drainage-the polymetallic sulfide deposit "Himmelfahrt fundgrube" in Freiberg (Germany). Isotopes in Environmental and Health Studies 38(2), 121-138.

Hughes, S.S., Smith, R., Hackett, W. and Anderson, S., 1999. Mafic volcanism and environmental geology of the eastern Snake River Plain. In: S.S. Hughes and G. Thackray (Editors), Guidebook to the geology of eastern Idaho. Idaho Museum of Natural History, Pocatello, Idaho, pp. 143-168.

Kaplan, I. and Rittenberg, S., 1964. Microbiological fractionation of sulphur isotopes. Journal of Gen. Microbiol 34, 195-212.

Karas, M., Bachmann, D. and Hillenkamp, F., 1985. Influence of the wavelength in high-irradiance ultraviolet laser desorption mass spectrometry of organic molecules. Analalytical Chemistry 57, 2935-2939.

Karas, M. and Kruger, R., 2000. Ion formation in MALDI: The cluster ionization mechanism. Chemical Reviews 103, 427-439.

Kargel, J.S., Kaye, J.Z., Head, J.W.I., Marion, G.M., Sassen, R., Crowly, J.K., Ballesteros, O.P., Grant, S.A. and Hogenboom, D.L., 2000. Europa's crust and ocean: origin, composition, and the prospects for life. Icarus 148, 226-265.

Karlo, J.H., Jorgenson, D.B. and Shineldecker, C.L., 1980. Sulfate minerals in Snake River Plain volcanoes. Northwest Science 54(3), 178-182.

Knochenmuss, R., Dubois, F., Dale, M.J. and Zenobi, R., 1996. The matrix suppression effect and ionization mechanisms in matrix-assisted laser desorption/ionization. Rapid Communications in Mass Spectrometry 10, 871-877.

Kotler, J.M., Hinman, N.W., Yan, B., Stoner, D.L. and Scott, J.R., 2008. Glycine identification in natural jarosites using laser-desorption Fourier transform mass spectrometry: Implications for the search for life on Mars. Astrobiology 8, 253-266.

Kuntz, M., Champion, D., Spiker, E. and Lefebvre, R., 1986. Contrasting magma types and steady-state, volume-predictable volcanism along the great rift, Idaho. GSA bulletin 97, 579-594.

Kuntz, M., Covington, H. and Schorr, L., 1992. An overview of basalitc volcanism of the eastern Snake River Plain, Idaho. In: P. Link, M. Kuntz and L. Platt (Editors), Regional geology of eastern Idaho and western Wyoming. Geological Society of America memoir, pp. 227-267.

Kuntz, M.E., 1989. Geology of the Craters of the Moon lava field, Idaho. In: K.L. Ruebelmann (Editor), Snake River Plain-Yellowstone Volcanic Province. American Geophysical Union, Washington D.C., pp. 51-56.

Leeman, W., Vitaliano, C. and Prinz, M., 1976. Evolved lavas from the Snake River Plain: Craters of the Moon National Monument, Idaho. Contributions to Mineralogy and Petrology 56, 35-60.

Lefticariu, L., Pratt, L.M. and Ripley, E.M., 2006. Mineralogic and sulfur isotopic effects accompanying oxidation of pyrite in millimolar solutions of hydrogen peroxide at temperatures from 4 to 150 °C. Geochimica et Cosmochimica Acta 70, 4889-4905.

Leveille, R. and Datta, S., 2007. Basaltic caves and lava tubes: astrobiological targets on Earth and Mars, Lunar and Planetary Science XXXVIII, Houston, TX.

Leveille, R. and Datta, S., 2009. Lava tubes and basaltic caves as astrobiological targets on Earth and Mars: A review. Planet. Space Sci, 10.1016/j.pss.2009.06.004.

Mangold, N., Gendrin, A., Gondet, B., LeMouelic, S., Quantin, C., Ansan, V., Bibring, J., Langevin, Y., Masson, P. and Neukum, G., 2008. Spectral and geological study of the sulfate-rich region of West Candor Chasma, Mars. Icarus 194, 519-543.

Martinez-Frias, J., Amaral, G. and Vazquez, L., 2006. Astrobiological significance of minerals on Mars surface environment. Reviews in Environmental Science and Biotechnology 5, 219-231.

McCord, T.B., Hansen, G., Fanale, F., Carlson, R., Matson, D.L., Johnson, T., Smythe, W., Crowley, J., Martin, P., Ocampo, A., Hibbitts, C.A., Granahan, J. and Team, N., 1998. Salts on Europa's surface detected by Galileo's near infrared mapping spectrometer. Science 280, 1242-1245.

McCord, T.B., Hansen, G.B., Matson, D.L., Johnson, T.V., Crowley, J.K., Fanale, F.P., Carlson, R.W., Smythe, W.D., Martin, P.D., Hibbitts, C.A., Granahan, J.C. and Ocampo, A., 1999. Hydrated salt minerals on Europa's surface from the Galileo near-infrared mapping spectrometer (NIMS) investigation. Journal of Geophysical Research 104, 11827-11851.

McJunkin, T.R., Tremblay, P.L. and Scott, J.R., 2002. Automation and control of an imaging internal laser desorption Fourier transform mass spectrometer (I^2LD-FTMS). Journal of the Association for Laboratory Automation (JALA) 7, 76-83.

Morris, R.C., Anderson, R.C., Earl, S., McCurry, M. and Pearson, L., 1995. A Mineral and Biotic Survey of Two Caves at Craters of the Moon National Monument. Environmental Science and Research Foundation.

Parnell, J., Cullen, D., Sims, M., Bowden, S., Cockell, C., Court, R., Ehrenfreund, P., Gaubert, F., Grant, W., Parro, V., Rohmer, M., Sephton, M., Stan-Lotter, H., Steele, A., Toporski, J. and Vago, J., 2007. Searching for Life on Mars: Selection of Molecular Targets for ESA's Aurora ExoMars Mission. Astrobiology 7, 578-604.

Peck, S.B., 1974. Unusual mineralogy of the Crystal Pit Spatter Cone, Craters of the Moon National Mounument, Idaho. NSS Bulletin 36(1), 19-24.

Poels, K., Van Vaeck, L. and Gijbels, R., 1998. Microprobe speciation analysis of inorganic solids by Fourier transform laser mass spectrometry. Analytical Chemistry 70, 504-512.

Reid, M., 1995. Processes of mantle enrichment and magmatic differentiation in the eastern Snake River Plain: Th isotope evidence. Earth and Planetary Science Letters 131, 239-254.

Richardson, C., Hinman, N., McHenry, L., Kotler, J. and Scott, J., 2009a. Secondary sulfate mineralization and basaltic chemistry of Craters of the Moon National Monument, Idaho: A view into the martian subsurface. Chemical Geology, submitted.

Richardson, C., Hinman, N., McJunkin, T., Kotler, J. and Scott, J., 2008. Exploring biosignatures associated with thenardite by geomatrix-assisted laser desorption/ionization Fourier transform ion cyclotron resonance mass spectrometry (GALDI-FTICR-MS). Geomicrobiology Journal 25(7), 432-440.

Richardson, C., Hinman, N. and Scott, J., 2009b. Effect of thenardite on the direct dectection of aromatic amino acids: Implications for the search for life in the solar system. International Journal of Astrobiology 8(4), 291-300.

Rye, R.O., Bethke, P.M. and Wasserman, M.D., 1992. The stable isotope geochemistry of acid sulfate alteration. Economic Geology 87, 225-262.

Sakimoto, S., Gregg, T., Hughes, S.S. and Chadwick, J., 2003. Re-assessing plains-style volcanism on Mars, Sixth International Conference on Mars, pp. 3197.pdf.

Scott, J.R., McJunkin, T.R. and Tremblay, P.L., 2003. Automated analysis of mass spectral data using fuzzy logic classification. Journal of the Association for Laboratory Automation (JALA) 8(2), 61-63.

Scott, J.R. and Tremblay, P.L., 2002. Highly reproducible laser beam scanning device for an internal source laser desorption microprobe Fourier transform mass spectrometer. Review of Scientific Instruments 73(3), 1108-1116.

Smith, B., 1999. Infrared spectral interpretation: A systematic approach. CRC Press, Boca Raton, FL.

Smock, A., Bottcher, M. and Cypionka, H., 1998. Fractionation of sulfur isotopes during thiosulfate reduction by *Desulfovibrio desulfuricans*. Arch. Microbiology 169, 460-463.

Stefansson, A.B., 1992. The Prihnukagigur Pit of southwest Iceland. National Speleological Society News 50(202-208).

Stout, M.Z., Nicholls, J. and Kuntz, M.A., 1994. Petrological and mineralogical variations in 2500-2000 yr B.P. lava flows, Craters of the Moon lava field, Idaho. Journal of Petrology 35(6), 1681-1715.

Taylor, B. and Wheeler, M., 1994. Sulfur and oxygen-isotope geochemistry of acid mine drainage in the western United States. In: C. Alpers and D. Blowes (Editors), Environmental geochemistry of sulfide oxidation. Am. Chem. Soc. Symp. Ser., pp. 481-514.

Thorseth, I., Furnes, H. and Tumyr, O., 1995. Textural and chemical effects of bacterial activity on basaltic glass: an experimental approach. Chemical Geology 119, 139-160.

Toran, L. and Harris, H., 1989. Interpretation of sulfur and oxygen isotopes of sulphates generated by bacterial and abiological oxidation. Geochimica et Cosmochimica Acta 53, 2341-2348.

Van Vaeck, L., Adriaens, A. and Adams, F., 1998. Microscopical speciation analysis with laser microprobe mass spectrometry and static secondary ion mass spectrometry. Spectrochim Acta B 53, 367-378.

Wood, W.W. and Low, W.H., 1986. Aqueous geochemistry and diagenesis in the easter Snake River Plain aquifer system, Idaho. Geological Society of America Bulletin 97, 1456-1466.

Wyrick, D., Ferrill, D., Morris, A., Colton, S. and Sims, D., 2004. Distribution, morphology, and origins of martian pit crater chains. Journal of Geophysical Research 109, E06005.

Yan, B., Stoner, D.L., Kotler, J.M., Hinman, N.W. and Scott, J.R., 2007a. Detection of biosignatures by geomatrix-assisted laser desorption/ionization (GALDI) mass spectrometry. Geomicrobiology Journal 24, 379-385.

Yan, B., Stoner, D.L. and Scott, J.R., 2007b. Direct LD-FTMS detection of mineral-associated PAHs and their influence on the detection of other organics. Talanta 72, 634-641.

Zhu, M., Xie, H., Guan, H. and Smith, R., 2006. Mineral and lithologic mapping of martian low albedo regions using OMEGA data, Lunar and Planetary Science XXXVII pp. 2173.pdf.

Zolotov, M.Y. and Shock, E.L., 2001. Composition and stability of salts on the surface of Europa and their oceanic origin. Journal of Geophysical Research 106(E12), 32815-32827.

APPENDIX A: DISTRIBUTION OF ORGANIC COMPOUNDS IN THE SOLAR SYSTEM: PLANETARY BODIES

The emergence of complex organic molecules in our solar system depends, in part, on the occurrence of organic compounds, whose type and distribution are controlled by the processes that form them from existing organic molecules. Thus, Earth-based telescopic and space-based instrumental detection and characterization of reservoirs of organic compounds is crucial to understanding the formation of organic molecules. The composition of organic molecules and the relationships between organic-molecule reservoirs remain active topics of extraterrestrial research.

With the exception of Mars, Europa, and Titan, planetary bodies are considered unsuitable for extant or extinct life, although these bodies offer valuable insight into surficial and atmospheric organic-chemical processes that lead to formation and accumulation of organic molecules. Therefore, this section will summarize evidence on the distribution and formation of organic molecules on planetary bodies in our solar system; although, it is very exciting that methane has been recently discovered on an extrasolar planetary body by space-based spectroscopy [338]. Reviews of planetary bodies have been published previously [339,340,341].

A1.1. THE KUIPER BELT AND CENTAURS

The Kuiper belt is a disk-shaped region between 30 to 200 AU beyond Neptune. The icy objects of the Kuiper belt follow heliocentric orbits. They are variably sized, with tens of thousands of them measuring greater than 100 km in diameter [342]. They have undergone minimal chemical and physical modifications from solar UV radiation [343]. Their current chemical composition likely reflects their original composition and, hence,

that of the solar proto-nebula. Dark refractory material and volatiles dominate the composition, making detection of organic constituents difficult. Unfortunately, chemical characterization of these bodies is also hindered by their small size and great distance from Earth.

Neptune's gravitational field occasionally ejects Kuiper belt objects from their orbits, relegating them to an unstable elliptical orbit among the Jovian planets (Jupiter, Saturn, Uranus, and Neptune) [344]. These objects, called Centaurs, are closer to Earth and, therefore, more easily observed than their parent Kuiper belt objects. Some Centaurs show variations in dust and evaporated gas content and composition, suggesting that Centaurs formed at different temperatures. Consequently, the compositions of these Centaurs and Kuiper-belt objects may be compositionally similar to short-lived comets [345,346].

Earth-based infrared spectroscopy shows that the surface composition and characteristics of Centaurs vary significantly. Several objects absorb strongly at the same infrared wavelengths as does the organic material, tholin, suggesting it may be present [347,348]. Tholins are high molecular weight, synthetic, macromolecular compounds produced from irradiated gaseous or solid mixtures of simple hydrocarbons, water, or nitrogen. They contain combinations of nitrogen heterocycles, amino acids, pyrimidines, and/or purines [349,350]. Additional surface components of Centaurs are water ice, minor amounts of methanol, $(CH_2)_6N_4$ (a photolytic product of methanol), amorphous carbon, and kerogen-like organic molecules [351,352]. The surface compositions of Centaurs are likely representative of all Kuiper belt objects [343].

Organic ices (hydrates) of carbon dioxide and carbon monoxide along with refractory minerals likely comprise the interiors and surfaces of Kuiper belt objects [353]. The largest and most easily studied of the Kuiper-belt objects is Pluto. Spectroscopic data show that Pluto's surface, which is compositionally similar to the Neptunian satellite, Triton, contains varying amounts of CH_4, CO, and tholin ices (see Figure A1.1.) [354]. These CH_4, CO, and tholin ices, which are produced by photochemical reactions of N_2 and CH_4 in Pluto's atmosphere [355], subsequently condense and precipitate onto Pluto's surface. Like Triton, Pluto also has other complex organic compounds (HCN, C_2H_4, C_2H_6, C_2H_2, and nitriles) that likely formed by photochemical reactions in the atmosphere [356].

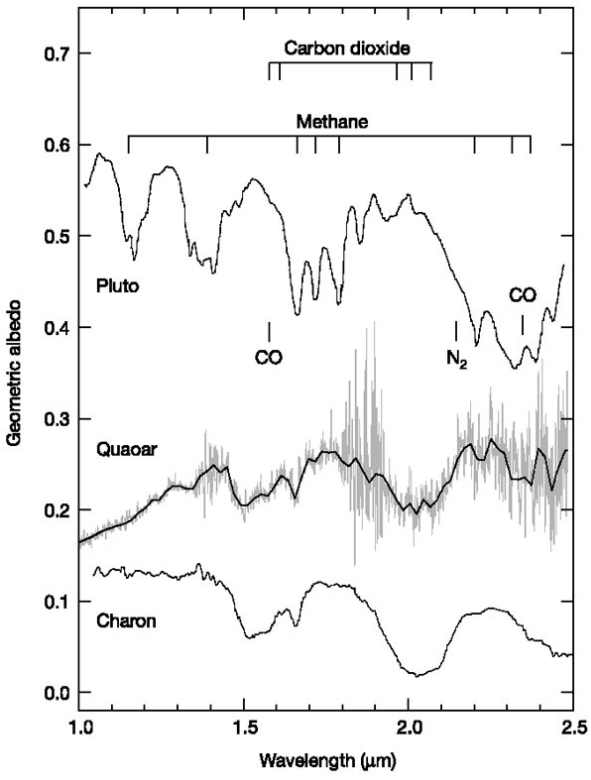

Figure A1.1. Near-infrared spectra of Pluto, Pluto's moon Charon, and the large Kuiper belt object Quaoar Wavelengths of solid CO, CO_2, N_2 and CH_4 are shown. Reprinted from [357] by permission from Macmillian Publishers Ltd: Nature, Jewitt, D.C. and Luu, J., **432**, 731 (2004), copyright (2004).

A1.2. GIANT PLANETS

Atmospheric compositions of the Jovian planets, determined by infrared and ultraviolet spectroscopy from orbiting spacecraft (Voyager 1, Voyager 2, Galileo, and Cassini) and terrestrial-based instruments, are dominated by hydrogen and helium with minor concentrations of CH_4 and other carbon-bearing compounds (see Table A1.1.) [358]. The carbon-bearing compounds are the result of three different mechanisms of CH_4 dissociation. The first is photolysis of singly bonded carbon resulting in CH_3 radicals. The CH_3 radicals subsequently react with atomic H to form simple hydrocarbons, such as ethane (C_2H_6), 154thane (C_2H_4), and acetylene (C_2H_2) [359,360]. Other complex organic molecules, such as C_4H_2 and C_6H_6 are produced by further photochemical reactions of the simpler hydrocarbons (ethane, ethane, and acetylene) [361,362]. The second formation mechanism of organic compounds in the Jovian planetary atmospheres is the reaction of magnetically trapped ions (H^+, CH_3^-) with atmospheric CH_4, which produces a cloud of simple and more complex hydrocarbons (see Table A1.1.) [363]. The last mechanism is the synthesis of organic molecules from CH_4 during lightning storms. This interaction can drive non-equilibrium organic reactions leading to formation of C_2H_6, C_4H_2, and C_6H_6. The exact formation processes of this last mechanism and its relative importance are poorly understood [364,365].

Hydrogen cyanide (HCN) and its polymers are likely formed in the atmospheres of the Jovian planets by photolysis of CH_4 and NH_3 [366]. The polymers are precursors to polypeptides and amino acids [367,368]. The occurrence of HCN and its polymers may potentially account for Jupiter's banded coloration and for the changes observed after

impact of comet P/Shoemaker-Levy 9 with Jupiter in 1994 [367,369]. The occurrence of HCN polymers on Saturn may cause the brown-orange color of the planet [367].

A1.3. SATURN'S ICY MOONS

NASA's Cassini spacecraft entered Saturn's orbit in summer 2004. One primary objective of the mission was detection and characterization of surficial and atmospheric composition of Saturn's icy moons (all of Saturn's moons except Titan). Cassini data reveal that the icy moons are physically and chemically diverse.

Table A1.1. Chemical composition of atmospheres of the Jovian planets [370-374].

	Jupiter	**Saturn**	**Uranus**	**Neptune**
Major compounds	**mixing ratio relative to H_2**			
H_2	1	1	1	1
He	0.15	0.06	0.18	0.18
CH_4	0.001-0.003	0.002	0.03	0.03
Minor compounds	**ppm**			
C_2H_6	1-2	1-3	trace	1-3
C_2H_2	0.03	0.07	0.1	0.1
C_2H_4	0.007	trace		
C_3H_8		trace		
C_3H_4	0.003	trace		
C_6H_6	0.002			
HCN	trace	trace		0.001
CO	0.002	0.002	0.01	1
CO_2	trace	trace	trace	trace

A1.3.1. Phoebe

Phoebe is Saturn's outermost moon. The elliptical retrograde orbit, unusual for moons, supports one interpretation that it may be a gravitationally captured Kuiper-belt object [375,376]. Further, the surface composition of Phoebe is unlike any surface composition observed in the outer solar system. The unusual, heterogeneous surface composition may reflect a thin veneer of cometary or intersolar material [377].

Spectroscopic data of Phoebe's surface shows the presence of PAHs, CO_2, amorphous carbon, nitriles, tholin, and cyanide compounds bound in a matrix of water ice [377-380]. CO_2 is ubiquitous on Phoebe and, along with these other compounds, accounts for the low albedo of the surface [377]. The origin of PAHs on Phoebe is still uncertain, although similar molecules are found on another of Saturn's satellites, Iapetus [378].

A1.3.2. Iapetus

Iapetus is Saturn's third largest moon. The surface is divided into a low-albedo hemisphere and a water-rich high-albedo hemisphere [381,382]. This difference in albedos is atypical in the solar system and represents different surface compositions in the two hemispheres. The composition of the high-albedo hemisphere is dominated by water ice with minor, but ubiquitous amounts of tholin [383]. Conversely, the low-albedo hemisphere is composed of several organic compounds; PAHs with aromatic and aliphatic bonds have been detected spectroscopically [378], while modeling experiments suggest the presence of spatially variable tholin, poly-HCN, and low concentrations of water ice [383,384]. Additionally CO_2, a photodissociation product trapped in water ice and organic solids, is ubiquitous in the low-albedo hemisphere [379,385,386]. The occurrence of CO_2 and the existence of PAHs suggest a possible evolutionary link with Phoebe and possibly with carbonaceous meteorites and interstellar dust [377,378].

A1.3.3. Enceladus

Embedded in Saturn's largest planetary ring is the volcanically active moon, Enceladus. Its atmosphere is composed with minor amounts of CH_4, CO, and CO_2 [387-389]. Additionally, the organic compounds, acetylene and propane, were detected from an outgassing volcanic plume. The presence of these organic compounds suggests that

Enceladus potentially has a thermally active carbon-bearing interior [388,390,391], which results in the accumulation of surficial CH_4, CO_2, and water ice [392].

Of the remaining icy moons, few are found to contain carbon-bearing molecules. These moons include Rhea, Hyperion, Mimas, Tethys, and Dione, all of which have trace amounts of atmospheric CO_2 [393,394]. Atmospheric CO_2 in the moons, detected by Cassini's VIMS (Visible and Infrared Mapping Spectrometer), is likely a dissociation product of interaction of Saturn's magnetosphere with existing tholin and cyanogens [393]. Minor amounts of surficial organic compounds (CH_4, nitriles, and tholin), detected by radiometric and infrared instrumentation are likely interstitially bound in a rock and water ice matrix [395].

A1.4. TITAN

The atmosphere of Saturn's moon, Titan, is approximately 90% molecular N_2 with up to 8% CH_4 (see Table A1.2.). CH_4 is essential in the production of atmospheric hydrocarbons, CO_2, CO, nitriles, and amorphous organic solids [339,396,397]. The interaction of cosmic rays, UV radiation, and magnetospheric radiation with CH_4 forms a methyl radical (CH_3) [398], which subsequently reacts to form tholin (see Figure A1.2.).

Photoionization of N_2 to N ions leads to the formation of nitriles, which subsequently react with methyl radicals to form hydrocarbons (see Figure A1.2.) [399,400]. These atmospheric reactions are common resulting in formation of increasingly more complex organic compounds (propane, butane, polyacetylene, and cyanoacetylene) [401-403]. Benzene, a precursor of PAHs, is found in an opaque haze cloud in the upper layers of the atmosphere [397,401,404,405].

Table A1.2. Organic inventory on Titan based on data from [397,408].

Major constituent	Percentage		
N_2	82–90		
CH_4	1–8		
Minor carbon compound	**ppm**	**Minor carbon compounds**	**ppm**
C_2H_6	20	C_4H_2	0.01
C_2H_4	1—4	CO_2	0.01
C_2H_2	1	CO	10-50
C_3H_8	1—10	HCN	1
C_3H_4	0.01	C_2N_2	0.02
C_6H_6	—	HC_3N	0.1–0.03
C_8H_2	—	CH_3CN	0.003
C_4N_2	—		

—detected but abundance not determined

Temperature fluxuations in Titan's atmosphere result in continual exchange between surficial and atmospheric CH_4 [396], resulting in a global CH_4 cycle with atmospheric (CH_4 cloud) and liquid reservoirs and evaporation/precipitation transfer mechanisms, analogous to the terrestrial water cycle [406]. Evidence of liquid CH_4 reservoirs derives from morphological, radar backscattering, and climatic models [407]. The CH_4 inventory in these lakes is roughly 30–30,000 km^3, a hundred times more than known hydrocarbons reserves on Earth [407]. Further, although temperatures are too cold for liquid water, the high concentrations of CH_4, and abundance of complex organic compounds suggests that life potentially could have evolved during warmer periods during Titan's past.

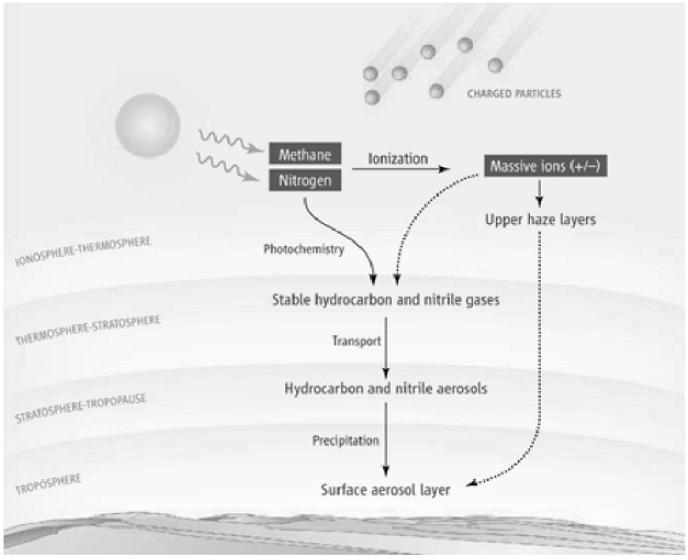

Figure A1.2. Formation of hydrocarbons, nitriles and tholin by interaction of UV radiation and charged particles from Saturn's magnetosphere react with N_2 and CH_4 in the upper layers of the atmosphere. From [397], Atreya, Science **316**, 5826 (2007). Reprinted with permission from AAAS.

A1.5. TRITON

Neptune's largest moon, Triton, was investigated directly by Voyager 2 spacecraft. Voyager mission data and ground-based telescopic observations suggest solid CO_2, CH_4, CO, and H_2O on Triton's surface [409-411] likely in an N_2-ice matrix [412].

Models of vapor pressure, temperature, atmospheric pressure, and surface organic composition suggest a variety of organic gases should be stable in the atmosphere [343]. Organic gases form by sublimation of N_2, CH_4, and CO ices. These gases are subsequently destroyed by solar winds and photolyzed by UV radiation [413-416], producing small organic compounds, such as HCN, C_2H_2, C_2H_4, and C_2H_6 [343]. These products subsequently condense as a result of Triton's cold temperature and precipitate on the surface [413-415]. However, either because of rapid sublimation or dilution by more abundant N_2, CH_4, and CO, these organic compounds have not been detected on Triton's surface [411]. Of these more abundant gases, CH_4 appears to be photochemically degraded in the atmosphere and is replenished by either sublimation of solid organic

compounds or volcanic outgassing. This CH_4 cycle is apparently similar to that of Saturn's moon, Titan, but differs because of Triton's lower temperature and thinner atmosphere [417].

A1.6. Galilean Satellites

Jupiter's largest moons (Io, Europa, Ganymede, and Callisto) are called the Galilean moons. With the exception of Io, each contains a significant concentration of surficial water ice [418], along with hydrated silicates and trapped volatiles [419]. Furthermore, infrared spectroscopy data from the Voyager and Galileo spacecraft suggest carbon-bearing compounds are incorporated in these surficial components [420-422].

A1.6.1. Europa

Spectroscopic and gravimetric data confirm that Europa's surface is a 100–150 km thick ice layer overlying a potentially liquid water ocean [422,423]. The existence of the liquid water interior is still uncertain, although magnetic, spectroscopic, and morphologic observations from the Voyager and Galileo spacecrafts support its presence [422,424,425]. A subsurface ocean could contain organic compounds, possibly emanating from hydrothermal vents on the ocean floor [426,427]. Unfortunately, any inferences of the composition of the subsurface ocean are only speculative.

Comets delivered an estimated minimum of 1 to 10 Gt of carbon and other biogenic elements (H, O, P, N, and S) to Eurpoa based on modeling experiments using cometary densities, cometary impact velocities, and escape thresholds of Europa's atmosphere [428]. Hence, Europa has the necessary components for formation of organic compounds.

The presence of liquid water, organic matter, and volcanic activity suggests the possibility of extant or extinct life. These characteristics, in conjunction with past conditions, could generate biochemical compounds and induce polymerization to provide the necessary ingredients for emergent life.

A1.6.2. Ganymede and Callisto

Ice on Ganymede, the largest moon in the solar system, covers approximately 50%–90% of the surface and is estimated to be 1,000 km thick [429]. Additionally, the surface has minor concentrations of CO_2, tholin, and cyanogens (compounds with a $[CN]_2$ component) interstitially bound in the water ice [420]. The presence of these carbon-bearing compounds mirrors organic compounds on Callisto, suggesting similar origin for organic compounds on the two moons [420].

Callisto has a heavy cratered surface devoid of tectonic activity [421] and a CO_2-dominated atmosphere [430]. The CO_2 likely originated from degradation of existing organic compounds supplied by cometary impacts [431] or degassed from the interior [430]. Atmospheric CO_2 is degraded by irradiation from Jupiter's magnetosphere, producing CO and amorphous carbon on both Callisto and Ganymede [420].

A1.7. The Terrestrial Planets

The four innermost solar bodies are called the terrestrial planets. Their atmospheres result from internal thermal activity and cometary impacts. Compositionally, these atmospheres differ from the atmospheres of the Jovian planets. Spectroscopic investigations using orbiting spacecraft and Earth-based telescopes show that the terrestrial planets are depleted in organic compounds relative to the large Jovian planets.

A1.7.1. Mercury

The lack of a substantial atmosphere on Mercury and its proximity to the Sun causes temperature to reach 440°C. At this temperature, organic compounds are unstable. Thus, long-term preservation of organic compounds on Mercury is unlikely. Only two spacecraft have investigated Mercury, the Mariner 10 orbiter, which was launched in the mid 1970's, and the MESSENGER spacecraft, which did a flyby in early 2008 and is scheduled to enter Mercury's orbit in 2011. A future joint mission between Japan's Aerospace Exploration Agency and the European Space Agency is tentatively scheduled for launch in 2013.

A1.7.2. Venus

Venus is the closest planet to Earth and comparable in mass, diameter, density, and chemical composition but lacks liquid water. Further, Venus has a dense corrosive atmosphere (with pressures up to 90 bar) and a runaway greenhouse effect causing surface temperatures to reach 450°C [432,433]. In addition to CO_2, the atmosphere contains trace amounts of CO and possibly carbonyl sulfide (OCS) [434]. The extreme surficial and atmospheric conditions on Venus make it unlikely for synthesis and preservation of organic compounds.

A1.7.3. Mars

Viking 1 and 2 were launched in the mid 1970's. A primary objective was the detection of biological processes in the martian soil. Instrumentation aboard the landers was designed to detect photosynthetic, metabolic, and respiration by-products of microbial communities that might be present in the martian regolith. The main instrument for detecting biological processes was a gas chromatography-mass spectrometer with high sensitivity and broad applicability. Unfortunately, no organic carbon was detected

using this technique. These results, or lack of results, could be explained by the presence of an oxidant, possibly H_2O_2 [435,436]. Without a protective atmosphere, the martian regolith is continually exposed to solar UV radiation, which could result in photochemical production of oxidants and subsequent oxidation of any organic molecules that might be present [437,438].

The Planetary Fourier Spectrometer aboard the Mars Express Orbiter detected CH_4 in the martian atmosphere [439]. Its presence was confirmed using the Earth-based Fourier Transform Spectrometer [440]. Atmospheric CH_4 concentrations are between 0 and 30 ppbv (parts per billion by volume), with a global mixing ratio of 10 ppbv [439]. Theories of the origin of atmospheric CH_4 include release as a by-product of methanogenic metabolism in the martian soil [440], emission through degassing by thermal activity [439], and introduction by cometary delivery [441].

In May 2008, Phoenix mission landed in the northern polar region of Mars to look for evidence of liquid water, biologically necessary elements (C, P, N, H), and evidence of organic compounds potentially indicative of life [442]. With only a week on the surface at this time, the Phoenix mission has taken two samples, but no chemical analyses have been completed [443]. NASA's Mars Science Laboratory Rover, scheduled to land in summer 2010 has a primary objective of identifying potential signatures of extinct or extant life [444]. The Sample Analysis at Mars Instrument Suite (SAM), will search for organic compounds using gas chromatography, mass spectrometry, and tunable laser spectrometry. Further, SAM can detect some light biogenic elements, such as H, O, and N.

A1.8. SNC Meteorites

The SNC (shergotite-nakhlite-chassignite) meteorite classification system is based primarily on oxygen isotope fractionation in meteoritic materials that indicate an extraterrestrial origin [445] and also correlate with compositional and isotopic measurements of the martian atmosphere taken by Viking spacecraft [446]. The chemistry of gas inclusions in the SNC meteorites (e.g., N_2, CO_2, and various noble gases) serve as geochemical fingerprints linking these meteorites to Mars, which has a unique atmospheric composition [447,448].

Martian meteorites are classified according to their primary mineralogy and petrologic relationships. All martian meteorites are considered to be achondritic stony meteorites. Stony meteorites are similar in composition to terrestrial rocks that have been differentiated or processed by igneous processes resulting in distinct textures and mineralogies; achondritic meteorites are stony meteorites that lack chondrules. Achondritic meteorites account for only 8% of classified meteorites compared to the iron-nickel and chondritic meteorites that constitute the remaining 92% percent of classified meteorites [449]; some meteorites are still unclassified. The shergotites are named after Shergotty, a 5 kg meteorite that fell in the Bihar State of India in 1865 [449]. There are 6 identified shergotites, all recovered from India, Nigeria, and various localities in Antarctica [445]. The term “shergotites” includes meteorites with basaltic and lherzolitic composition, although the lherzolitic shergotities have only been found in Antarctica [450]. The nakhlites are also igneous rocks and are named after the archetype meteorite, Nakhla, which fell in 1911 at El-Nakhla el-Bahariya in northern Egypt [449]. Two other nakhlites, Layfette and Governador Valadares, have uncertain histories; they may be

from the Nakhla fall [451]. Since 2000, four additional nakhlites have been discovered; two in northwest Africa and two from separate localities in Antarctica [452]. There are only two chassignite (Chassigny) meteorites, which are the only known martian dunite samples. The first was observed to fall in Haute-Marne, France in 1815 [453-455]. The second Chassigny meteorite, NWA 2727, was found in North West Africa [456].

Our understanding of martian organic matter is limited to what is known from the SNC meteorites because of the lack of detection of organic matter by Viking landers. SNC meteorites contain many complex organic molecules. Aromatic, alkyl-substituted aromatic, oxygen-containing, and nitrogen-bearing aromatic hydrocarbons (see Table A1.3.) were detected in the Nakhla meteorite, EETA 79001, by pyrolosis GC-MS [459]. Additionally, stepped-heating combustion experiments released CO_2 between 200–400°C, suggesting the presence of carbon-bearing compounds. The amount of CO_2 release is equivalent to approximately 1,000 ppm of carbon [460,461].

Meteorite ALH84001 does not fall specifically into the SNC classification system, but it is still considered to have a martian origin [457] based on oxygen isotopic composition and gas chemistry [445]. Geochronological investigations estimated the age of the meteorite to be 4.5 ± 0.13 Ga, which is 3 to 4 billion years older than the other SNC class meteorites. Although the age of ALH84001 has raised questions about its designation as the oldest known martian meteorite [458], it is now generally accepted to have originated from Mars [452].

Table A1.3. Distribution of organic compounds detected in martian meteorites based on data from [459,467,468].

High mass organic compounds detected in EETA79001[*,#]	
aromatic and alkyl-substituted	
benzene	C_6H_6
toluene	C_7H_8
naphthalene	$C_{10}H_8$
ethenylbenzene	C_8H_8
oxgyen-containing	
phenol	C_6H_5OH
nitrogen-containing	
benzonitrile	C_6H_5CN
High mass organic compounds detected in ALH84001[+]	
phenanthrene	$C_{14}H_{10}$
pyrene	$C_{16}H_{10}$
chrysene	$C_{18}H_{12}$
benzopyrene	$C_{20}H_{12}$
anthanthrene	$C_{22}H_{12}$
benzopenylene	$C_{22}H_{12}$
coronene	$C_{24}H_{12}$
kerogen-like compound	
amino acids (considered to be terrestrial contamination)	

* a Nakhla meteorite has same organic compounds with addition of biphenyl ($C_{12}H_{10}$),
[#] using pyrolsis-GC-MS,
[+] using LD-MS

In 1996, McKay et al. [462] issued an astonishing report that ALH84001 contained signsof extraterrestrial life, supported by the appearance of nanofossils, biogenic magnetite, nd PAHs. One of the stronger arguments in support of extraterrestrial biogenic influences in ALH84001 is chemical zonation in the carbonate globules. The sequence of Mn-carbonate deposition, followed by Fe-carbonate deposition, followed by Fe-sulfide formation is commonly observed in terrestrial environments where microbial processes control solution chemistry and hence, mineral solubility [463]. The sequence of chemical environments necessary to produce these structures abiotically is complicated. Hence, McKay et al. [462] dismiss an abiotic origin for this sequence as unlikely in ALH84001's history. Another piece of evidence is the presence of small, elongated, single-crystal magnetite grains. Although McKay et al. [462] acknowledge that some of

these structures can form abiotically, their statement that the elongated magnetite crystals in ALH84001 are biogenic is supported by other work that suggests that these structures can be biologically mediated in the form of magnetofossils produced by bacterial magnetosomes [463].

McKay et al. [462] consider possible sources of contamination from Antarctic groundwaters that contain terrestrial organic compounds and microorganisms. Further, they discuss the possibility of sample preparation contaminants and artifacts introduced during some of the analytical procedures. The controversial observation of the nanofossils generated contentious debate and is now considered the weakest evidence for extraterrestrial life. The nanofossils observed by McKay et al. [462] are found in carbonate globules. The nanofossils are purportedly similar in size, shape, and texture to bacterially induced carbonate precipitates in terrestrial samples. Sample-preparation issues, specifically, Au/Pd coatings used in electron-microscopy studies can affect sub-micron morphology. Bradley et al. [464] suggests that Au/Pd imparts fine-scale segmentation and that the segmentation increases as the thickness of the coatings increases. This argument has effectively placed nearly insurmountable doubt on the the veracity of purported nanofossils in ALH84001 [462] by calling them ‘microscopy artifacts’ [465].

McKay et al. [462] boldly conclude that “Although there are alternate explanations for each of these phenomena taken individually, when they are considered collectively, particularly in view of their spatial association, that they are evidence for primitive life on early Mars.” While carbon isotopic values and others lines of evidence have discredited the finding of signs of life in ALH84001, examination of the bulk matrix

material and carbonate globules indicate that these materials are indeed of extraterrestrial origin based on isotopic studies of the PAHs present in the meteorite [466]. Multiple species of polycyclic aromatic hydrocarbons (see Table 7) [462,467] and amino acids (glycine, serine, alanine) were also detecting using LD-MS and HPLC, but some were considered to be products of terrestrial contamination [467,468], especially the amino acids that are thought to be contaminants from Antarctic meltwater [466]. Discussions related to martian meteorite ALH84001 are likely to continue. A benefit to the scientific community is that intense scrutiny of the data has altered the rationale and methods in the search for martian life. Multiple methods (e.g., morphological, chemical, mineralogical, and isotopic) are needed to unequivocally identify signs of extraterrestrial life [469,470].

A1.9. REFERENCES

342. J. Luu and D. Jewitt, Annu. Rev. Astron. Astrophys. **40**, 63 (2002).

343. D. P. Cruikshank, Space Sci. Rev **116**, 421 (2005).

344. D. Durda and A. Stern, Icarus **145**, 220 (2000).

345. H. Levison and M. Duncan, Icarus **127**, 13 (1997).

346. K. Meech and J. Belton, Astron. J **100**, 1323 (1990).

347. E. Dotto, M. Barucci and C. De Bergh, Earth Moon Planets **92**, 157 (2003).

348. D. P. Cruikshank, H. Imanaka and C. M. Dalle Ore, Adv. Space Res **36**, 178 (2005).

349. C. Sagan and B. N. Khare, Nature **277**, 102 (1979).

350. G. McDonald, L. Whited, C. DeRuiter, B. N. Khare, A. Patnaik and C. Sagan, Icarus **122**, 107 (1996).

351. F. Poulet, J. Cuzzi, D. P. Cruikshank, T. L. Roush and C. M. Dalle Ore, Icarus **160**, 313 (2002).

352. M. P. Bernstein, S. Sandford, L. Allamandola, S. Chang and M. Scharberg, Astrophys. J. **454**, 327 (1995).

353. J. Luu and D. Jewitt, Astrophys. J. Suppl. S. **112**, 2310 (1996).

354. S. Doute, B. Schmitt, E. Quirico, T. C. Owen, D. P. Cruikshank, C. De Bergh, T. R. Geballe and T. L. Roush, Icarus **142**, 421 (1999).

355. V. Krasnopolsky and D. P. Cruikshank, J. Geophys. Res **104**, 21979 (1999).

356. L. Lara, W. Ip and R. Rodrigo, Icarus **130**, 16 (1997).

357. D. Jewitt and J. Luu, Nature **432**, 731 (2004).

358. J. Fortney, Science **305**, 1414 (2004).

359. T. Encrenaz, Planet Space Sci. **51**, 89 (2003).

360. B. Bezard, T. Encrenaz, E. Lellouch and H. Feuchtgruber, Science **283**, 800 (1999).

361. G. Gladstone, M. Allen and Y. L. Yung, Icarus **119**, 1 (1996).

362. D. Strobel, J. Atmos. Sci **30**, 489 (1973).

363. J. Friedson, A. Wong and Y. L. Yung, Icarus **158** (2002).

364. S. Desch, W. Borucki, C. Russell and A. Bar-Nun, Rep. Prog. Phys. **65**, 955 (2002).

365. J. Magalhaes and W. Borucki, Nature **349**, 311 (1991).

366. A. T. Tokunaga, S. Beck, T. R. Geballe, J. Lacy and E. Serabyn, Icarus **48**, 283 (1981).

367. C. N. Matthews, Adv. Space Res **19**, 1087 (1997).

368. R. Glaser, B. Hodgen, D. Farrelly and E. McKee, Astrobiology **7**, 455 (2007).

369. C. Griffith, B. Bezard, T. Greathouse, E. Lellouch, J. Lacy, D. Kelly and M. Richter, Icarus **170**, 58 (2004).

370. M. Summers and D. Strobel, Astrophys. J. **346**, 495 (1989).

371. W. Hubbard, Science **275**, 1279 (1997).

372. J. I. Lunine, Annu. Rev. Astron. Astrophys. **31**, 217 (1993).

373. J. Moses, B. Bezard, E. Lellouch, G. Gladstone, H. Feuchtgruber and M. Allen, Icarus **143**, 244 (2000).

374. C. Nixon, R. Achterberg, B. Conrath, P. Irwin, N. Teanby, T. Fouchet, P. Parrish, P. Romani, M. Abbas, A. LeClair, D. Strobel, A. Simon-Miller, D. Jennings, F. Flasar and V. Kunde, Icarus **188**, 47 (2007).

375. T. Johnson and J. I. Lunine, Nature **435**, 69 (2005).

376. D. P. Simonelli, J. Kay, D. Adinolfi, J. Veverka, P. C. Thomas and P. Helfenstein, Icarus **138**, 249 (1999).

377. R. N. Clark, R. H. Brown, R. Jaumann, D. P. Cruikshank, R. M. Nelson, B. J. Buratti, T. B. McCord, J. I. Lunine, K. H. Baines, G. Belluci, J. Bibring, F. Capaccioni, G. Cerroni, A. Coradini, V. Formisano, Y. Langevin, D. L. Matson, V. Mennella, P. D. Nicholson, B. Sicardy, C. Sotin, T. M. Hoefen, J. M. Curchin, G. Hansen, K. Hibbitts and K. Matz, Nature **435**, 66 (2005).

378. D. P. Cruikshank, E. Wegryn, C. M. Dalle Ore, R. H. Brown, J. Bibring, B. J. Buratti, R. N. Clark, T. B. McCord, P. D. Nicholson, Y. J. Pendleton, T. C. Owen, G. Filacchione, A. Coradini, G. Cerroni, F. Capaccioni, R. Jaumann, R. M. Nelson, K. H. Baines, C. Sotin, G. Belluci, M. Combes, Y. Langevin, B. Sicardy, D. L. Matson, V. Formisano, P. Drossart and V. Mennella, Icarus **193**, 334 (2008).

379. B. J. Buratti, K. Soderlund, J. Bauer, J. A. Mosher, M. D. Hicks, D. P. Simonelli, R. Jaumann, R. N. Clark, R. H. Brown, D. P. Cruikshank and T. Momary, Icarus **193**, 309 (2008).

380. A. Coradini, F. Tosi, A. Gavrishin, F. Capaccioni, P. Cerroni, G. Filacchione, A. Adriani, R. H. Brown, G. Belluci, V. Formisano, E. D'Aversa, J. I. Lunine, K. H. Baines, J. Bibring, B. J. Buratti, R. N. Clark, D. P. Cruikshank, M. Combes, P. Drossart, R. Jaumann, Y. Langevin, D. L. Matson, T. B. McCord, V. Mennella, G. Hansen, C. A. Hibbitts, M. Showalter, C. Griffith and G. Strazzulla, Icarus **193**, 233 (2008).

381. A. R. Hendrix and C. Hansen, Icarus **193**, 344 (2008).

382. F. Vilas, S. Larson, K. Stockstill and M. Gaffey, Icarus **124**, 262 (1996).

383. B. J. Buratti, D. P. Cruikshank, R. H. Brown, B. C. Clark, J. Bauer, R. Jaumann, T. B. McCord, D. P. Simonelli, C. A. Hibbitts, G. Hansen, T. C. Owen, K. H. Baines, G. Belluci, J. Bibring, F. Capaccioni, G. Cerroni, A. Coradini, P. Drossart, V. Formisano, Y. Langevin, D. L. Matson, V. Mennella, R. M. Nelson,

P. D. Nicholson, B. Sicardy, C. Sotin, T. L. Roush, K. Soderlund and A. Muradyan, Astrophys. J. **622**, L149 (2005).

384. P. Wilson and C. Sagan, J. Geophys. Res. **100**, 7531 (1995).

385. E. Palmer and R. H. Brown, Icarus **195**, 434 (2008).

386. T. C. Owen, D. P. Cruikshank, C. M. Dalle Ore, T. R. Geballe, T. L. Roush, C. de Bergh, Y. J. Pendleton and B. N. Khare, Icarus **149**, 160 (2001).

387. M. Y. Zolotov, Geophys. Res. Lett. **34** (2007).

388. M. Y. Zolotov, in *EOS Trans. AGU*; *Vol. 88* (Fall Meet. Suppl. Abstract P32B-0540, 2007).

389. J. H. Waite, M. Combi, W. Ip, T. E. Cravens, R. L. McNutt, W. Kasprzak, R. Yelle, J. Luhmann, H. Niemann, D. Gell, B. Magee, G. Fletcher, J. I. Lunine and W. Tseng, Science **311**, 1419 (2006).

390. D. L. Matson, J. C. Castillo, J. I. Lunine and T. V. Johnson, Icarus **187**, 569 (2007).

391. R. P. Hodyss, P. V. Johnson, J. D. Goguen, A. L. Lane, C. S. Boxe, J. L. Kirschvink, Y. L. Yung and I. Kanik, EOS **87** (2006).

392. R. H. Brown, R. N. Clark, B. J. Buratti, D. P. Cruikshank, J. W. Barnes, R. M. Mastrapa, J. Bauer, S. Newman, T. Momary, K. H. Baines, G. Belluci, F. Capaccioni, G. Cerroni, M. Combes, A. Coradini, P. Drossart, V. Formisano, R. Jaumann, Y. Langevin, D. L. Matson, T. B. McCord, R. M. Nelson, P. D. Nicholson, B. Sicardy and C. Sotin, Science **311**, 1425 (2006).

393. R. N. Clark, R. Brown, K. H. Baines, G. Belluci, J. Bibring, B. J. Buratti, F. Capaccioni, G. Cerroni, M. Combes, A. Coradini, D. P. Cruikshank, P. Drossart, G. Filacchione, V. Formisano, R. Jaumann, Y. Langevin, D. L. Matson, T. B. McCord, V. Mennella, R. M. Nelson, P. D. Nicholson, B. Sicardy, C. Sotin, J. M. Curchin and T. M. Hoefen, America Astronomical Society **37**, 705 (2005).

394. G. Filacchione, F. Capaccioni, T. B. C. McCord, A., P. Cerroni, G. Belluci, F. Tosi, E. D'Aversa, V. Formisano, R. H. Brown, K. H. Baines, J. Bibring, B. J. Buratti, R. N. Clark, M. Combes, D. P. Cruikshank, P. Drossart, R. Jaumann, Y. Langevin, D. L. Matson, V. Mennella, R. M. Nelson, P. D. Nicholson, B. Sicardy, C. Sotin, G. Hansen, K. Hibbitts, M. Showalter and S. Newman, Icarus **186**, 259 (2007).

395. S. Ostro, R. West, M. Janssen, R. Lorenz, H. Zebker, G. Black, J. I. Lunine, L.

Wye, R. M. Lopes, S. Wall, C. Elachi, L. Roth, S. Hensley, K. Kelleher, G. Hamilton, Y. Gim, Y. Anderson, R. Boehmer, W. Johnson and t. C. R. Team, Icarus **183**, 479 (2006).

396. C. P. McKay and H. D. Smith, Icarus **178**, 274 (2005).

397. S. Atreya, Science **316**, 843 (2007).

398. E. Wilson and S. Atreya, Planet Space Sci. **51**, 1017 (2003).

399. B. Tran, J. Joseph, J. Ferris, P. Persans and J. Chera, Icarus **165**, 379 (2003).

400. S. Atreya, E. Adams, H. Niemann, J. Demick-Montelara, T. C. Owen, M. Fulchignoni, F. Ferri and E. Wilson, Planet Space Sci. **54**, 1177 (2006).

401. J. H. Waite, D. T. Young, T. E. Cravens, A. J. Coates, F. J. Crary, B. Magee and J. Westlake, Science **316**, 870 (2007).

402. Y. L. Yung, M. Allen and J. P. Pinto, Astrophys. J. Suppl. S. **55**, 465 (1984).

403. A. Coustenis, A. Salama, B. Schulz, S. Ott, E. Lellouch, T. Encrenaz, D. Gautier and H. Feuchtgruber, Icarus **161**, 383 (2003).

404. K. Rages and J. Pollack, Icarus **55**, 50 (1983).

405. D. Clarke and J. Ferris, Icarus **127**, 158 (1997).

406. J. I. Lunine and S. Atreya, Nature Geo. **1**, 159 (2008).

407. R. M. Lopes, K. Mitchell, S. Wall, G. Mitri, M. Janssen, S. Ostro, R. Kirk, A. Hayes, E. Stofan, J. I. Lunine, R. Lorenz, C. Wood, J. Radebaugh, P. Paillou, H. Zebker and F. Paganelli, EOS **88**, 569 (2007).

408. D. Gautier and F. Raulin, in *Huygens:science, payload and mission*, edited A. WIlson, ESA Special Report SP-1177, (1997), p. 359.

409. K. Tryka, R. Brown, V. Anicich, D. P. Cruikshank and T. C. Owen, Science **261**, 751 (1993).

410. D. P. R. Cruikshank, T., T. C. Owen, E. Quirico and C. De Bergh, in *Ices in the Solar System*, edited B. Schmitt, C. De Bergh, and M. Festou, Kluwer, Dordrecht (1998), p. 655.

411. E. Quirico, S. Doute, B. Schmitt, C. De Bergh, D. P. Cruikshank, T. C. Owen, T. R. Geballe and T. L. Roush, Icarus **139**, 159 (1999).

412. W. Grundy, M. Buie and J. Spencer, Astron. J. **123**, 1039 (2002).

413. W. Thompson, S. Singh, B. N. Khare and C. Sagan, Geophys. Res. Lett. **16**, 981 (1989).

414. D. Strobel and M. Summers, in *Neptune and Triton*, edited D. P. Cruikshank, University of Arizona Press, Tucson, (1995), p. 1107.

415. J. Elliot, D. Strobel, M. Zhu, J. Stansberry, L. Wasserman and O. Franz, Icarus **143**, 425 (2000).

416. R. B. Bohn, S. Sandford, L. Allamandola and D. P. Cruikshank, Icarus **111**, 151 (1994).

417. Y. L. Yung and W. DeMore, *Photochemistry of planetary atmospheres*, Oxford, New York (1999).

418. O. Kuskov and V. Kronrod, Icarus **151**, 204 (2001).

419. O. Gomis and G. Strazzulla, Icarus **194**, 146 (2008).

420. T. B. McCord, W. Carlson, W. Smythe, G. Hansen, R. Clark, C. A. Hibbitts, F. Fanale, J. Granahan, M. Segura, D. L. Matson, T. Johnson and P. Martin, Science **278**, 271 (1997).

421. A. Showman and R. Malhotra, Science **286**, 77 (1999).

422. M. Kivelson, C. Khurana, C. Russel, R. Volwerk, R. Walker and C. Zimmer, Science **289**, 1340 (2000).

423. R. Pappalardo, M. Belton, H. Breneman, M. Carr, C. Chapman, G. Collins, T. Denk, S. Fagents, P. Geissler, B. Giese, R. Greeley, R. Greenberg, J. Head, P. Helfenstein, G. Hoppa, S. Kadel, K. Klaasen, J. Klemaszewski, K. Magee, A. S. McEwen, J. Morre, W. Morre, G. Neukum, C. Phillips, L. Prockter, G. Schubert, D. Senske, R. Sullivan, B. Tufts, E. Turtle, R. Wagner and K. WIlliams, J. Geophys. Res. **104**, 24015 (1999).

424. D. Stevenson, Science **289**, 1305 (2000).

425. M. Carr, M. Belton, C. Chapman, M. Davies, P. Geissler, R. Greenberg, A. S. McEwen, B. Tufts, R. Greeley, R. Sullivan, J. Head, R. Pappalardo, K. Klaasen, T. Johnson, J. Kaufman, D. Senske, J. N. Moore, G. Neukum, G. Schubert, J. Burns, P. C. Thomas and J. Veverka, Nature **391**, 363 (1998).

426. T. Reynolds, S. W. Squyres, D. Colburn and C. P. McKay, Icarus **56**, 246 (1983).

427. C. Chyba, Nature **406**, 391 (2000).

428. E. Pierazzo and C. Chyba, Icarus **157**, 120 (2002).

429. W. Calvin, R. Clark, R. Brown and J. Spencer, J. Geophys. Res. **100**, 19041 (1995).

430. R. Carlson, Science **283**, 820 (1999).

431. M. Delitsky and A. L. Lane, J. Geophys. Res. **103**, 31391 (1998).

432. W. DeMore and Y. L. Yung, Science **217**, 1209 (1982).

433. P. Drossart, G. Piccioni, J. C. Gérard, M. A. Lopez-Valverde, A. Sanchez-Lavega, L. Zasova, R. Hues, F. W. Taylor, B. Bézard, A. Adriani, F. Angrilli, G. Arnold, K. H. Baines, G. Bellucci, J. Benkhoff, J. P. Bibring, A. Blanco, M. I. Blecka, R. W. Carlson, A. Coradin, A. D. Lellis, T. Encrenaz, S. Erard, S. Fonti, V. Formisano, T. Fouchet, R. Garcia, R. Haus, J. Helbert, N. I. Ignatiev, P. Irwin, Y. Langevin, S. Lebonnois, D. Luz1, L. Marinangeli, V. Orofino, A. V. Rodin, M. C. Roos-Serote, B. Saggin, D. M. Stam, D. Titov, G. Visconti, M. Zambelli and C. Tsang, Nature **450**, 641 (2007).

434. R. Carlson, K. H. Baines, T. Encrenaz, F. Taylor, P. Drossart, L. Kamp, J. Pollack, E. Lellouch, A. Collard, S. Calcutt, D. Grinspoon, P. Weissman, W. Smythe, A. Ocampo, G. Danielson, F. Fanale, T. Johnson, H. Kieffer, D. L. Matson, T. B. McCord and A. Soderblom, Science **253**, 1541 (1991).

435. H. Hartman and C. P. McKay, Planet Space Sci. **43**, 123 (1995).

436. J. A. Hurowitz, N. J. Tosca, S. M. McLennan and M. A. A. Schoonen, Earth Planet. Sc. Lett. **255**, 41 (2007).

437. V. Oyama, B. Berdahl and G. Carle, Nature **265**, 100 (1977).

438. T. Encrenaz, B. Bezard, T. Greathouse, L. Richter, J. Lacy, S. Atreya, A. Wong, S. Lebonnis, F. Lefevre and F. Forget, Icarus **170**, 424 (2004).

439. V. Formisano, V. Atreya, E. T., N. Ignatiev and M. Giuranna, Science **306**, 1758 (2004).

440. V. Krasnopolsky, J. Maillard and T. C. Owen, Icarus **172**, 537 (2004).

441. M. Kress and C. P. McKay, Icarus **168**, 475 (2004).

442. Phoenix Mars Mission, http://phoenix.lpl.arizona.edu/science03.php, accessed on 06/04/08.

443. Phoenix Mars Mission,http://phoenix.lpl.arizona.edu/06_03_pr.php, accessed on 06/04/08.

444. M. Cabane, P. Coll, C. Szopa, G. Israel, F. Raulin, R. Sternberg, P. Mahaffy, A. Person, C. Rodier, R. Navarro-Gonzalez, H. Hiemann, D. Harpold and W. Brinckerhoff, Adv. Space Res. **33**, 2240 (2004).

445. R. N. Clayton and T. K. Mayeda, Geochim. Cosmochim. Acta **60**, 1999 (1996).

446. M. H. Carr and H. Wanke, Icarus **98**, 61 (1992).

447. K. Marti, J. S. Kim, A. N. Thakur, T. J. McCoy and K. Keil, Science **267**, 1981 (1995).

448. G. Turner, S. F. Knott, R. D. Ash and J. D. Gilmour, Geochim. Cosmochim. Acta **61**, 3835 (1997).

449. H. Y. McSween, Annu. Rev. Earth Pl. Sc. **17**, 119 (1989).

450. H. Y. McSween and K. Keil, Geochim. Cosmochim. Acta **64**, 2155 (2000).

451. A. H. Treiman, Meteoritics **18**, 409 (1983).

452. A. H. Treiman, Chem. Erde-Geochem. **65**, 203 (2005).

453. A. Banin, Adv. Space Res. **18**, 231 (1996).

454. A. Banin, Adv. Space Res. **18**, 233 (1996).

455. R. L. Mancinelli, Adv. Space Res. **18**, 241 (1996).

456. P. Beck, J. A. Barrat, P. Gillet, M. Wadhwa, I. A. Franchi, R. C. Greenwood, M. Bohn, J. Cotten, B. V. de Moortele and B. Reynard, Geochim. Cosmochim. Acta **70**, 2127 (2006).

457. A. H. Treiman, A. K. Maloy and C. K. Shearer, Meteorit. Planet. Sci. **40**, A157 (2005).

458. C. L. Harper, L. E. Nyquist, B. Bansal, H. Wiesmann and C. Y. Shih, Science **267**, 213 (1995).

459. M. A. Sephton, I. P. Wright, I. Gilmour, J. W. de Leeuw, M. M. Grady and C. T. Pillinger, Planet Space Sci. **50**, 711 (2002).

460. I. Wright, M. Grady and C. Pillinger, Nature **340**, 220 (1989).

461. A. Jull, C. Courtney, D. Jeffrey and J. Beck, Science **279**, 366 (1998).

462. D. S. McKay, E. K. Gibson, K. L. ThomasKeprta, H. Vali, C. S. Romanek, S. J. Clemett, X. D. F. Chillier, C. R. Maechling and R. N. Zare, Science **273**, 924 (1996).

463. R. P. Blakemore, Annu. Rev. Microbiol. **36**, 217 (1982).

464. J. P. Bradley, R. P. Harvey and H. Y. McSween, Nature **390**, 454 (1997).

465. R. A. Kerr, Science **278**, 1706 (1997).

466. L. Becker, B. Popp, T. Rust and J. L. Bada, Earth Planet. Sc. Lett. **167**, 71 (1999).

467. L. Becker, B. Popp, T. Rust and J. L. Bada, in *Life Sciences: New Insights Into Complex Organics In Space*, Pergamon, Oxford (1999), Vol. 24, p. 477.

468. J. L. Bada, D. P. Glavin, G. D. McDonald and L. Becker, Science **279**, 362 (1998).

469. J. F. Banfield, J. W. Moreau, C. S. Chan, S. A. Welch and B. Little, Astrobiology **1**, 447 (2001).

470. J. W. Schopf, A. B. Kudryavtsev, D. G. Agresti, T. J. Wdowiak and A. D. Czaja, Nature **416**, 73 (2002).

APPENDIX B: DEFINITION OF MASS DEFECT

The mass defect is the number to the right of the decimal and is used in a variety of mass spectrometry applications, but maybe none as important as peak identification. The mass defect is related to the nuclear binding energy released upon formation and subsequent stabilization of the nucleus of any given isotope. The mass defect arises since the mass of the nucleus is slightly lower compared to the sum of its constituent matter. The mass defect can be used to calculate the nuclear binding energy, with the equation:

$$\text{Mass of bound system} = \text{sum of masses of its parts} - (\text{binding energy})/c^2.$$

Thus, the mass of a helium nucleus is thus a bit less than two times the proton mass plus two times the mass of a neutron. The mass of any nucleus is less than the sum of the separate masses of its protons and neutrons. In other words, sticking protons and neutrons together somehow causes some of their mass is converted into energy (by the equation $e=mc^2$). By convention, the mass defect of ^{12}C is defined as having zero atomic mass units, and the mass defect of any other isotope is calculated as the difference between the actual mass of the isotope and the isotope's nominal mass (Hall et al. 2003). As a result, ^{1}H has a larger mass defect because it has not lost mass by combining with neutrons. See Figure below for relative mass defects of common elements.

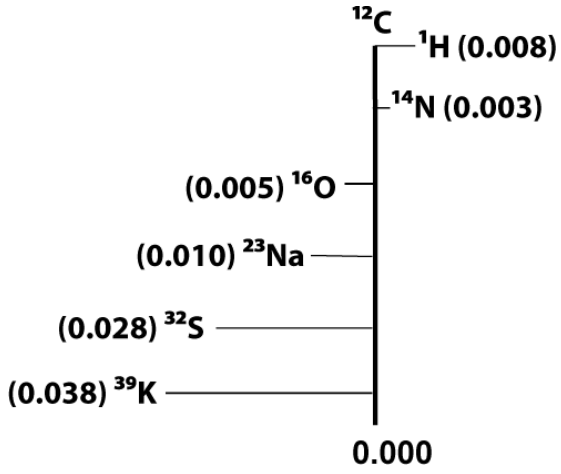

Figure illustrating the relative mass defects (depected by horizontal line) of some common organic and inorganic elements.

Hall, M., Ashrafi, S., Obegi, I., Petesch, R., Peterson, J., Schneider, L., 2003. 'Mass defect' tags for biomolecular mass spectrometry. Journal of Mass spectrometry 3 8, 809-816.

APPENDIX C: PHREEQC INPUT FILE FOR COM BASALTIC WEATHERING MODEL AND SUBSEQUENT SECONDARY MINERAL FORMATION

PHREEQC input file corresponding to Figure 4.5

```
Title :  weathering of basalts at COM
SOLUTION 1  Pure water

            pH      7.0
      temp    25.0  CO2(g) -3.5
            pE      12.5    O2(g) -0.68
equilibrium_phases

            CO2(g)  -3.5 10

save solution 1
END

Title :  dissolution of Blue Dragon
Solution 2          Equilibration with basalt
use solution 1
EQUILIBRIUM_PHASES
CO2(g)      -3.5    10
Diopside
Quartz
Fayalite
pyrite              0.0001
Ilmenite
Plagioclase

phases

Plagioclase
      Na.6Ca.4Al1.4Si2.6O8 + 5.6 H+ = \
            0.6 Na+ + 0.4 Ca++ + 1.4Al+++ + 2.8 H2O + 2.6 SiO2

save solution 2
end

use solution 2
Reaction 1   evaporation in multiple steps

H2O -1
5.53 in 1 step     # 55.3 moles *-1= -55.3 moles of H2O removed

EQUILIBRIUM_PHASES
CO2(g)      -3.5    10
dolomite

save solution 3
end

use solution 3
Reaction 2  second step of evaporation
```

```
H2O -1  5.53 in 1 step

EQUILIBRIUM_PHASES
CO2(g)      -3.5    10
calcite
dolomite

save solution 4
end

use solution 4
Reaction 3   thirst step of evaporation
H2O -1
5.53 in 1 step

EQUILIBRIUM_PHASES
CO2(g)      -3.5    10
calcite
dolomite

save solution 5
end

use solution 5
Reaction 4   fourth step of evaporation
H2O -1
5.53 in 1 step

EQUILIBRIUM_PHASES
CO2(g)      -3.5    10
calcite
dolomite

save solution 6
end

use solution 6
Reaction 5    fifth step of evaporation
H2O -1
5.53 in 1 step

EQUILIBRIUM_PHASES
CO2(g)      -3.5    10
calcite
dolomite

save solution 7
end

use solution 7
Reaction 6          sixth step of evaporation
H2O -1
5.53 in 1 step

EQUILIBRIUM_PHASES
CO2(g)      -3.5    10
```

```
calcite
dolomite

save solution 8
end

use solution 8
Reaction 7 seventh step of evaporation
H2O -1
5.53 in 1 step

EQUILIBRIUM_PHASES
CO2(g)     -3.5    10
calcite
dolomite

save solution 9
end

use solution 9
Reaction 8 eighth step of evaporation
H2O -1
5.53 in 1 step

EQUILIBRIUM_PHASES
CO2(g)     -3.5    10
calcite
dolomite

save solution 10
end

use solution 10
Reaction 9 ninth step of evaporation
H2O -1
5.53 in 1 step

EQUILIBRIUM_PHASES
CO2(g)     -3.5    10
calcite
dolomite

save solution 11
end

use solution 11
Reaction 10 Final step of evaporation
H2O -1
5.53 in 1 step

EQUILIBRIUM_PHASES
CO2(g)     -3.5    10
calcite
dolomite
save solution 12
end
```